A New Converter Topology for High-Speed High-Starting-Torque Three-Phase Switched Reluctance Motor Drive System

By

Ehab Elwakil

Submitted in partial fulfilment of the requirements for the degree of

Doctor of Philosophy

Department of Electronics and Computer Engineering

School of Engineering and Design

Brunel University

London, UK

January, 2009

Acknowledgements

My full gratitude and thanks are to Allah the one who helped me and gave me life, power and time to finish this work.

I am also grateful to my supervisor, Dr Mohamed K. Darwish for his outstanding and continuous help, advice and support.

Also, I would like to pass my special gratitude to the soul of my father, to my mother, my wife and kids for their patience and their emotional support along the time of conducting this research.

All thanks are to the Egyptian government represented by the Egyptian Cultural and Education Bureau for sponsoring this research in full, and to my respectable teachers and colleagues in the department of power electronics and energy conversion in the national Electronics Research Institute (ERI) in Egypt for nominating me for this scholarship.

Abstract

Switched reluctance motor (SRM) has become a competitive selection for many applications of electric machine drive systems recently due to its relative simple construction and its robustness. The advantages of those motors are high reliability, easy maintenance and good performance. The absence of permanent magnets and windings in rotor gives possibility to achieve very high speeds (over 10000 rpm) and turned SRM into perfect solution for operation in hard conditions like presence of vibrations or impacts. Such simple mechanical structure greatly reduces its price. Due to these features, SRM drives are used more and more into aerospace, automotive and home applications. The major drawbacks of the SRM are the complicated algorithm to control it due to the high degree of nonlinearity, also the SRM has always to be electronically commutated and the need of a shaft position sensor to detect the shaft position, the other limitations are strong torque ripple and acoustic noise effects.

The aim of this research is to design a new drive circuit topology of the SRM to meet the requirement of high-speed and/or high-starting torque applications.

To accomplish this aim, the following objectives have been conducted:

1. A survey of the fundamental background of the SRM design, applications, and theory of operation was established.
2. All converter topologies which have been used as an SRM drive circuits in the literature were critically reviewed, compared and classified according to their major field of application.
3. Upon completion of the literature review, decision was made to select the asymmetric converter topology as it is widely used in different applications and to modify the converter topology by inserting the switched capacitance circuit which acts as a variable capacitor and utilising this feature to profile the phase current waveform.

4. Two topologies of the switched capacitance circuit have been analysed, mathematically modelled, and experimentally verified to examine the behaviour of the switched capacitance circuit as a variable capacitor.
5. A survey has been conducted on the software packages which are commonly used to model and simulate the switched reluctance machine and the Magnet software was selected for its capability to model the motor with its real mechanical dimensions and utilising the FEM analysis to evaluate the magnetic characteristics of the motor besides the PSPICE-complying models of the passive and power electronic components of its circuit modeller.
6. A 3 phase 6/4 switched reluctance motor has been modelled and the drive circuit was designed by modifying the conventional asymmetric converter by inserting the switched capacitance circuit within the converter to act as a variable capacitor connected in series with the motor phase.
7. Simulation results were obtained and a comparison was held between the conventional asymmetric converter results without using the switched-capacitance circuit and the results obtained after modifying the converter by inserting the switched-capacitance circuit. The effect of the modification on different parameters of the drive circuit was discussed and criticised.

The contribution to knowledge of this research in the field of SRM drive circuits is represented in the following points:

- The Literature Review, which represents a comprehensive critical review of the machine design and its converters, which has been published as a journal article in 2006, such a review is not established in the literature up to the date of writing this thesis.
- introducing a new converter topology with a new switching strategy utilising the switched capacitance circuit to modify the conventional asymmetric converter

which is considered as a new topology of the converters used to drive such a type of electric motors which has not been covered in any of the literature published in this topic.

- Developing an SRM model using Magnet software which was not found in the literature.
- The contribution to solve the problem of torque ripples and acoustic noise through phase current shaping without varying the dwell angle.
- The contribution to present a new design which is perfect for applications where high speed and/or high starting torque is required.

The simulation results were very promising and it opens the door for more research to be conducted to enhance the performance of the suggested topology and to introduce the concept of utilising the switched capacitance circuit to modify other converter topologies of the SRM drive systems in the future.

Table of Contents

List of Tables

List of Figures

List of Symbols

θ	Rotor angle (position)
ϕ	Flux linkage
ω	Angular speed
φ	Phase angle
ψ	Phase shift
γ	C_2/C_1
τ	Switching interval period
Λ	Tooth pitch
δ	Air gap length
θ_a	Advance angle
θ_{al}	Aligned position
θ_{co}	Commutation angle
θ_d	Dwell angle
Δi	Hysteresis current window
θ_{omax}	Maximum overlap angle
β_r	Rotor pole arc
θ_r	Rotor position
θ_{rn}	Normalised rotor position
β_s	Stator pole arc
ω_s	Switching angular frequency
ϕ_s	Stator flux linkage
ΔT	Time period
θ_u	Unaligned position
A_o, A_n, B_n	Fourier coefficients
C	Capacitance
C_{eff}	Effective capacitance
D	Duty cycle
D_r	Rotor external diameter
D_{ri}	Rotor internal diameter
D_s	Stator external diameter
D_{si}	Stator internal diameter
D_w	Winding-wire diameter
f	frequency
F	Magneto-motive force
f(t)	Switching function
$f'(t)$	Complementary switching function
f_s	Switching frequency
g	Air gap width
h_r	Rotor tooth-height
h_s	Stator tooth-height
i	Instantaneous phase current
$\hat{I}$	Peak value of current
i^*	Current command signal
i_{ac}	Phase ac current

I_m	Maximum current
I_p	Peak flat tip of current signal
I_{ph}	RMS phase current
i_s	Stator current
K_b	EMF constant
L	Inductance
L_a	Aligned inductance
L_{as}	Aligned saturation inductance
L_{cs}	Stator-core axial length
L_{ph}	Phase inductance
L_u	Unaligned inductance
N_{ph}	Number of turns per stator-phase
P_r	Number of rotor poles
q	Number of phases
R	Resistance
R_m	Motor phase resistance
S	Switch
T	Torque
T	Period
t_{off}	OFF time
t_{on}	ON time
t_r	Rotor tooth width
t_s	Stator tooth width
u_s	Stator voltage
v	Instantaneous voltage
V^*	Converter command signal
v_{ac}	Phase ac voltage
v_c	Capacitor voltage
V_m	Maximum voltage
V_{ph}	RMS phase voltage
v_s	Supply voltage
$\hat{v}_{xx}$	Peak value of voltage
W_c	Magnetic co-energy
W_f	Magnetic field energy
W_m	Mechanical energy
X_c	Capacitive reactance
X_L	Inductive reactance
X_{ph}	Phase reactance
y_r	Rotor internal radius
y_s	Stator steel thickness
Z_{ph}	Phase impedance

List of Abbreviations

AI	Artificial intelligence
ANFIS	Adaptive Neuro-fuzzy inference system
ANN	Artificial neural network
DCDS	Double-capacitance, double-switch
EMF	Electromotive force
EMI	Electromagnetic interference
FEM	Finite element mesh
GFA	Genetic fuzzy algorithm
MF	Membership function
MMF	Magnetomotive force
PID	Proportional+ integral+ derivative
PWM	Pulse width modulation
SCC	Switched capacitance circuit
SCDS	Single-capacitance, double-switch
SRM	Switched reluctance motor
TR	Torque ripple
ZCS	Zero current switching
ZVS	Zero voltage switching
PIC	Programmable interface controller in some literatures referred to as programmable intelligent computer
DSP	Digital signal processor

Chapter 1

Introduction

1.1 Preface

The switched reluctance motor (SRM) represents one of the earliest electric machines which was introduces two centuries back in the history. It was not widely spread in industrial applications such as the induction and DC motors due to the fact that at the time when this machine was invented, there was no simultaneous progress in the field of power electronics and semiconductor switches which is necessary to drive this kind of electrical machines properly. The problems associated with the induction and DC machines together with the revolution of power electronics and semiconductors late in the sixties of the last century (1969), led to the re-invention of this motor and redirected the researchers to pay attention to its attractive features and advantages which help with overcoming a lot of problems associated with other kinds of electrical machines such as; brushes and commutators in DC machines, and slip rings in wound rotor induction machines, besides the speed limitation in both kinds. The simple design and robustness of the switched reluctance machine made it an attractive alternative for these kinds of electrical machines for many applications recently, specially that most of its disadvantages which are mentioned in the following chapter could be eliminated or minimized using the high speed and high power semiconductor switches such as the power Thyristors, power GTO, power transistors, power IGBT, power MOSFET. The availability and the inexpensive cost of these power switches nowadays besides the presence of microcontroller, microprocessors, PIC and DSP chips makes it a strong opponent to other types of electrical machines.

In industry, there is a very wide variety of designs of the switched reluctance machines which are used as motors or generators, these designs vary in number of phases, number of poles for both stator and rotor, number

of teeth per pole, the shape of poles and whether a permanent magnet is included or not.

These previous options together with the converter topology used to drive the machine lead to an enormous number of designs and types of switched reluctance machine systems, which means both the switched reluctance machine with its drive circuit to suit different applications with different requirements. It is to be noted that it is well known to those who are interested in this kind of electrical machines that the drive circuit and the machine is one integrated system, one part of such a system can't be separately designed without considering the other part.

A Switched Reluctance (SR) machine is a rotating electric machine where both stator and rotor have salient poles. The stator winding is comprised of a set of coils, each of which is wound on one pole. SR motors differ in the number of phases wound on the stator. Each of them has a certain number of suitable combinations of stator and rotor poles.

When operated as a motor, the machine is excited by a sequence of current pulses applied at each phase. The individual phases are consequently excited, forcing the motor to rotate. The current pulses need to be applied to the respective phase at the exact rotor position relative to the excited phase.

The inductance profile of SR motors is triangular shaped, with maximum inductance when it is in an aligned position and minimum inductance when unaligned. When the voltage is applied to the stator phase, the motor creates torque in the direction of increasing inductance. When the phase is energized in its minimum inductance position, the rotor moves to the forthcoming position of maximal inductance. The profile of the phase current together with the magnetization characteristics define the generated torque and thus the speed of the motor.

There are several advantages of the switched reluctance machine that gives it preference over other types of electrical motors in many applications, these advantages are: [1-5].

1. Simple design and robust structure.
2. Unwind rotor.

3. Lower cost.[6]
4. High starting torque without the problem of inrush currents compared with induction motor.
5. Suitable for high speed applications.
6. High reliability due to the electric and magnetic independency of the machine phases.
7. Suitable for high temperature applications compared to other machines of similar ratings.
8. Motor torque is independent of the phase current polarity.
9. Four quadrant operations.
10. A wide constant torque or power region in the torque speed characteristics.
11. High efficiency throughout every part of torque speed range.

1.2 SRM Applications

Many of the applications are categorized as low power, medium power, high power, and high speed drives for rotary motor drive. Some emerging applications and underwater applications are shown as well as few applications for linear switched reluctance motors. [1]

1.2.1 Low Power Drives

In this category, drives less than 3 hp are considered, this has been a successful range for many applications of switched reluctance motors such as, plotter drive, air handler motor drive, hand fork lift/pallet truck motor drive, door actuator system, washers, and dryers.

1.2.2 Medium Power Drives

This segment is generally in the range of less than 300 kW for general purpose, variable speed applications. New applications do not come in large numbers and don’t create huge markets for the switched reluctance machine drives in the medium power range. However, SRM drive systems have been

developed within the medium power range for general purpose industrial applications (up to 140 hp), train air conditioning drives (40 kw), and mining drive (300 kw) applications.

1.2.3 High Power Drives

There have been some efforts to develop SRM drives up to 1000 hp for fan and pump applications. At this high power level, the SRM converter is very competitive due to the fact that at high power levels, the inverter switches do not come with anti-parallel diodes as a single package which leads to a significant reduction in the converter cost added to the cheaper cost of the SRM compared with other AC or DC drives.

1.2.4 High Speed Drives

The SRM is a natural choice for high speed applications due to its robust rotor construction and its high power density. The performance sensitivity to high temperatures in the SRM is minimal compared with the permanent magnet synchronous and brushless dc motor and induction motor drive systems. Some existing products are available in the market for high speed applications such as screw rotary compressor drive at 4500 rpm, centrifuge for medical applications with high speed at 30000 rpm, aircraft jet engine starter motor generator at 27000 rpm, at the same time, the SRM can be used in the regeneration mode to supply electric power to the aircraft, the regeneration speed range is between 27000 and 50000 rpm. Also, fuel lube pump motor drive for a gas turbine engine for is another aerospace application of the SRM.

1.2.5 Emerging Applications

Variable speed applications can be found in hand power tools, fans, pumps, drives for freezers and refrigerators, automotive applications such as antilock brake drives, transportation and machine tool spindles. Also, underwater applications for marine propulsion system for surface, submersible, and flexible steering propulsion units. Finally, linear drive

applications such as direct drive based elevator door openers, semiconductor fabrication plants for material handling, low speed direct propulsion drive transit systems, automatic direct drive base door openers in office and commercial environments, and slide tables.

1.2.6 High volume Applications

Due to its simplicity of construction and resulting economy in its manufacture, SRMs are expected to gravitate toward high volume but inexpensive variable speed applications, such as hand power tools, fans, pumps, drives for freezers and refrigerators, automotive applications such as antilock brake drives and ripple torque minimized electronically controlled steering system and transportation and machine tool spindles where torque ripple is not a serious concern.

1.2.7 Underwater Applications

This drive system is also under consideration for underwater propulsion applications. The main features sought after for marine propulsion systems for surface, submersible, and flexible-steering propulsion units are the enhanced control, greater efficiency, reduced acoustic noise, high reliability, and equipment layout flexibility. One such application involves a 7.5 kw drive system with a partial stator and a rotor completely in water. The other application is an underwater marine drive unit for propulsion of remotely operated vehicles.

1.2.8 Linear Drive Applications

The linear switched reluctance motor is emerging for select applications. The trend is to use direct drive systems whereby the rotary to linear mechanical converters such as the lead screw, gears, etc., can be dispensed with both to reduce the cost of the system and to make the system compact and highly reliable. The linear switched reluctance motors have been in long use in XY table drive systems. Also it is found in direct drive based elevator door openers, semiconductor fabrication plants for

material handling, low speed direct propulsion drive transit systems, automatic direct drive based door openers in office and commercial environments, machine tools, slide tables, and in futuristic levitation systems for urban transit systems.

1.3 Aim of this Research

The aim of this research is to design a new topology of SRM drive circuit which is capable of shaping the phase current waveform in order to minimize the rise time and the fall time which in turn leads to two significant results, first, to achieve a more flat current pulse within the same pulse width (the same dwell angle), hence increasing significantly the net developed torque as the latter is proportional to the square of the phase current, secondly, is to meet the condition of better performance at higher speeds.

The new topology is a modification of the conventional asymmetric converter topology, Figure 2.6. The modification is achieved by inserting a switched capacitance circuit in series with the motor phase as shown in Figure 5.4.

The switched capacitance circuit in this case acts as a variable capacitor which may be varied by changing the duty cycle of the two semiconductor switches so that the value of the equivalent capacitance tracks the variation of the phase inductance profile of the machine causing a significant change in both the amplitude and the shape of the current waveform.

The novelty of introducing the switched capacitance circuit to the field of SRM drives is a main feature of this research. The main applications of the switched capacitance circuits in electrical power field are the power active filters and reactive power generation, while no research has been conducted to introduce it to the field of SRM drive circuits.

The thesis consists of six chapters, broken down as follows:

Chapter 1 is an introduction of the aim and the break down of the thesis.

Chapter 2 is a critical review of the SRM designs and the different topologies of the SRM drive circuits with a critical comparison showing the advantages and the disadvantages of each topology together with the suitable applications for it. Also, a brief description of the different control schemes is presented.

Chapter 3 presents the fundamentals and theory of operation of the switched reluctance motor showing the mathematical equations that govern the electrical, the magnetic and the mechanical characteristics of the machine.

Chapter 4 shows the mathematical and analytical derivation of the characteristics of two different topologies of switched capacitance circuits to be considered in this research which are the single capacitance double switch, and the double capacitance double switch circuits, deducing the relation between the effective capacitance and the duty cycle of the semiconductor switches.

Chapter 5 presents the modeling of a 3-ph, 6/4 switched reluctance machine using the Magnet software and simulation results are presented and discussed in details for each of the above two cases.

And finally the conclusions and future work are presented in chapter 6.

Chapter 2

Literature Review

2.1 Introduction

Switched reluctance motors (SRM) and their drives for industrial applications are considered in many references to be of recent origin. Krishnan, referred the first proposal of a variable reluctance motor for variable speed application to 1969, and the originality of the motor itself to 1842 [1].

Some other authors dated back the first acknowledged application of Switched Reluctance Motor to the late 1830s [7]. Since that date, the Switched Reluctance Motor was proposed but with major drawbacks, which severely limited the applications of this motor in industry, these major drawbacks are:

- Necessity of electronic commutation [8].
- Complicated analysis due to non-linear characteristics.
- Difficulty of control.
- Need to shaft position sensor.
- Torque ripples.
- Acoustic noise.

However, if considering the fact that the Switched Reluctance Motor together with its drive and control circuits should be designed as one single block, it can be appreciated why the SRM was not applicable since the early date on which it was invented; that is because of the unavailability of fast, inexpensive, high-power switching devices and control techniques at that time till the late 1960s, at which, most of the SRM drawbacks could be overcome [7]. Many researchers paid attention to the analysis and modelling of the SRM since that date, specially with the great development of software

packages, which helped with accurate modelling of the machine parameters such as PSPICE and MATLAB—[9-30].

This fact is more appreciated when one knows that unlike DC or induction motors, the Switched Reluctance Motor can't run directly neither from a DC nor an AC supply, instead a power converter must supply unipolar current pulses, timed accurately according to the inductance profile to produce positive torque in the motoring operation mode [31].

It is of great importance to overview the various designs of Switched Reluctance Motors as both the motor design and its drive circuit are severely inseparable.

2.2 Configurations of Switched Reluctance Motor

The Switched Reluctance Motor is a doubly salient, single excited machine, which has a number of critical parameters should be considered in its design process; these parameters are : the dimensions of stator and rotor laminations, winding details, number of poles, pole arcs, and number of phases[1]. These critical parameters determine the electrical, magnetic, mechanical, and thermal capabilities of the Switched Reluctance Motor.

The variety of combinations of number of phases with stator and rotor number and shapes of poles led to a wide range of possible designs of the SRM. The Rotary Switched Reluctance Motors, which is the scope of this research, could primarily be divided into Radial field and Axial field machines, Figure 2.1.

Within the radial field rotary machines, there are two possible designs, if the stator and the rotor of the machine are symmetrical about their centre lines and equally spaced around their periphery, this may be referred to as a regular structured machine as this term was first adopted by T. Miller [31].

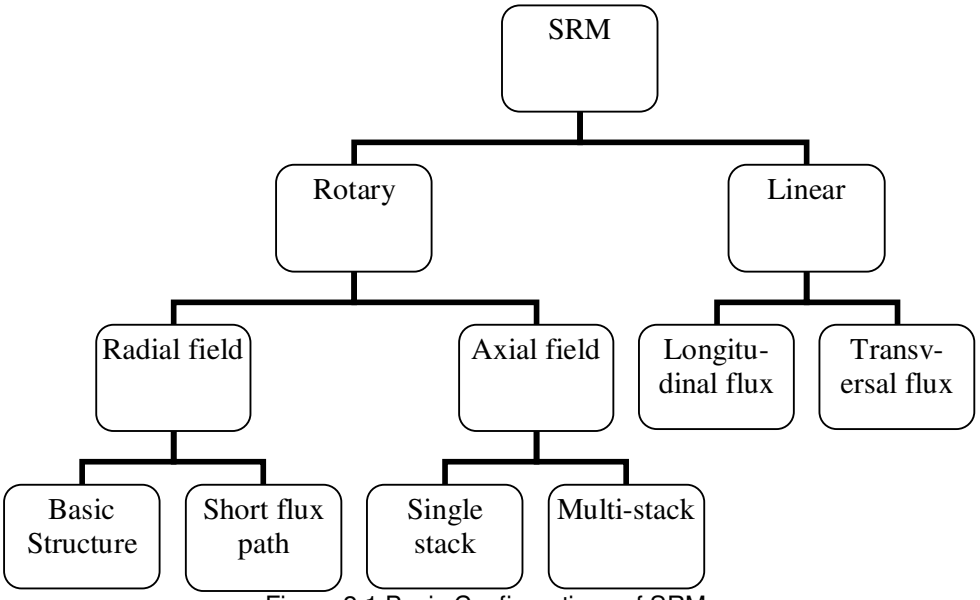

Figure 2.1 Basic Configurations of SRM.

In the early 1990s, an alternative arrangement, called the dual rotor pitch machine was introduced in the design of a five-phase 10/8 SRM but with its rotor having two separate pole pitches, the authors introduced the position theory as an extension to the basic modelling theory to encompass the boarder range of SRMs [31]. The position theory added a new categorization concept to SRMs on basis of the relative position of rotor poles with respect to the nearest stator poles, according to which, machines could be categorized to one position, two positions, or four positions machine [31].

Researches related to the machine design have been carried out to overcome the major drawbacks of SRM, specially those related to acoustic noise and torque ripples. One other problem with the SRM arises only in single and two phase machines, which is the existence of dead zones which may lead to the failure of the motor to self start at certain positions of the rotor.

The hybrid SRM was proposed to overcome this problem in the late 1980s, this type of motor utilizes a PM inserted either in the rotor or in the stator iron in order to guarantee the possibility of providing starting torque at all rotor positions. The idea of hybrid or PM SRM was applied later to multi phase (3 and above) machines to enhance the torque/volume ratio and to boost the efficiency of the machine [32, 33]. Other solutions were proposed

to solve the self starting problem such as, the stepped-gap motor, Figure 2.2 which was proposed in 1986 [34], and the homopolar SRM, which was applied to a two phase SRM design as shown in Figure 2.3 [35].

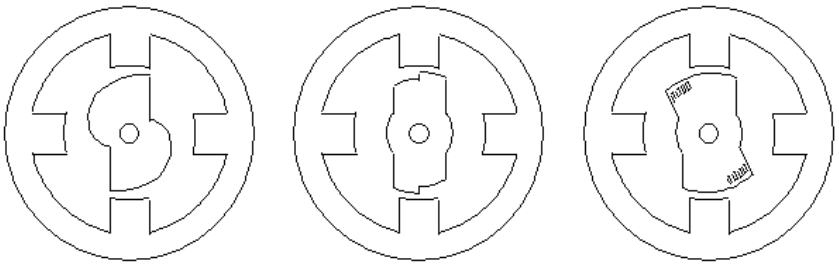

Figure 2.2 Different implementations of Stepped- gap Switched Reluctance Motors.

The axial field SRM in which the flux path is parallel to the shaft was proposed in the early 1970s to meet the applications in which the total length may be constrained, such as ceiling fans. The axial field SRMs have the advantage of lower core losses than the radial field motors, however, they have higher mutual inductance and higher magnetic pull on the rotor [1].

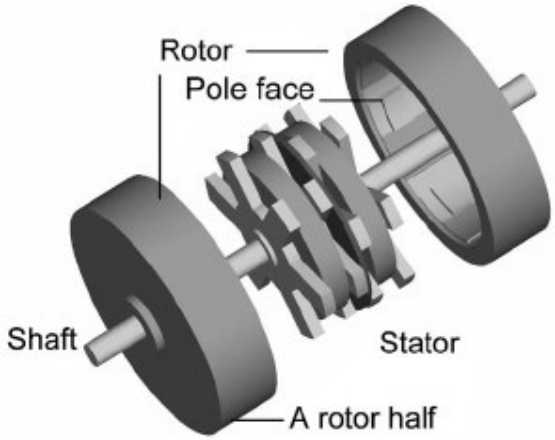

Figure 2.3 Two-phase homopolar SRM.

There are various configurations of SRM designs which were proposed to improve the overall performance of the machine, e.g. a c-core stator was proposed in [36] as shown in Figure 2.4 to increase torque capability and efficiency and also to provide a higher flexibility in winding design, while a new pole tip shape was suggested in [37], and a new notched teeth rotor shape was suggested in [38] to reduce the torque ripple rate as shown in Figure 2.5.

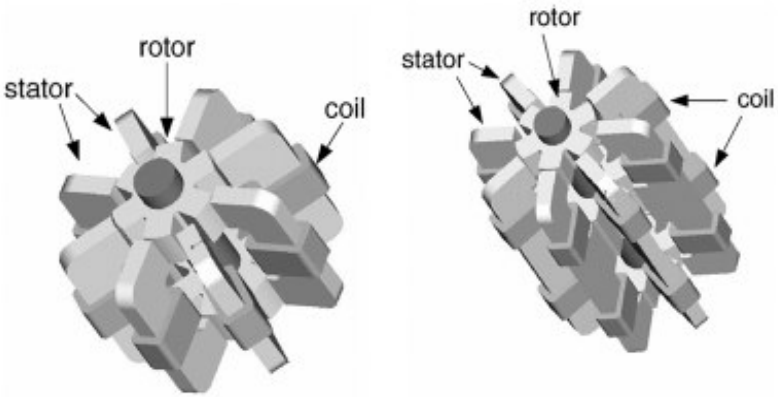

Figure 2.4 Structure of c-core stator SRM.

In [4], a novel SRM with wound-cores which is made of grain-oriented silicon steel was proposed to reduce the weight and volume of the SRM, hence increasing the power/weight and power/volume capability.

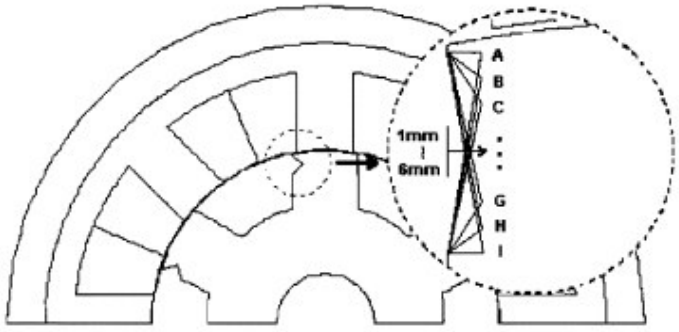

Figure 2.5 Notched rotor teeth.

2.3 Converter Topologies for Switched Reluctance Motor Drives

It is essential before considering the different topologies of Switched Reluctance Motor drive circuits to introduce the following features of the motor which give it an attractive advance over other types of AC machines; and affects the design of the drive circuit, these features are:

1. The torque in a SRM is independent of the polarity of the phase excitation current, which means only one switch per phase winding is required to energize or de-energize this phase.

2. There is always one switch connected in series with a phase winding, which makes the SRM self protected against shoot-through fault.
3. The phases of the SRM are electrically and magnetically independent, which allows separate control of current and torque for each phase, and also allows possible operation of the machine in case of one phase winding failure, although with reduced output power.
4. The mutual coupling between phases in a SRM can be neglected, this also gives an advance for independent phase current and torque control.
5. The phase inductance of the SRM varies with the rotor position in either a linear or a nonlinear profile.

The previous facts about the SRM explain the expected function of the drive circuit for this type of AC machines, which could be concluded in three tasks; first, is to divert current into the phase only in the positive gradient period of its inductance profile. Second, is to shape the energizing current of each phase, including its amount and its rise and fall times, of course less rise and fall times are desired to maximize the torque productivity during motoring operation[17, 39][8]. Third task is to provide a path for the stored magnetic energy in the phase winding during the commutation period, otherwise it will result in excessive voltage stress across the phase winding, hence across the semiconductor switching element leading to its failure, this energy could be freewheeled, or returned to the DC source either by electronic or electromagnetic means.

There are several topologies suggested to achieve the above function of the drive circuit. These topologies are well classified in [1] based on the number of switches used to energize and commutate each phase.

The most common configuration of SRM drive circuit is the asymmetric type with freewheeling and regeneration capability, Figure 2.6. The performance of this converter depends on the switching strategy, which varies between simultaneous switching of T_1 and T_2, or switching one switch ON and OFF while the other is ON all time. Selecting the proper switching strategy, dwell angle and control technique (usually hysteresis current control) will define the efficiency and application of this converter.

The asymmetric converter is the most common for voltage source operation for low power levels [40].

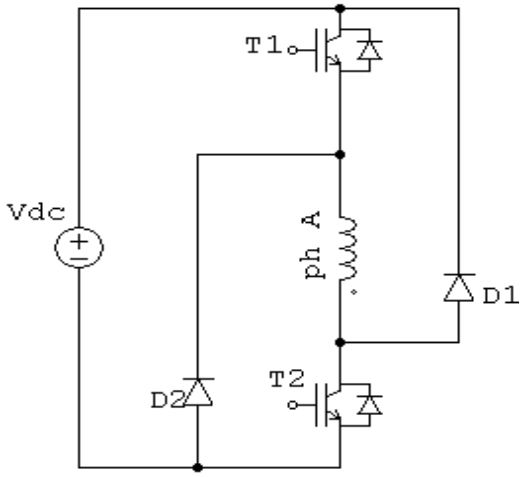

Figure 2.6 Asymmetric Bridge Converter.

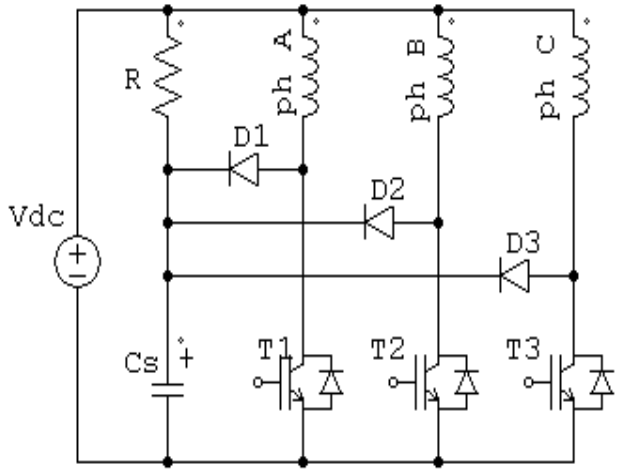

Figure 2.7 R-Dump Converter.

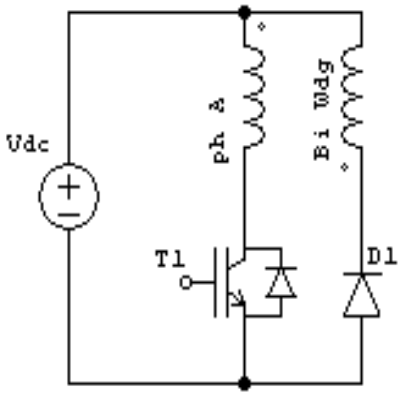

Figure 2.8 Bifilar Type Converter.

The R-dump converter, Figure 2.7, is one of the configurations which has one switch and one diode per phase. The value of R determines the power dissipation and the switch voltage. A compromise of R value should be done to achieve both reasonable stress on the switch (increases with higher R), and appropriate fall time of the current (increases with lower R). Analysis and detailed design procedure of this converter is explained in [41].

The Bifilar type converter, Figure 2.8, also has one switch and one diode per phase but with the capability of regenerating the stored magnetic energy to the supply by the bifilar winding. This converter is also utilizing one switch per phase. The bifilar converter has the drawbacks of reduced power density, and the high stress on the switching elements due to the bifilar windings inductance.

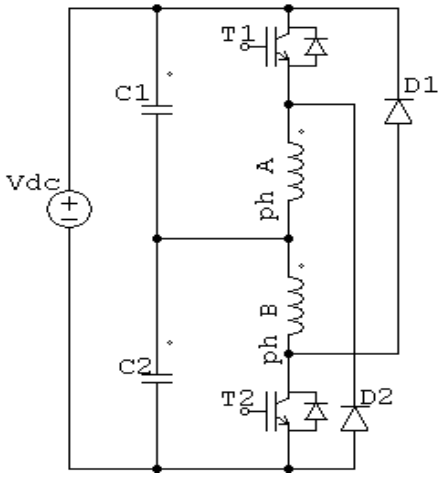

Figure 2.9 Split DC Supply Converter.

Figure 2.9 shows the split DC supply converter which allows freewheeling and regeneration. Proper design of the values of C_1 and C_2 should be done carefully to achieve charge balancing across the DC link. However, this converter utilizes only half the value of the DC supply, and also it is suitable only for motors with even number of phases.

One of the earliest drive circuits introduced for switched reluctance machines is the C-dump converter, shown in Figure 2.10. In this converter, the stored magnetic energy is partially diverted to the dump capacitor and recovered by a single chopper and sent to the DC source.

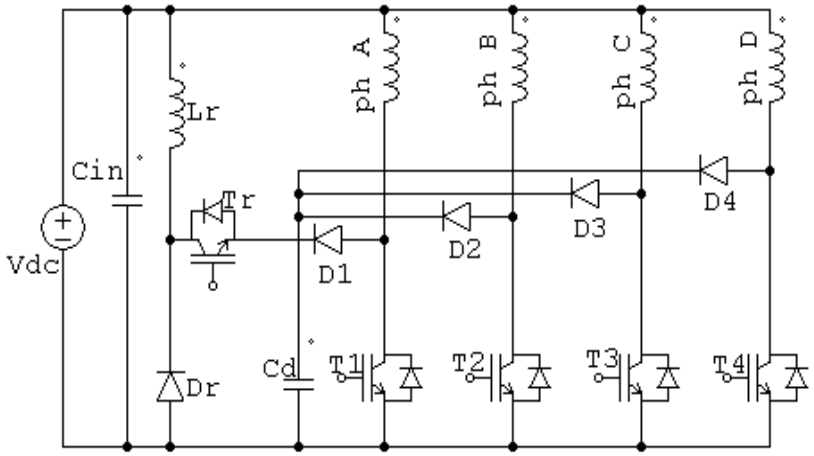

Figure 2.10 C–Dump Converter.

The C-dump converter has the drawback of disability to provide zero voltage across the phase winding during commutation period, which results in increased acoustic noise, and deterioration of the winding insulation. These drawbacks were overcome by adding a freewheeling transistor, which may be used for active energy recovery replacing the energy recovery coil further modifications were proposed to the conventional C-dump converter to eliminate its drawbacks while maintaining its attractive advantages [42, 43].

The variable DC link converter is an attractive configuration of SRM drives due to its advantages and its ability of operation in four-quadrant sensor-less applications.

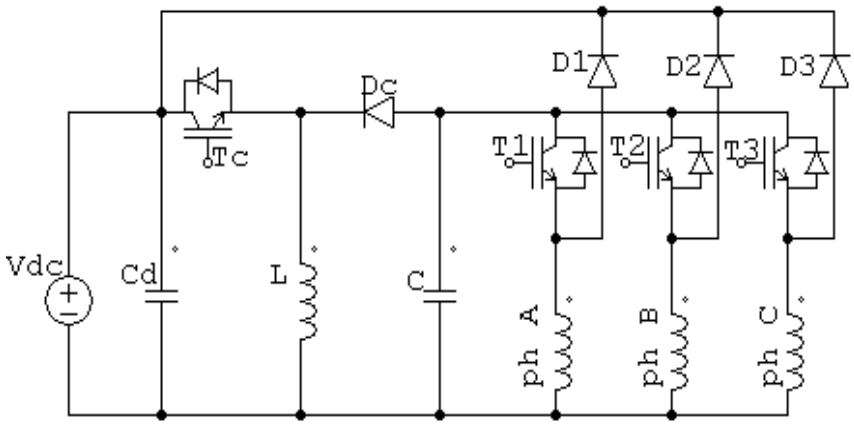

Figure 2.11 Variable DC Link Converter.

The variable DC link could be achieved by inserting a front end converter which may be a buck or a buck-boost converter. Figure 2.11 shows a variable DC link converter with a buck-boost front end stage. The machine input voltage can be varied from zero to twice the supply voltage, further, faster commutation of the current is achieved. A combination of the C-dump and the buck front end converters was proposed in [44] as a hybrid converter that possesses the advantages of both topologies and overcomes their major drawbacks.

All the above converter topologies are known as hard switching topologies, since the power switches and diodes are switched ON and OFF while their voltages and currents are nonzero. The converter topologies that enable soft switching are known as resonant topologies, one of which is shown in Figure 2.12 below.

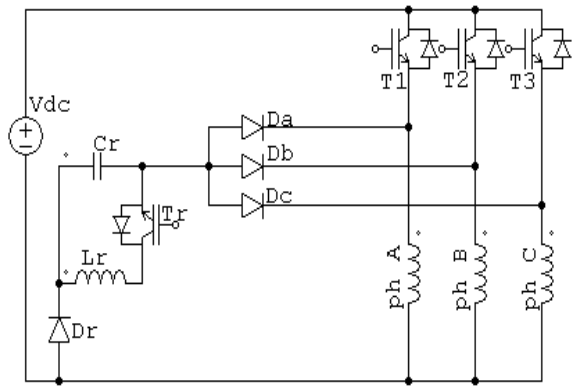

Figure 2.12 Resonant Converter.

The attractive advantage of zero switching losses which could be offered by the resonant circuit is contradicted by the losses in its passive elements, and the electromagnetic interference, EMI influenced by such circuits. There are several configurations within the resonant converter topology, depending on the resonance elements arrangement, (series or parallel), the soft switching technique (ZCS or ZVS), and the application (is phase current overlap required or not)[45, 46]. Few researches paid attention to the resonant converter topology because of the un-encouraging experimental studies [1].

More detailed study and suggestion of a new configuration based on the resonance principle and utilizing a switched capacitance circuit to perform as a variable capacitor is proposed in chapter 5 of this thesis.

The last converter topology to be presented in this section is the two stage power converter, Figure 2.13 in which the three phase AC supply is converted to a single phase variable frequency via a controlled rectifier/inverter, the other stage is the commutating stage which energizes phase windings [1].

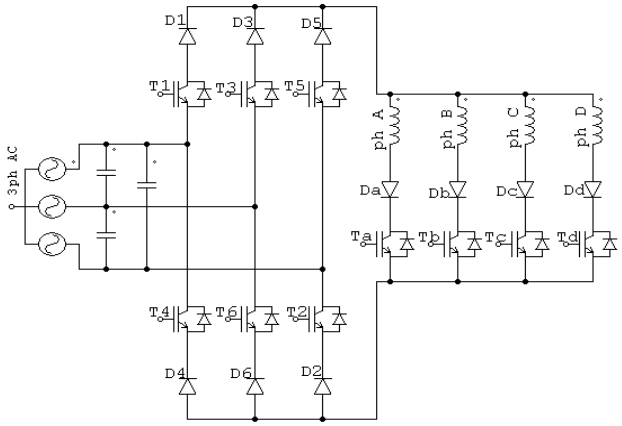

Figure 2.13 Two Stage Power Converter.

The two stage converter has the advantage of being capable of returning the power from the machine to the supply side directly with no limitations and eliminates the DC link capacitor. A comparison of the above discussed topologies showing the advantages and disadvantages together with useful application notes is presented in Table 2-1.

Table 2-1 Comparison of Common SRM Drive Circuits

Type	Switches /phase	Diodes /phase	Advantages	Disadvantages	Application Notes
Asymmetric Bridge	2	2	-Ideal for high performance current and torque control. -Allows greater flexibility in controlling machine current. -Capable of +ve, -ve, and zero voltage output. -Voltage stress across the switching element is restricted to V_{dc}.	-High switching losses. -Larger Heat sinks. -Not suitable for high power applications.	Low power levels inverters fed from a voltage source.
R- Dump	1	1	-Compactness of converter package. -Lower cost due to minimum number of switches and diodes.	-Unable to apply zero voltage output during current conduction. -Reduced system efficiency. -Rate of change of phase voltage is doubled.	Low speed, low switching frequencies.
Bifilar	1	1	-Compactness of converter package.	-High stress on switching element. -Reduced power density[1].	Not economical for large motors.

			-Lower cost due to minimum number of switches and diodes. -Capability of regeneration of stored energy.		
Split DC supply	1	1	-Compactness of converter package. -Lower cost due to minimum number of switches and diodes. -Capability of regeneration of stored energy.	-De-rating of the supply voltage. -Suitable only for motors with an even number of phases.	Fractional hp motors with even number of phases.
C –Dump	1	1	-Minimum switches number. -Independent phase current control.	-Current commutation is limited by the difference between the voltage across C_d and the DC link. -Not suitable for high speeds. -Lower efficiency. -Unable to provide zero voltage.	Low speed applications
C –Dump	1	1	-Minimum switches number.	-Only motoring operation is	Suitable only for

with freewheeling transistor			-Independent phase current control. -Lower cost than C-dump. -Higher power density than C-dump. -Less ripple on DC link capacitor. -Able to provide zero voltage.	possible. -High rating of the freewheeling switch. -complexity of control when phase currents overlap.	motoring operation.
Minimum switch with variable DC-link	1	1	-Higher DC source can be adopted -Lower core losses[1, 44]. -Lower switching losses. -Reduced acoustic noise.	-Lower commutation voltage. -Lower overall system efficiency. -Unsuitable for continuous generative operation[1].	-Suitable for four quadrant sensor-less applications. -Preferred in generation mode of operation.
Resonant converter	1	1	-Low switching losses (theoretically zero). -Superior quality of current waveform. -High switching frequency	-Lower power density. -EMI influence. -Higher rating of switching elements.	Suitable for high frequency applications (f>20kHz).

			capability.		
Two –stage power converter	1(+6)	1(+6)	-Lower cost. -Higher reliability. -Higher power density.	-Higher number of switches. -Not economical if regenerative operation is not substantial.	Suitable for variable speed, constant frequency generation using wind energy[8].

However, the selection of the proper converter for a certain application depends on many factors the designer has to compromise between them, such as; the hp capability, size and volume, economic considerations, speed requirements, switching frequency's range and whether the machine is used for motoring or for generation.

From the literature review and the above comparison between different topologies of converters which are utilised as an SRM drive circuits, it has been shown that the asymmetric converter topology is the most common topology which is used for most of the applications of the switched reluctance machines in industry, therefore this converter will be used after modification to implement the new converter topology aimed from this research.

Chapter 3

Fundamentals and Theory of Operation of SRM

3.1 Motor Construction

The Switched Reluctance Motor (SRM) consists of a salient pole stator and a salient pole rotor. Only the stator carries windings (wound field coils of a DC motor), the rotor has neither windings nor magnets and it is built up from a stack of steel laminations (hence the SRM is referred to as a doubly salient, singly excited motor) [47].

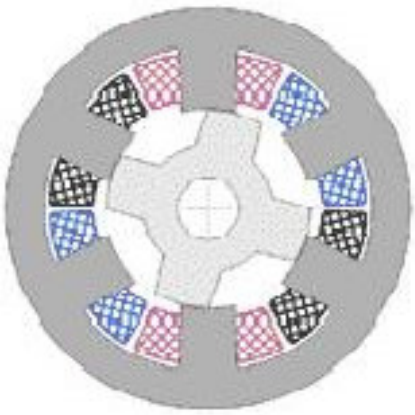

Figure 3.1 Basic Structure of SRM.

The SRM is classified as an AC synchronous machine, since the excitation sequence of stator phases should be synchronized with the rotor position to make the rotor rotates [47].

Each stator phase is consisted by connecting the two diametrically opposite windings in series, as shown in Figure 3.1.

The switched reluctance motor is similar to the step motor except that the former has fewer poles, larger step angle, and higher power output capability.

3.2 Theory of Operation

Figure 3.2 shows only two of the stator poles, and two of the rotor poles to explain how the torque is produced in SRM. At the position shown in Figure 3.2, the leading edge of the rotor pole meets the edge of the stator pole (at this position the inductance of phase A is minimum and the reluctance is maximum). If this stator pole is excited at this moment, (i.e, both the opposite poles of the stator are energized to constitute opposite magnetic poles), then the rotor pole is attracted to the stator pole causing the rotor to rotate in clockwise direction due to the fact that in a magnetic circuit the rotating member prefers to come to the minimum reluctance position at the instance of excitation.

As the rotor starts moving, the inductance is increased with the rotor position until it reaches its maximum value when the stator and rotor poles are completely aligned (fully overlapped). The inductance remains constant at its maximum as long as the two poles stay overlapped, this region is called the maximum inductance dead zone, where the name dead comes from zero torque production in this period.

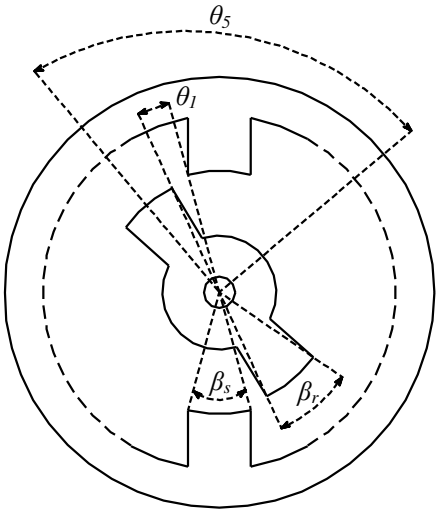

Figure 3.2 Single Element of SRM.

As the rotor continues rotating, the poles are not completely overlapped and the inductance starts to decrease until it reaches its minimum value when the two poles are apart from each other and it remains at this value until overlap occurs again, which is known as the minimum inductance dead zone.

The variation of phase inductance of the stator coil with the angle of rotation (θ) is illustrated in Figure 3.3.

While two rotor poles are aligned to the two excited stator poles, another set of poles is out of alignment with respect to a different set of the stator poles. The principle of operation depends on switching of currents into stator windings sequentially such that each phase is excited when its inductance is varying to produce positive or negative torque when the inductance is increasing or decreasing respectively, and only the sequence of excitation of stator phases determines the direction in which the rotor will rotate.

3.3 Torque Production

The Switched Reluctance Motor is an electric motor in which torque is produced by the tendency of its movable part to move to a position where the inductance of the excited winding is maximized. During motor operation, each phase is excited when its inductance is increasing and unexcited when its inductance is decreasing.

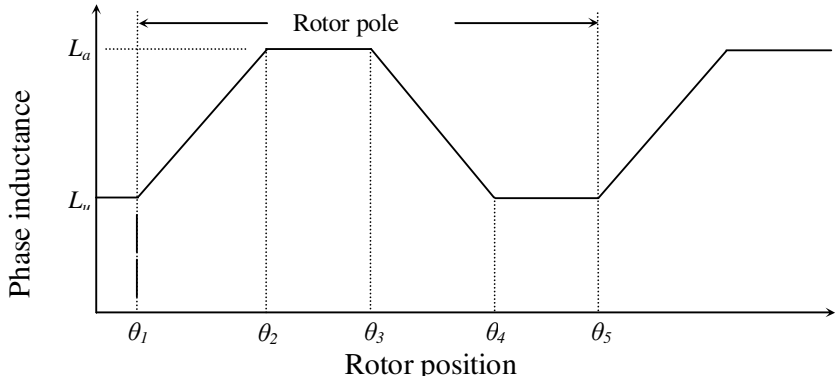

Figure 3.3 Ideal profile of phase inductance.

The air gap is minimum at the aligned position (the position at which a pair of rotor poles are exactly aligned with stator poles), the magnetic reluctance to the flux flow is at its lowest; it will be highest at the unaligned position. Thus, for a given phase, when the rotor is not aligned with the stator, the rotor will move to align with the excited stator pole [47].

The key to effective control of Switched Reluctance Motor is to switch the current from one phase to the next and to synchronize phase's excitation as a function of rotor position.

The current flowing in each stator phase is defined in magnitude, rise and fall times by the following parameters: motor resistance (including coil, wiring and on-state resistance of electronic switches), the inductance of the motor coil. The rise and fall times are directly proportional to coil inductance and inversely proportional to resistance.

The relation between the phase inductance, L and rotor position, θ can be deduced using Figure 3.3. The significant changes in the inductance profile are determined in terms of the stator and rotor pole arcs and number of rotor poles neglecting saturation. The stator pole arc is usually less than the rotor pole arc in most practical cases.

From Figure 3.3, different positions of the rotor can be derived as follows[1]:

$$\theta_1 = \frac{1}{2}\left[\frac{2\pi}{P_r} - (\beta_s + \beta_r)\right] \quad 3.1$$

$$\theta_2 = \theta_1 + \beta_s \quad 3.2$$

$$\theta_3 = \theta_2 + (\beta_r - \beta_s) \quad 3.3$$

$$\theta_4 = \theta_3 + \beta_s \quad 3.4$$

$$\theta_5 = \theta_4 + \theta_1 = \frac{2\pi}{P_r} \quad 3.5$$

Where β_s and β_r are the stator and rotor pole arcs respectively and P_r is the number of rotor poles.

The phase inductance has four distinct regions depending on the respective rotor position along one complete revolution:

1. Unaligned inductance region: this occurs in the intervals 0-θ_1 and θ_4-θ_5 at which the stator and rotor poles are not overlapping and the flux is predominantly determined by the air path, thus making the inductance minimum and almost constant. Thus, these two regions have no contribution to torque production.
2. Poles overlapping region: in this region, θ_1- θ_2, the stator and rotor poles begin to overlap and the flux path is mainly through the lamination of both poles, this increases the inductance with the rotor position, giving it a positive gradient, hence, if current is impressed in the winding during this region, it will produce a positive torque. The inductance reaches its maximum when the overlap of the two poles is complete.
3. Aligned inductance region: due to the fact that the two pole arcs of the stator and rotor are not equal, the movement of the rotor during the region θ_2-θ_3 doesn't change the complete overlap of the two poles, hence doesn't change the dominant flux path, and the inductance is kept constant at its maximum (aligned) value giving no contribution to the generated torque. This dead region serves on the other hand a useful function by allowing more time for the current to come to a lower value when it is commutated.
4. Poles departing region: in this region, θ_3-θ_4, the rotor pole continue moving away from alignment with the stator pole, which is the opposite process to region 1, hence the inductance change during this region is similar to that of region 1 but with a negative gradient.

3.4 Equivalent Circuit of a SRM

Neglecting the mutual inductance, an equivalent circuit of the SRM could be derived as follows:

The instantaneous voltage across the terminals of a single phase of a SRM winding is related to the flux linked in the winding by Faraday's law; equation 3.6

$$v = i R_m + \frac{d\phi}{dt} \qquad 3.6$$

Where, v is the terminal voltage, I is the phase current, R_m is the motor phase resistance, and ϕ is the flux linked by the winding, which varies as a function of rotor position θ, and the motor current I, hence, equation 3.6 can be expanded as:

$$v = i R_m + \frac{\partial \phi}{\partial i}\frac{di}{dt} + \frac{\partial \phi}{\partial \theta}\frac{d\theta}{dt} \qquad 3.7$$

Equation 3.7 governs the transfer of electrical energy to the SRM's magnetic field. Multiplying both sides of equation 3.6 by I, gives an expression for the instantaneous power in the SRM, equation 3.8

$$vi = i^2 R_m + i\frac{d\phi}{dt} \qquad 3.8$$

The left hand side of equation 3.8 represents the electrical input power, while the first term of the right hand side represents the ohmic losses in the motor winding, thus the second term of the right hand side must represent the sum of mechanical output power and any power stored in the magnetic field, since power is to be conserved. This is what equation 3.9 implies.

$$i\frac{d\phi}{dt} = \frac{d\ w_m}{dt} + \frac{d\ w_f}{dt} \qquad 3.9$$

Where, W_m is the mechanical energy, and W_f is the magnetic field energy. We can express the mechanical power as a function of torque, T and the speed,ω as:

$$\frac{d\ w_m}{dt} = T\ \omega = T\ \frac{d\theta}{dt} \qquad 3.10$$

Substituting from equation 3.10 into equation 3.9 we get:

$$i\ \frac{d\phi}{dt} = T\ \frac{d\theta}{dt} + \frac{d\ w_f}{dt} \qquad 3.11$$

Solving for T from equation 3.11 we get

$$T(\theta,\phi) = i\ \frac{d\phi}{d\theta} - \frac{d\ w_f}{d\theta} \qquad 3.12$$

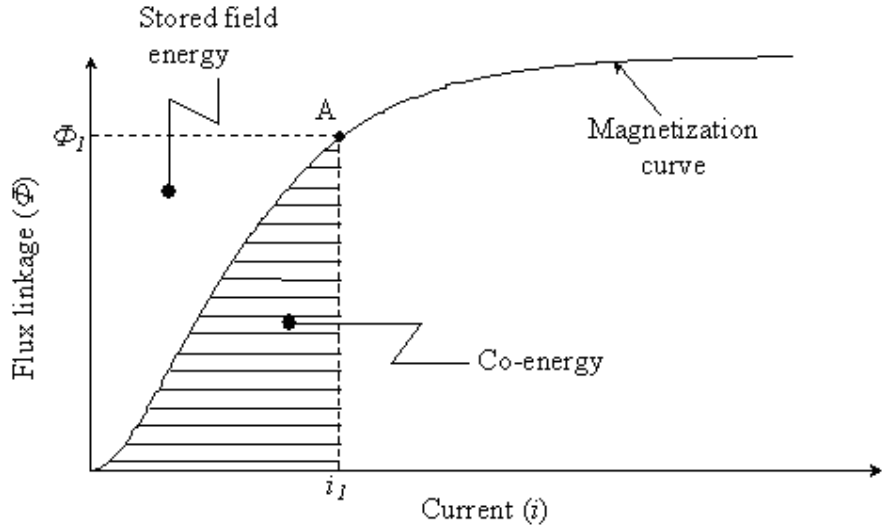

Figure 3.4 Magnetization Curve.

It is often desirable to express torque in terms of current rather than flux, hence appears the concept of co-energy, W_c instead of energy. To introduce the co-energy concept, consider the graphical interpretation of field

energy, Figure 3.4. Solving equation 3.11 for W_f at a constant shaft angle, gives:

$$w_f = \int_0^{\phi} i \, d\phi \qquad 3.13$$

This is represented by the area to the left of the curve of Figure 3.4. The co-energy for the same fixed angle, θ is given by:

$$w_c = \int_0^{i} \phi \, di \qquad 3.14$$

Which is represented by the area under the curve of Figure 3.4, it is shown from figure that the sum of the magnetic field energy and the co-energy for a fixed angle, θ is equal to the area of the rectangle which area is equal to (ϕ.i)

Hence we can write;

$$w_c + w_f = \phi \cdot i \qquad 3.15$$

Remember that we want to substitute W_f in equation 3.12 in order to express the torque in terms of current. Then from equation 3.15 we have:

$$d\,w_f = \phi \, di + i \, d\phi - d\,w_c \qquad 3.16$$

Substituting from equation 3.16 into equation 3.12 we get:

$$T(\theta,\phi) = \frac{i \, d\phi - (\phi \, di + i \, d\phi - d\,w_c)}{d\theta} \qquad 3.17$$

And

$$d\,w_c(\theta,i) = \frac{\partial w_c}{\partial \theta} d\theta + \frac{\partial w_c}{\partial i} di \qquad 3.18$$

For a constant current, from equation 3.17 the torque is simply given by

$$T = \frac{d\,w_c}{d\theta} \qquad 3.19$$

It is often assumed in SRM analysis that the motor remains magnetically unsaturated during operation, when this is assumed the relation between flux and current is given by:

$$\phi = L(\theta) \cdot i \qquad 3.20$$

Substituting from equation 3.20 into equation 3.14 we get

$$w_c = \frac{i^2}{2} L(\theta) \qquad 3.21$$

And from equation 3.19

$$T = \frac{i^2}{2} \frac{dL}{d\theta} \qquad 3.22$$

Also, substituting from equation 3.20 into equation 3.6 we get

$$v = i R_m + \frac{d[L(\theta) \cdot i]}{dt} = i R_m + L \frac{di}{dt} + i \frac{d\theta}{dt} \frac{dL}{d\theta} =$$

$$= i R_m + L \frac{di}{dt} + i\omega \frac{dL}{d\theta} \qquad 3.23$$

In equation 3.23, the three terms of the right hand side, and by analogy to a series DC machine, it represent the resistive voltage drop, the inductive voltage drop, and the induced EMF respectively. Hence, the induced EMF could be given as

$$e = i\omega \frac{dL}{d\theta} = i\omega K_b \qquad 3.24$$

Where K_b may be defined as the EMF constant similar to the DC series excited machine and is given here as $dL/d\theta$, which means that it depends on the rotor position and is obtained for a constant current at that position.
From the above derivation, the equivalent circuit of an SRM phase could be derived as shown in Figure 3.5.

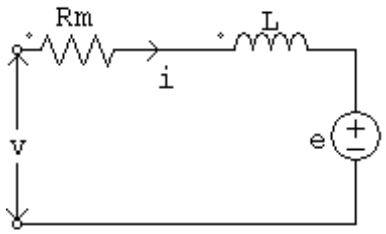

Figure 3.5 Single phase equivalent circuit of a SRM.

3.5 Static Characteristics of the SRM

The static characteristics of SRM include the flux linkage current curves, co-energy curves, and the static torque curves. In the following section, the experimental measurements of the parameters of the SRM is shown as stated in [48], which is the same parameters used in this case study.

3.5.1 Flux Linkage Current Curves

Flux linkage current curves represent the relationship between the phase flux linkage and phase current at different rotor positions. The two curves at the extreme aligned and unaligned rotor positions are considered experimentally, and the intermediate curves are obtained analytically.

3.5.1.1 Aligned rotor position

The flux linkage current curve at aligned rotor position is obtained experimentally as follows:

1- A certain phase of the motor is supplied by DC supply to ensure that the rotor is settled exactly at the aligned position. By measuring the current and DC supply, the phase resistance is obtained.
2- Then, the test is performed by exciting the same phase windings by a variable AC voltage. The current is measured at different voltage levels, and these data are used to obtain the flux linkage as a function of the excitation current.
3- If the phase current i_{ac} is measured at a certain voltage V_{ac}, then the phase impedance Z_{ph} is given by:

$$Z_{ph} = \frac{V_{ac}}{i_{ac}} \quad 3.25$$

And the phase reactance X_{ph} can be calculated from:

$$X_{ph} = \sqrt{Z_{ph}^{\ 2} - R^2} \quad 3.26$$

Where R is the phase resistance (is known from DC test).

4- The phase inductance is calculated by:

$$L = \frac{X_{ph}}{2\pi f} \quad 3.27$$

Where f is the frequency of AC supply (50 Hz.).

5- The flux linkage ϕ corresponding to the measured current is obtained by:

$$\phi = L \cdot i \quad 3.28$$

This procedure is repeated for different levels of excitation current to obtain the flux linkage as a function of that current.

3.5.1.2 Unaligned rotor position

The rotor must be fixed such that the poles of the excited phase are facing an inter-polar space of the rotor, since the rotor is at unaligned position. To achieve this position, two aligned positions are marked as shown in the previous test, for two different phases. The rotor is hold on mechanically in the midway between these two marked positions. At this position, one of these two phases is excited with AC voltage source, and the current is measured.

The flux linkage is obtained by using the same procedure discussed, from step 3 to step 5, for last subsection. There is no possibility for magnetic saturation at the unaligned position under normal operating condition. So, one value of flux is enough to get the slope of this characteristic, but for more accuracy more points are calculated.

Figure 3.6 shows the measured flux linkage current curves at both the two extreme aligned and unaligned rotor positions.

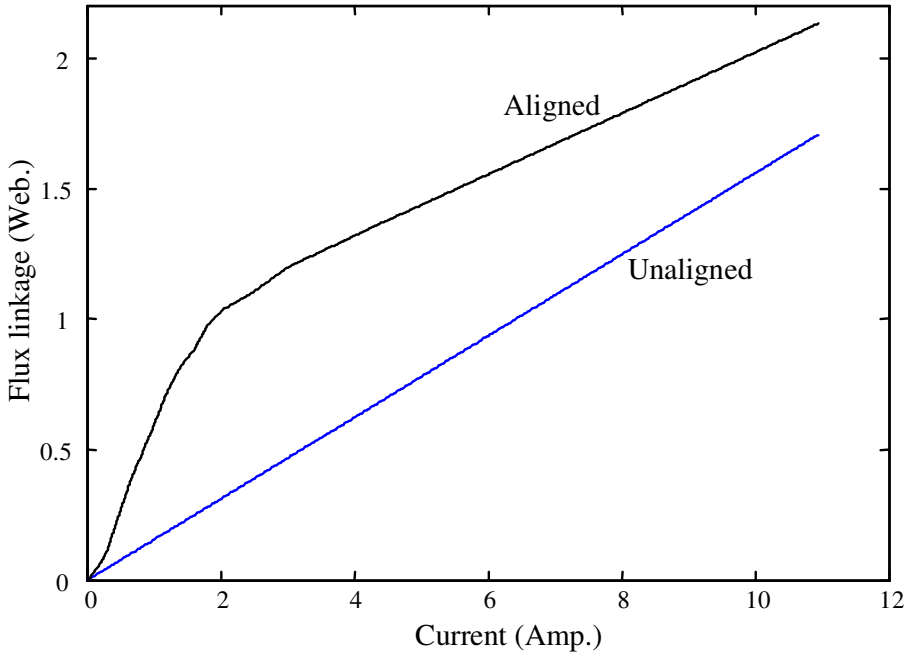

Figure 3.6 Measured flux linkage-current curves at aligned and unaligned positions.

3.5.1.3 Flux linkage current curves at intermediate rotor positions

As a complete view of flux current characteristics, the flux current curves at other intermediate rotor position angles must be obtained analytically after obtaining the measured flux linkage curves at both unaligned and aligned positions.

An analytical function that represents flux linkage characteristics over the entire half rotor pole pitch may be expressed as [49]:

$$\phi(i,\ \theta) = \sum_{n=0}^{N} \phi_n(i)\ \ Cos\ \ (nP_r\theta) \qquad 3.29$$

Where $\phi_n(i)$ are suitable expression depending only on the current variable, P_r is the number of rotor poles.

The first two terms in equation 3.29 are considered, because there are only two known available values for both aligned and unaligned rotor positions.

$$\phi(i,\ \theta) = \phi_0(i) + \phi_1(i)\ \ Cos\ \ (P_r\theta) \qquad 3.30$$

To find the values of $\phi_0(i)$ and $\phi_1(i)$ consider the following procedure:

By substituting in equation 3.30 assuming unaligned position ($\theta = \theta_u = 0$), also at aligned position ($\theta = \theta_{al} = 2\pi / P_r$). Then;

$$\phi_u(i) = \phi_0(i) + \phi_1(i) \quad 3.31$$

$$\phi_a(i) = \phi_0(i) - \phi_1(i) \quad 3.32$$

Solving the set of equations (3.31), and (3.32), then;

$$\phi_0(i) = \frac{1}{2}\ [\phi_u(i) + \phi_a(i)], \text{ and} \quad 3.33$$

$$\phi_1(i) = \frac{1}{2}\ [\phi_u(i) - \phi_a(i)] \quad 3.34$$

Where ϕ_u, and ϕ_a are the flux linkage at both unaligned and aligned positions.

By substituting equations 3.33, and equation 3.34 in equation 3.29, an expression for the flux linkage characteristics is obtained:

$$\phi\ (i,\ \theta) = L_u\ i + \frac{\phi_a(i) - L_u\ i}{2}\ [1 -\ Cos\ (P_r\theta)] \quad 3.35$$

By choosing a different values of θ (between $\theta = 0$, and $\theta = \pi / P_r$), the intermediate (ϕ, i) curves are obtained using equation 3.35. Usually choosing the step with equal spaces rotor position angles. In the current case, the intermediate flux linkage current curves obtained by spacing three mechanical degrees. The number of (ϕ, i) curves between aligned and unaligned positions are equal to fourteen curves as shown in Figure 3.7.

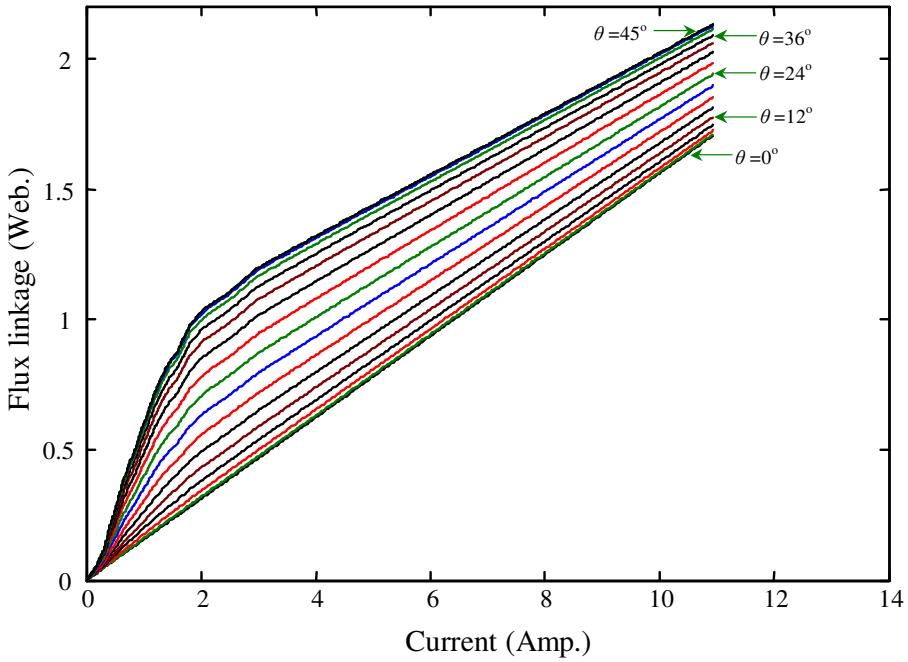

Figure 3.7 Flux linkage-current curves of 6/4 SRM.

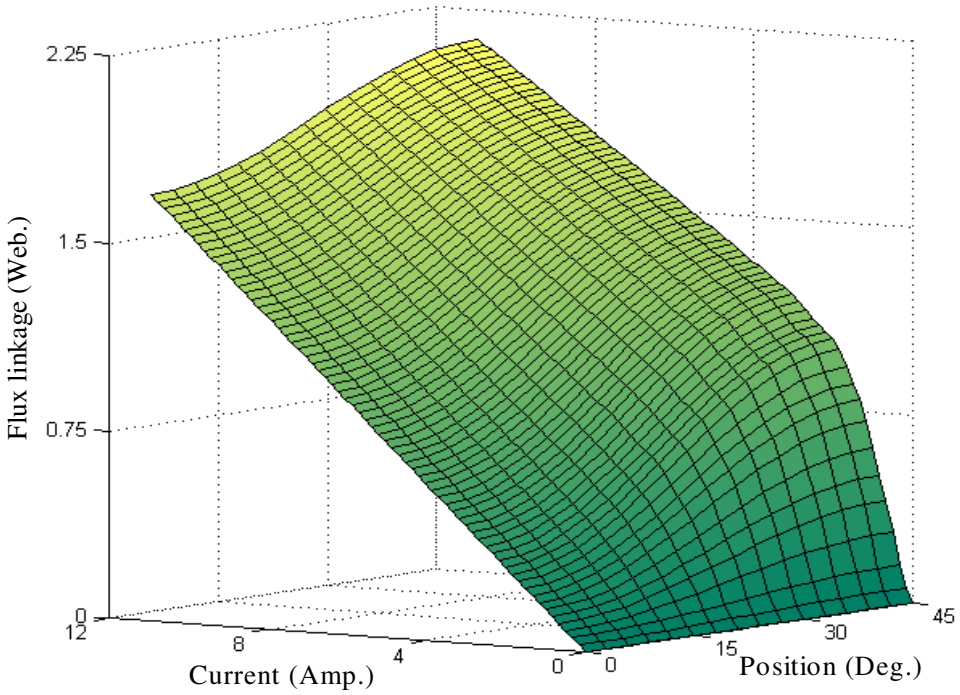

Figure 3.8 The three dimension of flux linkage, current, and position angle curves.

Thus, the flux linkage current data along half rotor pole pitch is completed, this data will be used to compute the co-energy curves, and it is reversed and stored in the form of $i(\theta, \phi)$ to be used later when solving the motor differential equations. Figure 3.8 illustrates the three dimensions of flux linkage, current, and rotor position curves.

Therefore, the vector of flux linkage can be obtained from the last estimated curves for any values of rotor position angle and stator current or by interpolation if it lies between any two closest curves as shown in Figure 3.8. The current values can be obtained form the corresponding values of both flux linkage and rotor position angle. Then, all data are stored in a look-up table matrix $i(\theta, \phi)$. In this matrix, the current values are arranged such that the flux linkage values represent the row index and rotor position angles represent the column index [48].

3.6 Torque-Speed Characteristics

The torque-speed operating point of the SRM is essentially programmable, and determined almost entirely by the control. This is one of the features that makes the SRM an attractive solution. The envelope of operating possibilities is limited by physical constraints such as the supply voltage and the allowable temperature rise of the motor under increasing load. In general this envelope is described by Figure 3.9 [2].

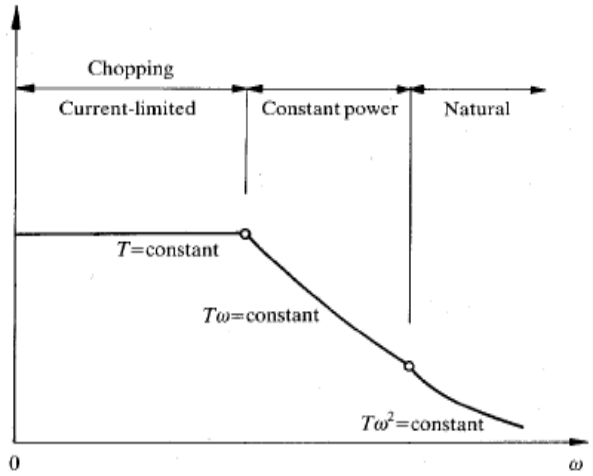

Figure 3.9 SRM Torque-Speed Characteristics.

Like other motors, torque is limited by the maximum allowed current, and speed is limited by the available bus voltage. With increasing shaft speed, a current limit region persists until the rotor reaches a speed where the back EMF of the motor is such that, given the DC bus voltage limitation we can get no more current in the winding, thus no more torque from the motor. At this point, called the base speed, and beyond, the shaft output power remains constant at its maximum. At higher speeds, the back EMF increases and the shaft output power begins to drop. This region is characterized by the product of torque and the square of speed remains constant [2].

3.7 Control Strategies of Switched Reluctance Motor Drives

There are different well known strategies of machine control depending on the application, these are, position, speed, current, and torque control. The switched reluctance machine is different from other types of DC and AC machines because of its poles saliency and nonlinearity. Further more, the current control strategy in SRM is different from torque control while these two are synonyms in DC drives.

The SRM produces discrete pulses of torque, and the proper design of the machine which allows overlapping inductance profile could make it possible to produce continuous torque. The developed torque is controlled by adjusting the magnitude of the phase current or by varying the dwell angle, which is recommended to be kept constant in order to reduce the torque ripples [1]. The control operation may be done using a position sensor feedback signal, or using sensor-less operation, by estimating the position from the magnetic characteristics of the machine [50-55].

In the following sections, a brief overview of the control principle of different schemes is presented.

3.7.1 Speed Control

The speed control scheme, Figure 3.10, consists of two loops, current loop and speed loop through which the speed error is processed and conditioned with the speed controller to obtain the current command signal, i^*, this current command is compared to the actual phase current feedback signal to generate the current error signal. This later is processed through the current controller to produce the command signal for the converter, v^*, and the switching of the phase is determined according to a predetermined window, Δi, of the hysteresis current controller. The currents are diverted into each phase according to its position information which maybe measured or estimated. In general, the speed control strategy consists of two actions, the first is to regulate the motor speed by adjusting the duty cycle of a PWM signal that activates the power converter, and the second action is to adjust the advanced firing angle as a function of the motor speed to improve motor efficiency and performance specially at high speeds [56].

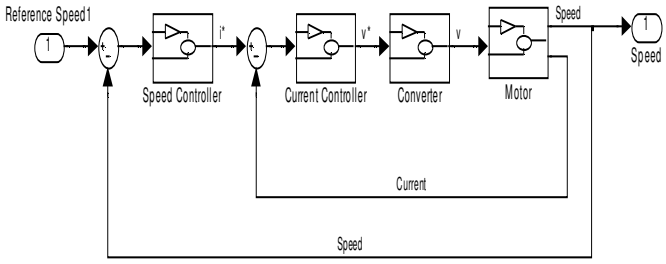

Figure 3.10 Speed Control Closed-loop Block Diagram.

3.7.2 Current Control

The SRM is operated either in current control or voltage control mode. The voltage control operation mode is cheaper in implementation but is not convenient for servo-type applications, in this case current control operation mode is essential [57].

The most significant parameter in the current control loop is the hysteresis band, which is desired to be as small as possible in order to reduce current ripples and to increase the bandwidth of the current loop, however the residual current ripple content, the high-variable switching frequency are the un-encouraging drawbacks of this approach [57].

3.7.3 Torque Control

Unlike DC and AC machines, the air-gap torque in the SRM has a nonlinear relationship with the excitation current which makes the control system more complex, since the torque is depending not only on the excitation current but on the rotor position as well. The method of torque control depends on the number of phases which are excited at the same instant, which severely affects the torque ripple content and consequently the speed ripples which in turn reduce the overall efficiency and performance of the drive system [1].

The designer of a SRM drive system has to aim at one of two conflicting concerns, maximizing the output torque, or maximizing the efficiency. The efficiency is maximized by minimizing the dwell (conduction) angle of the phase, while maximum torque is obtained when the dwell angle is maximized. In general, two strategies of dwell angle are followed, either constant or variable dwell angle, depending on the application. Different modes of SRM commutation are given in [40].

Although the switched reluctance machine has a strong similarity to the series excited DC and synchronous machines, it is different from these machines from the control point of view, more complications arise in the case of SRM due to the fact that the variable inductance of the motor is not only a function of the rotor position, but the phase excitation current as well, in contrast, for other machines, control strategies are based on the machine parameters being almost constant for the control range.

The control requirement could be classified to low performance and high performance categories based on torque ripples, and speed response specification.

The heart of any motor drive's control system is current control [1]. In most of the DC machine drives, torque control is synonymous with current control, but because of the nonlinearity of the SRM, this concept is significantly different.

3.8 Control Principle of SRM

Referring to Figure 3.11, the phase winding is switched ON during the positive gradient period of the inductance profile for motoring operation. The SRM produces discrete pulses of torque, and it could produce a continuous torque if proper design of overlapping inductance profile of different phases is achieved, on the other hand this overlap reduces the power density of the motor and complicates the control of the SRM drive [1].

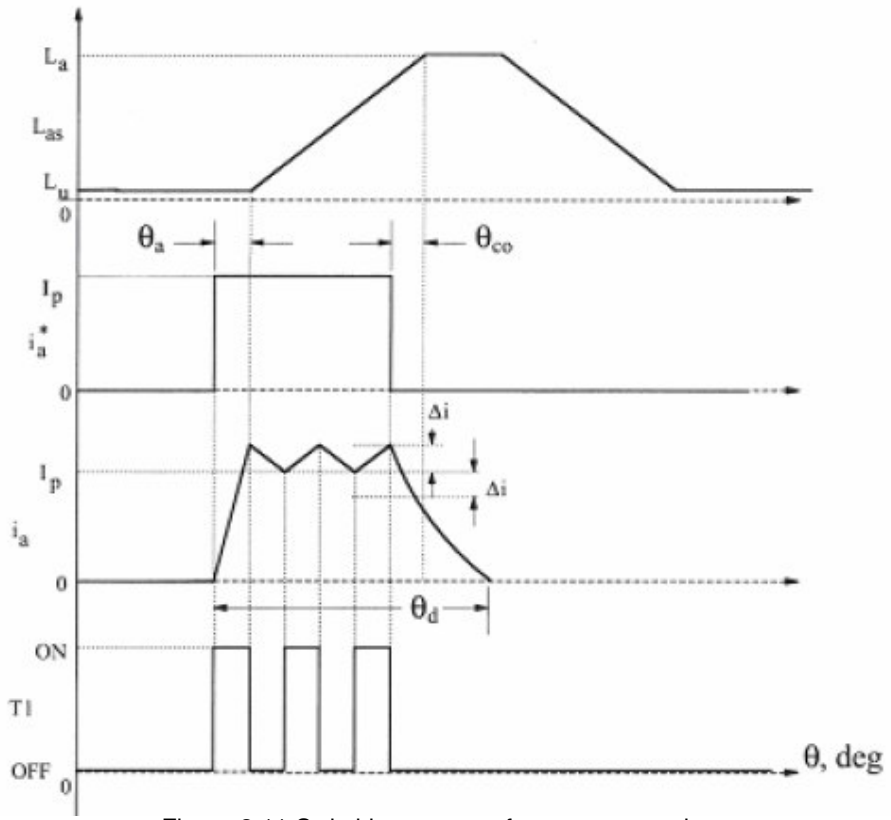

Figure 3.11 Switching strategy for motor operation.

The average torque is controlled by adjusting the magnitude of the phase current or by varying the dwell angle, θ_d. It is recommended, to reduce torque ripples, to keep the dwell angle constant and vary the magnitude of the phase current, which requires a current controller to be within the drive circuit of the motor adding a safe operation feature to this approach.

It is essential to divert the current into the winding at the instant of increasing inductance to ensure instantaneous torque production, but due to the fact that the current can't rise or fall instantaneously in an RL circuit, the voltage has to be applied with a certain advance angle, θ_a , Figure 3.11, and for the same reason current has to be commutated at a certain advance commutation angle θ_{co} in order to bring the current to zero before the negative gradient of the inductance profile is reached so that no negative torque may be produced. These two advance angles are function of the magnitude of the phase current and the speed of the rotor.

Figure 3.12 shows typical current waveforms for various advance angles and dwell angles [1].

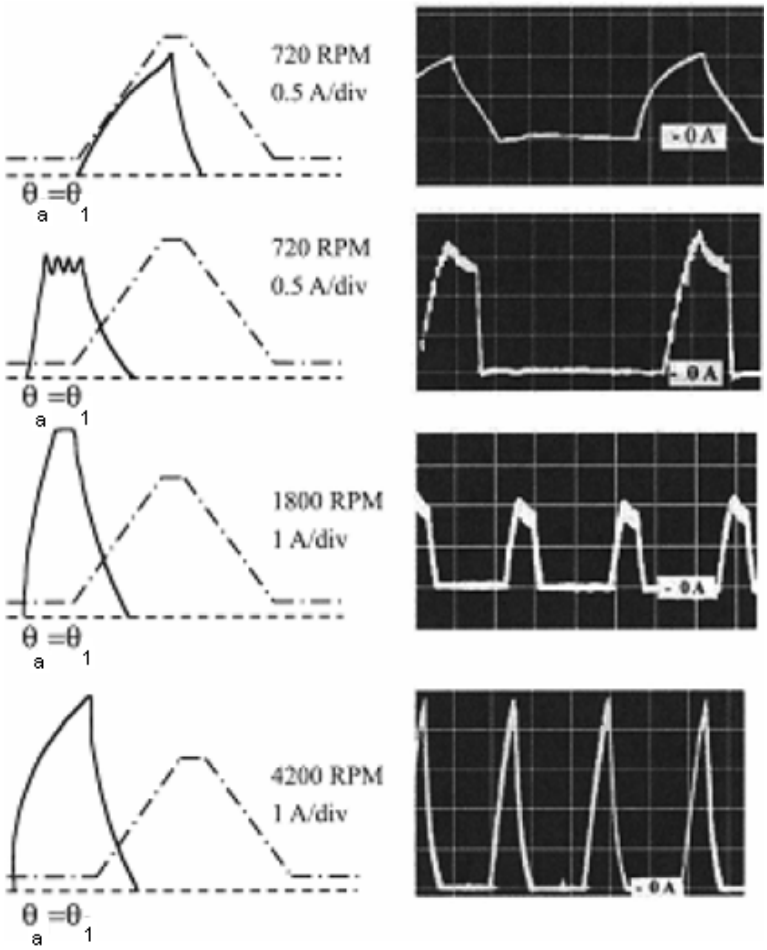

Figure 3.12 Typical current waveforms for various advance and dwell angles.

The shaft position feedback information is essential in all control strategies for generating switching commands for the power converter for the position feedback loop, and for the speed feedback loop which can be derived from the position data. There are several types of position sensors commonly used which are;

- Photo-transistors and photo-diodes.
- Hall effect elements.
- Pulse encoders.
- Variable Differential Transformers.

In the current control technique, the magnitude of the current flowing into windings is controlled using a control loop with a current feedback. The current in a motor phase winding is directly measured with a current/voltage

converter or a current sense resistor connected in series with the phase and compared with the desired value forming an error signal. This error is compensated via a control scheme such as PID and an appropriate control action is taken [47].

This method has the disadvantage that even if the phase current is maintained constant, the torque produced is not smooth not only because of control strategy and phase commutation but also because of the nonlinear relationship between torque and current. The torque ripples are undesirable because it contribute to the problem of audible noise, vibrations, and also introduce torque disturbances which manifest as velocity errors.

A solution to the problem of torque ripple is to profile the current such that torque is the controlled variable (torque control). Since torque can't be sensed directly, this can only be done using a prior information about the motor's torque-current-angle characteristics. The torque control strategy is based on following a contour for each phase of the SRM such that the sum of torque produced by each phase is constant and equal to desired torque, this desired total torque is calculated from the speed loop and is split into desired phase torque via shaping function [47].

In the following chapter, a new technique utilising the switched capacitance circuit to profile the phase current is discussed in details.

3.9 Sensor-less Operation of SRM Drives

Sensor-less operation of the SRM is desirable because of compactness in weight and volume, also lower cost is achieved due to the elimination of the mechanical assembly and mounting of the rotor position sensors. The driving factor behind sensor-less operation of any machine drive system including that of the SRM is the quest for low cost with high performance drive. Three broad classes of rotor position estimation have been emerged in research, these are the observer based scheme, the incremental inductance based measurement using current magnitude or fall and rise time and finally the inductance based estimation. A brief description of each of the previous techniques is given in the following sections [1].

3.9.1 Incremental Inductance Measurement [1]

This method uses the fact that the current rise and fall times are proportional to the incremental inductance, and under certain assumptions the rise and fall times reflect the incremental inductance and hence the rotor position itself. The only advantage of this method is that it only needs to measure the current and its rise and fall times to predict the rotor position and can use the active phase itself while it has many disadvantages.

3.9.2 Observer based rotor position estimation [1]

This technique depends on the real time solution of the SRM system equations which gives estimates of the current, speed and rotor position. To obtain this, it is required to know the rotor speed dynamics obtained through the electromechanical equation coupling the air gap torque to the mechanical system with rotor inertia and friction constants. For estimation, the machine model incorporating the error variables with their gain adjustment feature constitutes what is known as an observer.

3.9.3 Inductance Sensing

As the direct rotor position sensors don't provide any information about electrical characteristics of the motor because they are insensitive to inductance profile variation with rotor angle, and as the torque production is actually dependent on the rate of change of co-energy with rotor position, it appears that a desired instantaneous torque can be obtained from instantaneous inductance information rather than rotor position [47]. Since there is at least one idle phase in a SRM, the inductance of that phase can be sensed for the purpose of commutation control. The inductance can be estimated from the measurements of the motor terminal voltages and currents.

3.9.3.1 Phase Pulsing

A voltage pulse V is applied to an un-energized phase by the drive converter for a period of time ΔT and the change in coil current ΔI is measured. The inductance is obtained from:

$$L = \frac{\Delta T}{\Delta I} \quad 3.36$$

3.9.3.2 Frequency Modulation

Inductance information is encoded in a frequency modulated signal using a low voltage analogue circuit.

3.9.3.3 Phase Modulation

A low alternating voltage is applied to an un-energized phase and the phase angle difference between the input voltage and the resulting current is detected, the inductance is given by:

$$L = \frac{R \tan \varphi}{\omega} \quad 3.37$$

Where, φ is the phase angle.

3.9.3.4 Amplitude Modulation

A low level alternating voltage is applied to an un-energized phase and the amplitude of the resulting current is mapped to the coil inductance. The inductance can be expressed as:

$$L = \frac{1}{\omega} \sqrt{\frac{V_m^2}{I_m^2} - R^2} \quad 3.38$$

Where, V_m is the amplitude of the input alternating voltage, I_m is the current amplitude, and R is the resistance in the circuit.

3.9.3.5 Self-Voltage Technique

The inductance of the active phase is estimated in real time from measurements of the active phase current and phase flux. If I_{ph} is the current in the active phase linking a flux ϕ_{ph} then the phase inductance is given by:

$$L_{ph} = \frac{\phi_{ph}}{I_{ph}} \qquad 3.39$$

3.9.3.6 Artificial-Intelligence-based inductance estimation [58]

Most of the difficulty in understanding the operation and design of the switched reluctance machine drives originates from the fact that the switched reluctance machine is a doubly-salient, highly nonlinear machine. This makes it an ideal candidate to incorporate artificial intelligence in a switched reluctance machine drive.

Recently, extensive research work has been conducted in the field of sensor-less operation of switched reluctance machines utilising artificial-intelligence-based inductance estimation, artificial-intelligence-based position estimation and artificial-intelligence-based electromagnetic torque estimation as well as using artificial intelligence techniques for machine design and control. A brief illustration of some artificial-intelligence-based techniques is presented in the following sections.

As discussed earlier, the switched reluctance machine has a phase inductance which is a nonlinear function of the stator phase current and the rotor position. It is possible to use a fuzzy-logic-based estimator to estimate the phase inductance of the SRM. The inputs to this fuzzy estimator are the stator phase current and the rotor position while the output is the phase inductance. The universe of discourse for the two input variables is divided into an appropriate number of fuzzy sets for the stator current and an appropriate number of fuzzy sets for rotor position. In the fuzzification stage, the corresponding membership function values are obtained respectively. For this purpose, 7 triangular membership functions are used for the rotor

position, where the corresponding fuzzy sets are B_1 to B_7, shown in Figure 3.13 and 9 triangular membership functions for the stator current, where the corresponding fuzzy sets of which are A_1 to A_9. The universe of discourse for the output variable which is the phase inductance in this case is divided into 11 fuzzy sets, C_1 to C_{11} in Figure 3.13, in which, C_1 is used for the smallest inductance value which physically corresponds to zero rotor position and smallest stator current, while for the largest inductance value C_{11} is used.

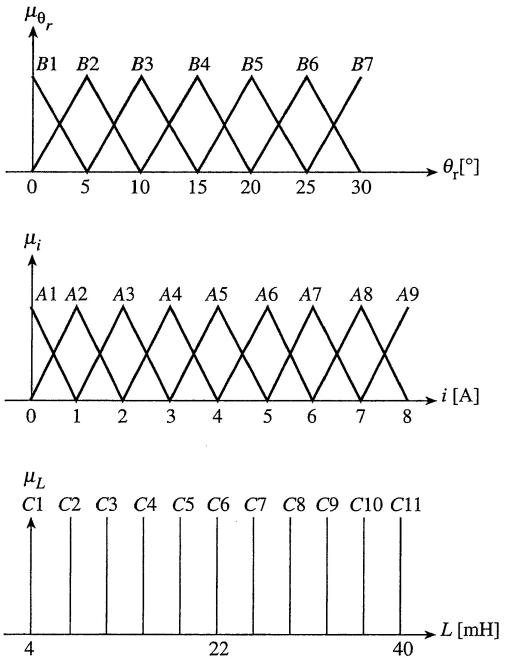

Figure 3.13 Input and output membership functions for fuzzy inductance estimation.

The phase inductance is determined by using the appropriate If-Then rules of the fuzzy-logic estimator which in general take the form “if i is A and θ_r is B then L is C”, where i, θ_r and L are the stator phase current, the rotor position and the phase inductance respectively.

The fuzzy output is computed by using the sup-min method, while the crisp output can be calculated in the defuzzification stage by using the height defuzzification technique described in [58], the crisp output in this case is the actual phase inductance.

Figure 3.14 shows an example of the estimated phase inductance being compared with the experimentally obtained one.[58]

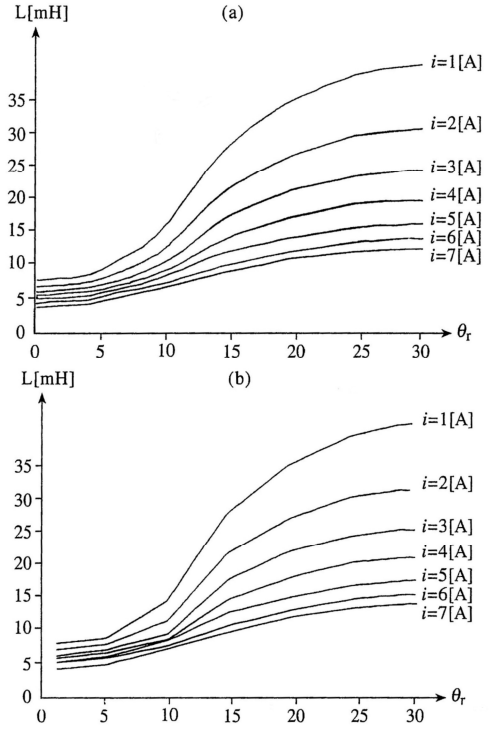

Figure 3.14 Phase inductance, (a) Experimentally obtained. (b) fuzzy-logic-based.

3.9.3.7 Artificial-Intelligence-based position estimation

Besides the conventional techniques used to estimate the rotor position in a switched reluctance machine, the universal function AI-based position estimators are ideal candidates in position-sensor-less SRM drives.

Figure 3.15 shows an ANN-based position estimator where it is assumed that the flux linkage-current characteristics of the switched reluctance machine are known and the ANN is used as a nonlinear function approximator of these characteristics.

The ANN can be a multilayer feed-forward neural network and the training can be based on back-propagation. [58]

The input to train the ANN are the input data pairs of the flux linkage, ϕ_s and the stator current, i_s while the corresponding output is the rotor position, θ_r.

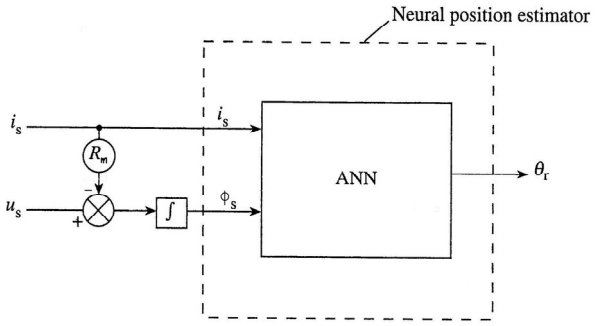

Figure 3.15 ANN-based position estimator.

However, to decide which side of the alignment the rotor is, angles from more than one phase has to be estimated. In the shown system of Figure 3.15, the stator voltage, u_s and the stator current, i_s are measured, and the flux linkage, ϕ_s is calculated from the measured values of u_s and i_s by integration. In this technique, errors are expected to occur which leads to an inaccurate estimation of the rotor position especially near the two extreme positions, the aligned and the unaligned position.

It is possible to have more accurate ANN-based position estimator where the role of the neural position estimator is not to approximate the static characteristics, but its role is to approximate the relationship between the output quantity which is the rotor position and the inputs which are the stator current and the stator flux under real operating conditions. In this case, an initial test stage where the motor is run under its real operating conditions and the input and output data are measured and used to train the ANN, a position sensor is needed only during this training data collection stage.

It is also possible to have another ANN-based position estimator scheme where the ANN directly estimates the position by using the monitored stator voltage and current. The training of this ANN can be used on data which is obtained in an initial test phase where apposition sensor is needed as well. Also, a fuzzy-neural estimator of Mamdani or Sugeno type can be used to replace the ANN to eliminate the problem of finding the number of hidden layers and hidden neurons.

Another system which uses an adaptive network fuzzy inference system (ANFIS) to estimate the rotor position was illustrated in [10] to estimate the rotor position of a 6/4 switched reluctance motor. This system which is shown in Figure 3.16 uses a first order Sugeno-style fuzzy system with two inputs, which are the flux linkage and the stator currents, and one output, which is the rotor position.

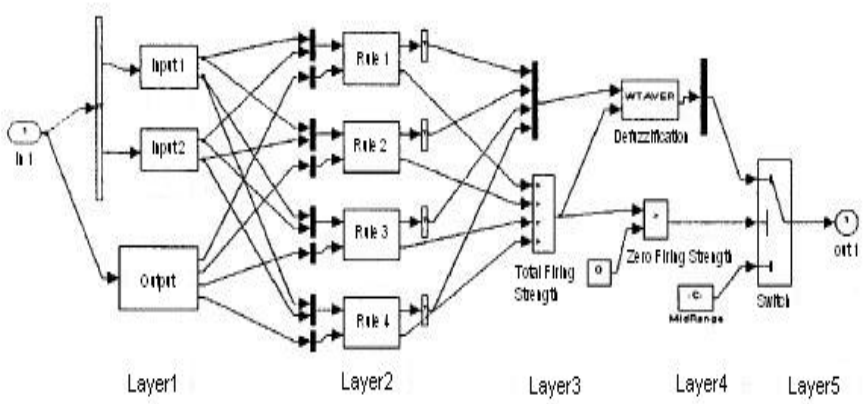

Figure 3.16 ANFIS structure for 2 inputs and 1 output.

An indirect method for rotor position estimation both at standstill and during running conditions has been presented in [10] by applying a reduced voltage to the stator phase windings for a short duration, the initial rotor position is accurately predicted, which ensures the starting of SRM at any initial rotor position without starting hesitation and also in the desired direction of rotation. The proposed method gave an accurate estimation of the rotor position with an error less than 0.1% for low current while the error was less than 0.5% for high current. This position estimation algorithm with the shown error percentages, ensures a sensor-less high performance and reliable SRM drive operation.

3.9.3.8 Artificial-Intelligence-based electromagnetic torque estimation

AI-based techniques could be used to estimate the electromagnetic torque in a switched reluctance machine drive, for this purpose, neural or fuzzy-neural networks can be used. [58]

The electromagnetic torque produced by a switched reluctance machine is a function of the rotor position and the stator flux linkage which in turn is a nonlinear function of the stator current. This is why it is difficult to implement a mathematical-model-based estimator of the electromagnetic torque, for this purpose an AI-based estimator could be used, where the inputs to this network can be the stator current and the rotor position.

To increase the robustness of the estimator, extra inputs can also be used such as, the turn-off angle and the stator current limit. Suggestion of the type and structure of such a network is given in [58].

Another ANFIS model is presented in [59] where an indirect method to measure the static flux linkage was used and then the co-energy method (via the principle of virtual displacement) was used to calculate the torque characteristics from data on flux linkage versus current and rotor position. A hybrid learning algorithm, which combines the back propagation algorithm and the linear least-squares estimation algorithm, identifies the parameters of the ANFIS. After training, the ANFIS flux linkage model and ANFIS torque model become in agreement with experimental flux linkage measurements and the calculated torque data. In the same research, an ANFIS current model and an ANFIS torque model were used to study SRM dynamic performance. The structure of the ANFIS and the ANFIS models for the estimation of flux linkage and torque are shown in Figure 3.17 and Figure 3.18 respectively.

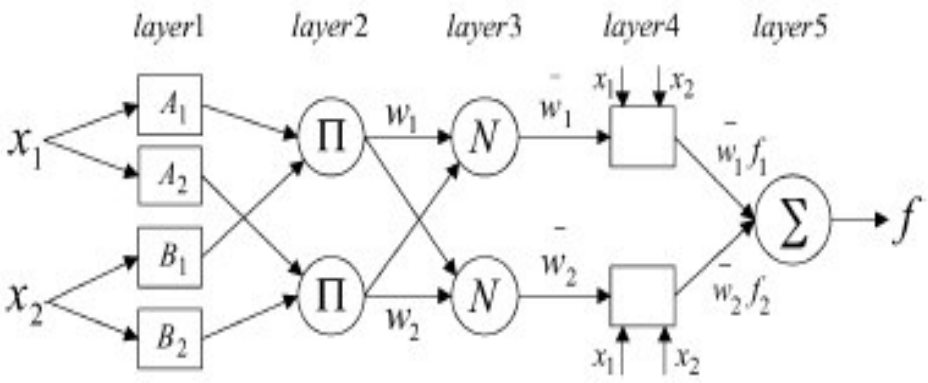

Figure 3.17 Structure of the ANFIS.

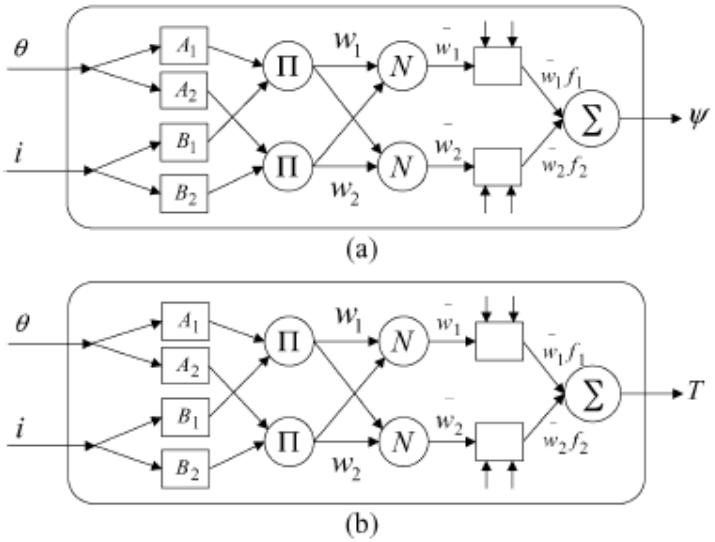

Figure 3.18 ANFIS models

(a) for calculating flux linkage (b) for calculating torque.

3.9.3.9 Artificial-Intelligence-based SRM design

The AI-based technique can be used to obtain the geometric parameters of a switched reluctance motor to meet a certain operating condition such as minimizing the torque oscillations at low-speeds.

An ANN is presented for this purpose which is a multilayer feed forward, back-propagation ANN, whose inputs are the geometrical parameters, the magneto-motive force and the rotor position, while its output is force.

The torque ripples in a switched reluctance motor can be minimised either by designing the motor with an optimum geometry or by shaping the stator current profile. It is useful, even if the stator current is shaped, it is useful to design the doubly salient geometry that minimizes the torque ripples. In Figure 3.19, an ANN-based force estimator is shown, the input layer of this ANN has 5 neurons and the five inputs are the three geometrical parameters (where Λ is the tooth pitch, δ is the air gap width, t_s is the stator tooth width and t_r is the rotor tooth width) and the other two inputs are the normalised rotor position, $\theta_{rn}=\theta_r/\Lambda$ and the magneto-motive force, F.

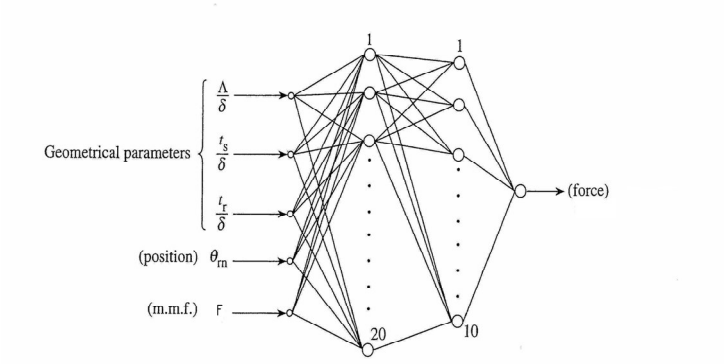

Figure 3.19 ANN-based force estimator.

The number of nodes in the hidden layers is found by trial and error. More details of the AI-based control of the switched reluctance machine is given in [58].

Another AI-based system is presented in [60], where a Genetic-Fuzzy Algorithm (GFA) is used to optimise the design parameters of a 8/6 four phase switched reluctance machine with two objective functions, the efficiency and the torque ripples.

Figure 3.20 shows a flow chart of that algorithm while Table 3-1 shows a comparison between the different design parameters and objective functions obtained by the initial design, the fuzzy method and the GFA method. Where, the shown parameters in the table represent; the stator pole-arc, the rotor pole-arc, the rotor tooth-height, the rotor internal radius, the stator tooth height, the stator steel thickness, the stator external diameter, the rotor external diameter, the number of turns per stator-phase, the efficiency and the torque ripple percentage respectively.

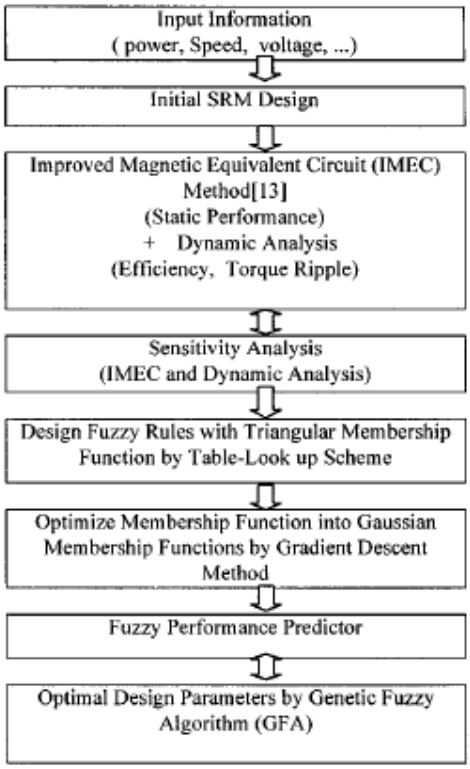

Figure 3.20 Optimal design of SRM by GFA.

Table 3-1 Comparison of design parameters and objective functions.[60]

Parameter	β_s°	β_r°	h_r (mm)	y_r (mm)	h_s (mm)	y_s (mm)	D_s (mm)	D_r (mm)	N_{ph}	η%	TR%
Initial	21	23	19.4	12.9	25.8	17.4	183.5	96.5	28	92.7	28.44
Fuzzy	20	23	19.3	15	23	15	176.9	100.3	28	92.1	15.4
GFA	20.3	23.7	19.2	14.6	20.5	14.7	170.3	99.3	26	93.1	10.4

The results as stated in [60] have shown an increase of 0.4% in the efficiency and a reduction of about 18% in the torque ripples compared with the initial design parameters.

The use of artificial intelligence have become familiar in the field of electrical machine drives in general and in particular in the field of switched reluctance machine drives as it is a very useful tool in the rotor position estimation which allows sensor-less operation of the switched reluctance machine, besides using it as has been shown in previous sections in

inductance estimation, torque estimation and the geometrical design of the motor.

As a matter of fact, the artificial intelligence is very useful to implement the designed system in this research as it will help to estimate the accurate values of the phase inductance at each switching instant of the switching-capacitance, as it is very critical in this case study to find the accurate value of inductance to resonate with the switched capacitance, as well as calculating the duty cycle, also the artificial intelligence techniques will be of great help with synchronising the switching instants of the main switches of the phase with the switches of the switched-capacitance circuit that is besides the improvement in the overall design and performance of the machine drive system as shown above.

Chapter 4

Switched Capacitance circuit applied to an SRM Driver topology

4.1 Proposed technique to profile the phase current

The idea of this technique aims at producing a current profile which is close to the ideal current waveform (ideally a square pulse) during the torque production period, which means, a current waveform with fast rising time, ideally zero, a flat top to produce maximum torque, a fast fall time, ideally zero. The ideal case is not achievable in practice, but the more close to ideal, the higher overall efficiency and power to weight capacity we get.

In the conventional converter systems utilized with SRM, switching on the current is done at a certain advance angle in order to allow the current to build up before the phase inductance reaches the positive gradient region, which leads to excessive conduction losses with zero torque production for a considerable period. Similarly, switching off the current is done at a certain advance angle in order to avoid the negative gradient region of the inductance, which leads to considerable reduction of the developed torque, hence the importance of profiling the current in the previous way is appreciated.

4.2 Switched capacitance circuit

There are a considerable variety of switched capacitance circuits depending on the number of capacitors and the number of switches utilized. Only two types of switched capacitance circuits will be considered here, these are the single capacitance double switch, SCDS and the double capacitance double switch, DCDS circuits for efficiency and size considerations of the drive circuit, as using a DCDS circuit with a 3-phase motor for example, means adding 6 capacitors and six semiconductor

switches to the drive circuit, which means, increased volume and weight and more switching losses.

4.2.1 Single Capacitance, Double Switch (SCDS) Circuit

A schematic diagram of a single capacitor double switch circuit is shown in Figure 4.1. The circuit consists of a capacitor, C and two semiconductor switches, S_1 and S_2 connected as shown.

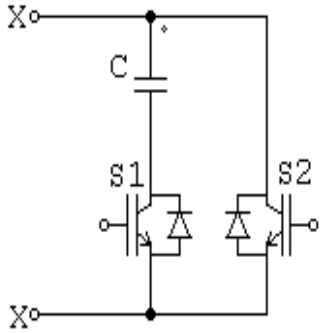

Figure 4.1 Single Capacitance Double Switch Circuit.

The switches S_1 and S_2 are switched ON and OFF alternately, i.e. if S_1 is ON, S_2 is OFF and vice versa. The effective capacitance, C_{eff} is the capacitance measured from terminals XX, which will be proven to vary with varying the duty cycle of the switching element resulting in a variable capacitance within the range between C and infinity for duty cycles of 1 and zero respectively.

To deduce the mathematical equations which describe the circuit operation, a current limiter should be connected to the circuit to limit the transient current value through the switches, this current limiter is an inductor and a small resistor connected in series with the switching capacitance circuit, as shown in Figure 4.2, the only difference which should be made when applying this circuit to an SRM motor phase, is to replace the fixed inductor with a variable inductor which varies as a function of the rotor position.

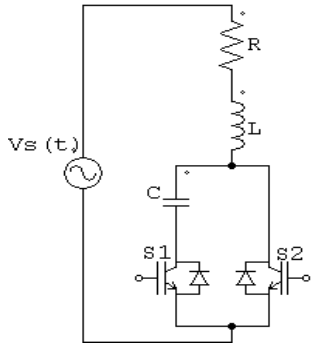

Figure 4.2 Switched capacitance circuit with a current limiter.

The circuit shown in Figure 4.2 has two branches connected alternately to the supply, the first branch contains L, R and C connected in series when S_1 is ON, and the second branch contains L and R connected in series when S_2 is ON.

The voltage equations of these two branches are as follows, depending on the duty cycle, D of the switching element, S_1:

At D=0;

$$v_s(t) = i(t)\ R + L\ \frac{di}{dt} \qquad 4.1$$

At D=1;

$$v_s(t) = i(t)\ R + L\ \frac{di}{dt} + v_c(t) \qquad 4.2$$

And the instantaneous current, i(t) is given by:

$$i(t)_) = c\ \frac{d\ v_c(t)}{dt} \qquad 4.3$$

If the supply voltage is given by;

$$v_s(t) = V_m \cos(\ \omega t + \psi\ ) \qquad 4.4$$

The instantaneous value of the current for each case is found to be:

For D=0;

$$i_1(t) = I_{1m} \cos(\ \omega t - \varphi_1\ ) \qquad 4.5$$

Where;

$$\varphi_1 = \tan^{-1} \frac{\omega L}{R} \qquad 4.6$$

And

$$I_{1m} = \frac{V_m}{\sqrt{R^2 + (\omega L)^2}} \quad 4.7$$

For D=1;

$$i_2(t) = I_{2m}\cos(\omega t - \varphi_2) \quad 4.8$$

Where;

$$\varphi_2 = \tan^{-1}\frac{(\omega L - \frac{1}{\omega c})}{R} \quad 4.9$$

And

$$I_{2m} = \frac{V_m}{\sqrt{R^2 + (\omega L - \frac{1}{\omega c})^2}} \quad 4.10$$

The steady state capacitor voltage, V_c will be given by equation 4.11

$$V_c(t) = \frac{I_{2m}}{\omega c}\sin(\omega t - \varphi) \quad 4.11$$

if we adjust R so that R << ωL and R<< $\frac{1}{\omega c}$, the phase angles φ_1 and φ_2 will be $\pm(\pi/2)$.

4.2.1.1 The Switching Function

Switching function is defined as the closing and opening interval pattern of switching by considering equal to 1 whenever the switch is ON and zero whenever the switch is OFF.

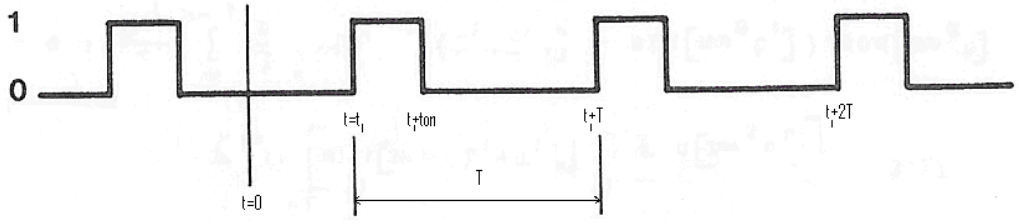

Figure 4.3 Switching Function.

The switching function takes the form of a train of pulses of a unity amplitude, Figure 4.3. The complexity of the generation of this train of pulses arises due to the fact that it has to be pulse width modulated in a pattern that controls the value of the equivalent capacitance between points XX, Figure 4.1. In the following is the derivation of the relation between the duty cycle of switch S_1, and the effective capacitance between XX.

Let the switching frequency be f_s, which means a period, T and an angular frequency ω_s, where;

$$T = \frac{1}{f_s} \qquad 4.12$$

And

$$\omega_s = 2\pi f_s \qquad 4.13$$

The angular duration of the unit-value period is 2πD rad, where D is the duty cycle, and the boundaries of the unit value period with respect to the time zero are 0 and 2πD rad.

From above the switching function can be expressed as:

$$f(t) = \sum_{n=1}^{\infty} A_n \cos(n\omega_s t) + B_n \sin(n\omega_s t) \qquad 4.14$$

Calculating for the coefficients of Fourier expansion, we get:

$$A_0 = \frac{1}{T}\int_{t_1}^{t_1+t_{on}} f(t)\,dt = \frac{t_{on}}{T} = D \qquad 4.15$$

$$A_n = \frac{2}{T}\int_{t_1}^{t_1+t_{on}} f(t)\cos(n\omega_s t)\,dt =$$

$$= \frac{2}{nT\omega_s}\left(\sin\left[n\omega_s(t_1+t_{on})\right] - \sin\left[n\omega_s t_1\right]\right) \qquad 4.16$$

$$B_n = \frac{2}{T}\int_{t_1}^{t_1+t_{on}} f(t)\sin(n\omega_s t)\,dt =$$

$$= -\frac{2}{nT\omega_s}\left(\cos\left[n\omega_s(t_1+t_{on})\right] - \cos\left[n\omega_s t_1\right]\right) \qquad 4.17$$

Substituting from equations 4.15, 4.16 and 4.17 into equation 4.14, we get:

$$f(t) = D + \frac{2}{T\,\omega_s}\sum_{n=1}^{\infty}\frac{1}{n}\{(\sin[n\,\omega_s(t_1+t_{on})]] - \sin[n\,\omega_s t_1])\cdot\cos[n\,\omega_s t - (\cos[n\,\omega_s(t_1+t_{on})] - \cos[n\,\omega_s t_1])\cdot\sin[n\,\omega_s t]\} \quad 4.18$$

For simplification, the switching instant is selected to be $t_1=-(t_{on}/2)$ which will reduce equation 4.18 to:

$$f(t) = D + \sum_{n=1}^{\infty}\frac{4\sin\left[\frac{n\,\omega_s t_{on}}{2}\right]}{nT\,\omega_s}\cdot\cos[n\,\omega_s t] \quad 4.19$$

And by substituting $\omega_s=2\pi/T$ into equation 4.19, we get

$$f(t) = D + \sum_{n=1}^{\infty}\frac{2\sin(nD\,\pi)}{n\,\pi}\cdot\cos(n\,\omega_s t) \quad 4.20$$

In the preceding calculation, $f(t)$ is the switching function of switch S_1, and the switching function of switch S_2 will be the complement function of it, hence

$$f'(t) = 1 - D - \sum_{n=1}^{\infty}\frac{2\sin(nD\,\pi)}{n\,\pi}\cdot\cos(n\,\omega_s t) \quad 4.21$$

The voltage across points XX, Figure 4.1, is given by:

$$v_{XX} = f(t)\cdot v_c(t) \quad 4.22$$

Where;

$$v_c(t) = \frac{1}{c}\int_0^t f(t)\cdot i(t)\,dt \quad 4.23$$

The voltage across the inductor,
Figure 4.2, is given by:

$$v_L(t) = L\frac{d}{dt}[f(t)\cdot i(t)] + L\frac{d}{dt}[f'(t)\cdot i(t)] =$$

$$= L\frac{d}{dt}[f(t)\cdot i(t) + f'(t)\cdot i(t)] \quad 4.24$$

Substituting $f(t)+f'(t)=1$, then:

$$v_L(t) = L \frac{d}{dt} \cdot i(t) \quad 4.25$$

Similarly the voltage across the resistor is given by:

$$v_R(t) = R \cdot i(t) \quad 4.26$$

Hence we can rewrite the voltage equation of the circuit,
Figure 4.2 as follows:

$$v_s(t) = R \cdot i(t) + L \frac{d}{dt} i(t) + \frac{1}{c} f(t) \int_0^t f(t) \cdot i(t)\, dt \quad 4.27$$

If the value of R is selected so that R << X_c and R<<X_L, then the resistive term in equation 4.27 could be neglected, therefore it could be rewritten as:

$$v_s(t) = L \frac{d}{dt} i(t) + \frac{1}{c} f(t) \int_0^t f(t) \cdot i(t)\, dt \quad 4.28$$

According to [61], if the switching frequency is high ($m \geq 10$), the above equation could be simplified for only the fundamental components to:

$$v_s(t) = [D^2 X_c - X_L] \cdot i(t) \quad 4.29$$

Where X_c and X_L are calculated at the supply frequency.
The peak value of the voltage v_{xx} is given in terms of total branch reactance by:

$$\hat{v}_{XX} = D^2 X_c \hat{I} \quad 4.30$$

And the effective capacitive reactance is given by:

$$X_{C_{eff}} = \frac{\hat{v}_{XX}}{\hat{I}} \quad 4.31$$

Substituting from equation 4.31 into equation 4.30 we get:

$$X_{C_{eff}} = D^2 X_c \quad 4.32$$

Hence;

$$c_{eff} = \frac{c}{D^2} \quad 4.33$$

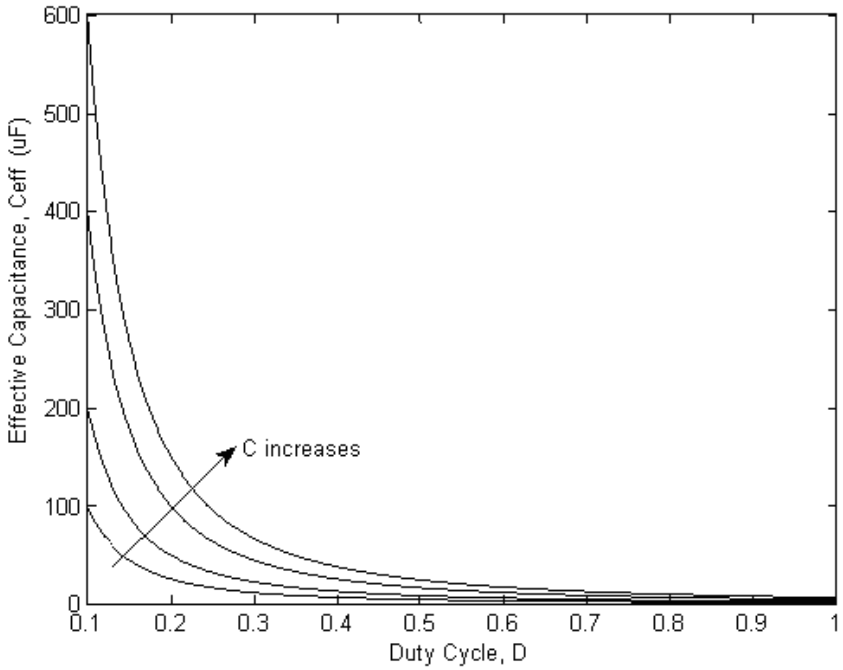

Figure 4.4 Relation between D and C_{eff} for SCDS circuit.

It is clear from the above discussion that this circuit could be used as a variable capacitor, depending on the duty cycle, starting with the value of the fixed capacitor at D=1, and increasing gradually with the reduction of D in an exponential proportion, Figure 4.4.

4.2.2 Double Capacitance, Double Switch (DCDS) Circuit

Another topology of the switched capacitance circuit, is the Double capacitance Double Switch circuit, Figure 4.5. In this topology, there are two branches of a fixed capacitor in series with a semiconductor switch in each branch.

The principle of operation of the DCDS circuit is the same as that of the SCDS one, hence the derivation of the relation between the duty cycle and the effective capacitance between A and B is similar, with the difference that it might be referred to either of the two branches C_1 or C_2.

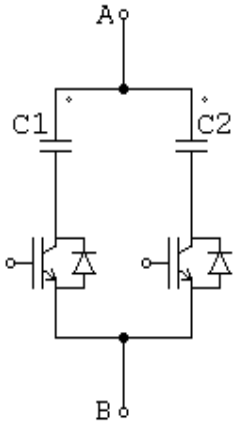

Figure 4.5 Double Capacitance Double Switch Circuit.

Using the same approach which has been used in the SCDS case, and applying it to Figure 4.6, we can write the voltage equations as stated in equation 4.34.

Referring to branch C_2, and at D=0, voltage equation is given by

$$v_s(t) = i(t)\ R + L\ \frac{di}{dt} + v_{c1}(t) \qquad 4.34$$

While at D=1, the voltage is given by equation 4.35

$$v_s(t) = i(t)\ R + L\ \frac{di}{dt} + v_{c2}(t) \qquad 4.35$$

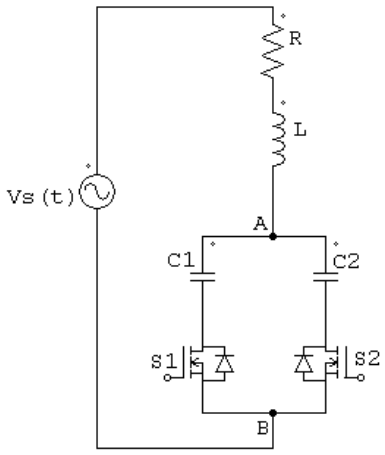

Figure 4.6 DCDS topology with a current limiter.

The current, i(t) is given by equations 4.36 and 4.37 at D=0 and D=1 respectively.

$$i(t) = c\frac{d\,v_{c1}(t)}{dt} \tag{4.36}$$

$$i(t) = c\frac{d\,v_{c2}(t)}{dt} \tag{4.37}$$

The voltage across AB is given by equations 4.38 and 4.39 as referred to branch C_1 or branch C_2 respectively. [61]

$$\hat{v}_{AB} = [D^2 X_{c1} + (1-D)^2 X_{c2}]\cdot \hat{I} \tag{4.38}$$

$$\hat{v}_{AB} = [D^2 X_{c2} + (1-D)^2 X_{c1}]\cdot \hat{I} \tag{4.39}$$

From equation 4.31 and referring to branch C_1 we get

$$X_{c_{eff}} = \frac{\hat{v}_{AB}}{\hat{I}} = [D^2 X_{c1} + (1-D)^2 X_{c2}] \tag{4.40}$$

Where X_{ceff} is the effective capacitive reactance between A and B

$$\frac{1}{\omega c_{eff}} = D^2\cdot\frac{1}{\omega c_1} + (1-D)^2\cdot\frac{1}{\omega c_2} \tag{4.41}$$

From which;

$$\frac{1}{c_{eff}} = D^2\frac{1}{c_1} + (1-D)^2\frac{1}{c_2} \tag{4.42}$$

$$\frac{1}{c_{eff}} = \frac{D^2 c_2 + (1-D)^2 c_1}{c_1 c_2} \tag{4.43}$$

Taking the reciprocal of equation 4.43 gives the value of C_{eff} in terms of the fixed capacitors of the two branches and the duty cycle referred to branch C_1.

$$c_{eff} = \frac{c_1 c_2}{D^2 c_2 + (1-D)^2 c_1} \tag{4.44}$$

Dividing both the numerator and the denominator of equation 4.44 by C_1 we get:

$$c_{eff} = \frac{c_2}{D^2 \cdot \frac{c_2}{c_1} + (1 - D)^2} \quad 4.45$$

Let;

$$\gamma = \frac{c_2}{c_1} \quad 4.46$$

Substituting from equation 4.46 into equation 4.45 we get:

$$c_{eff} = \frac{c_2}{\gamma D^2 + (1 - D)^2} \quad 4.47$$

Dividing both numerator and denominator by γ, we get;

$$c_{eff} = \frac{c_1}{D^2 + \frac{1}{\gamma}(1 - D)^2} \quad 4.48$$

Both equations 4.47 and 4.48 represent the effective capacitance between points A and B, Figure 4.6, where D is the duty cycle of the switch in series with C_1.

A plot of equation 4.47 is shown in Figure 4.7, for different values of γ.

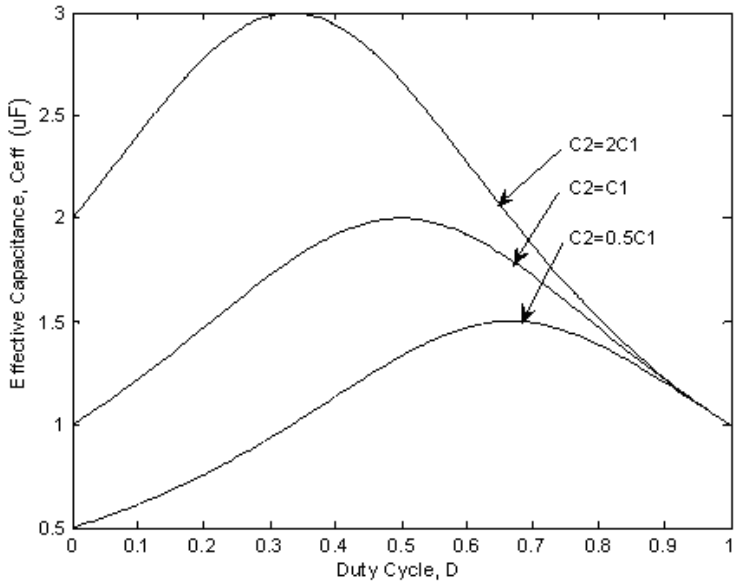

Figure 4.7 Relation between D and C_{eff} for DCDS circuit as referred to branch C_1.

If the duty cycle, D is referred to branch C_2 and using equation 4.39; we can get:

$$X_{c_{eff}} = \frac{\hat{v}_{AB}}{\hat{I}} = [D^2 X_{c2} + (1-D)^2 X_{c1}] \quad 4.49$$

$$\frac{1}{\omega c_{eff}} = D^2 \cdot \frac{1}{\omega c_2} + (1-D)^2 \cdot \frac{1}{\omega c_1} \quad 4.50$$

$$\frac{1}{c_{eff}} = D^2 \cdot \frac{1}{c_2} + (1-D)^2 \cdot \frac{1}{c_1} \quad 4.51$$

$$\frac{1}{c_{eff}} = \frac{D^2 c_1 + (1-D)^2 c_2}{c_1 c_2} \quad 4.52$$

Taking the reciprocal of equation 4.52, we get:

$$c_{eff} = \frac{c_1 c_2}{D^2 c_1 + (1-D)^2 c_2} \quad 4.53$$

Dividing by C_2

$$c_{eff} = \frac{c_1}{\frac{1}{\gamma} D^2 + (1-D)^2} \quad 4.54$$

And dividing by γ

$$c_{eff} = \frac{c_2}{D^2 + \gamma (1-D)^2} \quad 4.55$$

Equations 4.54 and 4.55 represent the value of the effective capacitance in terms of the fixed capacitors C_1 and C_2, where D is the duty cycle of the switch in series with C_2.

A plot of equation 4.54 is shown in Figure 4.8, for different values of γ.

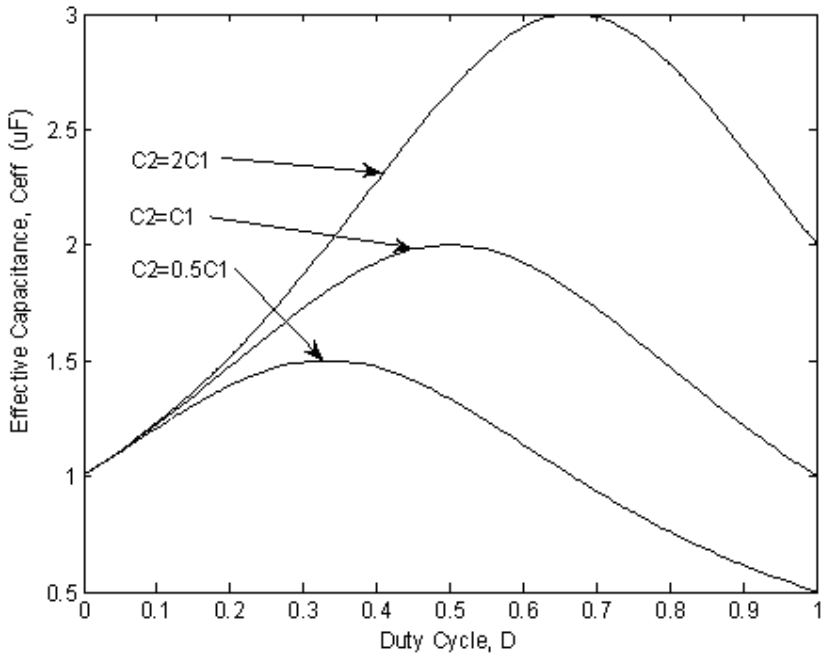

Figure 4.8 Relation between D and C_{eff} for DCDS circuit as referred to branch C_2.

The feature of this topology is that the maximum effective capacitance between points A and B, Figure 4.5, could be up to the sum of both fixed capacitors (C_1+C_2), also it gives more flexibility to obtain the same value of the effective capacitance at two different settings (a high and a low value) of the duty ratio, due to the bell function shape of the relation, Figure 4.7and Figure 4.8.

4.3 Implementation of the Switched-capacitance Circuit

The schematic diagram of Figure 4.9 shows a simple verification of a switched capacitance circuit formed by two capacitors, each capacitor is connected in series with two MOSFET switches and the two parallel branches are connected to an inductor across a sinusoidal power supply.

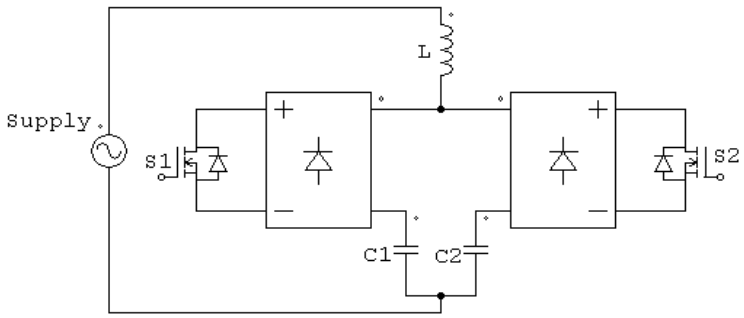

Figure 4.9 Schematic diagram of the implemented switched capacitance circuit.

The two cases discussed above in this chapter have been implemented in the Lab to verify the theoretical relations deduced above between the duty cycle and the effective capacitance for the two cases, the single-capacitance, double-switch case and the double-capacitance, double-switch case.

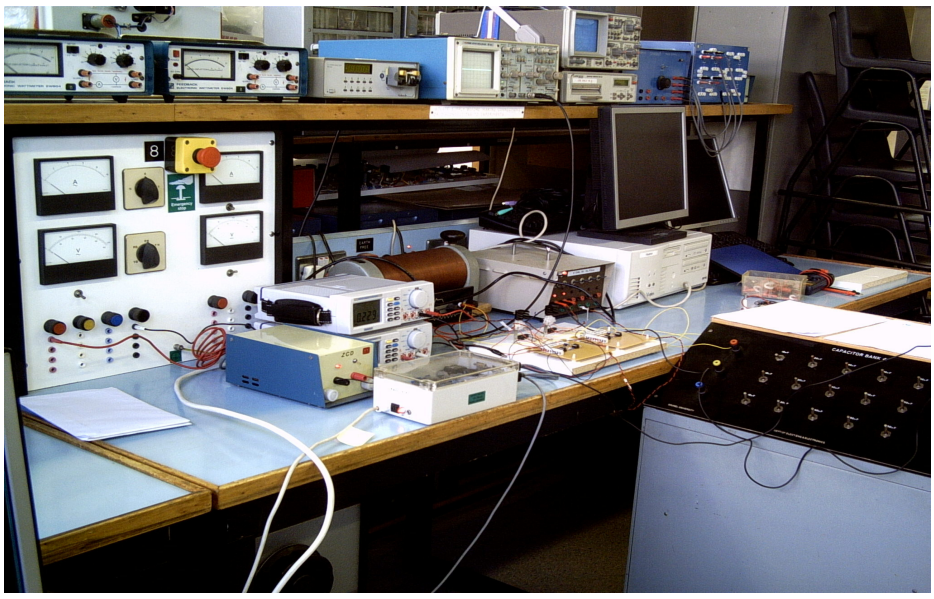

Figure 4.10 Experimental setup of the SCC.

The experimental system is setup as shown in Figure 4.10 which shows the following components from right to left; the capacitor bank, the PC, the DC power supply, the two switches with their drive circuits, the iron-cored coil, multi-meters, the AC mains, zero crossing detector circuit, and the microprocessor board respectively.

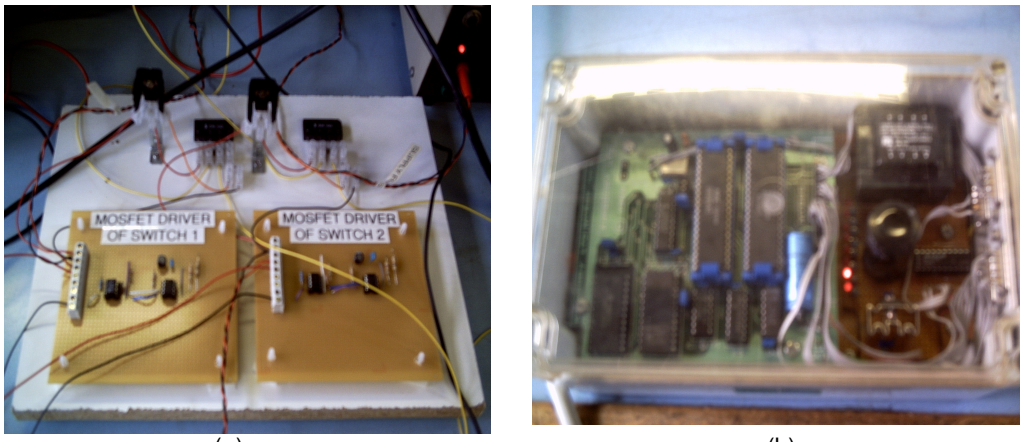

(a) (b)

Figure 4.11 (a) Drive circuit of the MOSFET switches. (b) Microprocessor board.

The switching signal is fed to the driver circuit of the power MOSFET (STP11NK40Z) as shown in Figure 4.11(a), this switching signal is obtained from the output port of a 8085 microprocessor board Figure 4.11(b), this board is Kimberry Ltd product, model MT885. A simple assembly program is written to generate a switching signal which has a duty cycle varying between 0.1 and 0.9 while a zero detector circuit is used to detect the supply frequency and synchronize it with the generated pulse from the microprocessor port, the output of the zero detector circuit is supplied to the input port of the microprocessor.

The power diode rectifier bridge shown in Figure 4.9 is used to rectify the AC current through the MOSFET switch.

The duty cycle of the power switch is varied from 0.1 to 0.9 and the voltage and current are measured, from which the capacitive impedance could be calculated and hence the effective capacitance of the circuit assuming that the ohmic resistance of the circuit is negligible.

The plot of the duty cycle against the effective capacitance for the single-capacitor double-switch circuit is shown in Figure 4.12 for the value of the single capacitor, C=10μF.

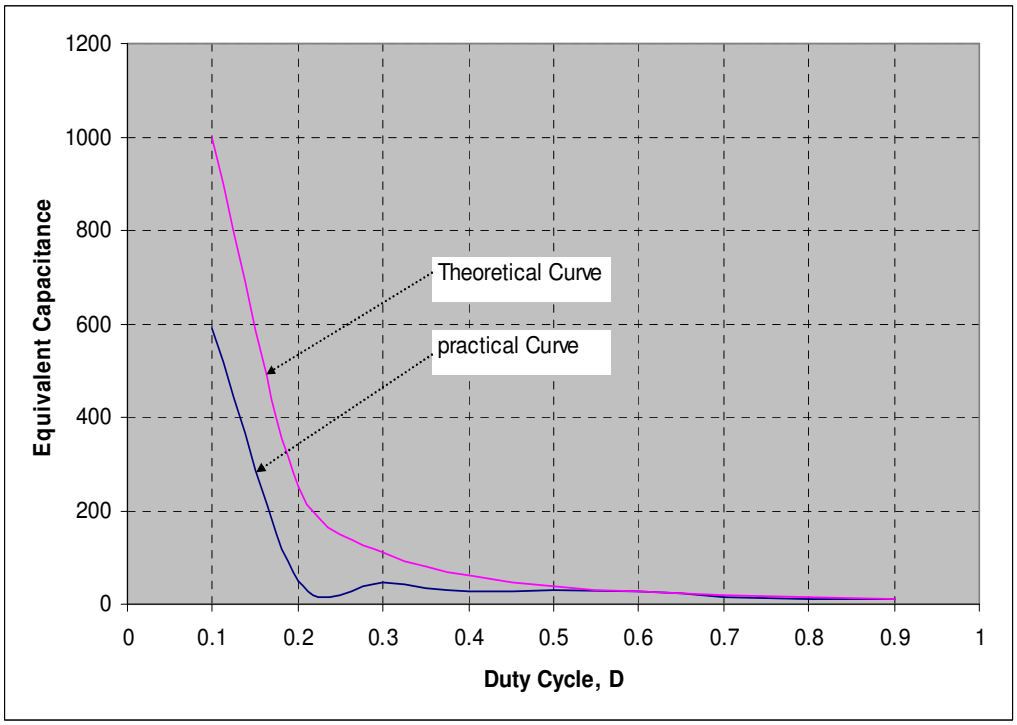

Figure 4.12 Experimental plot of D against C_{eff} for SCDS circuit.

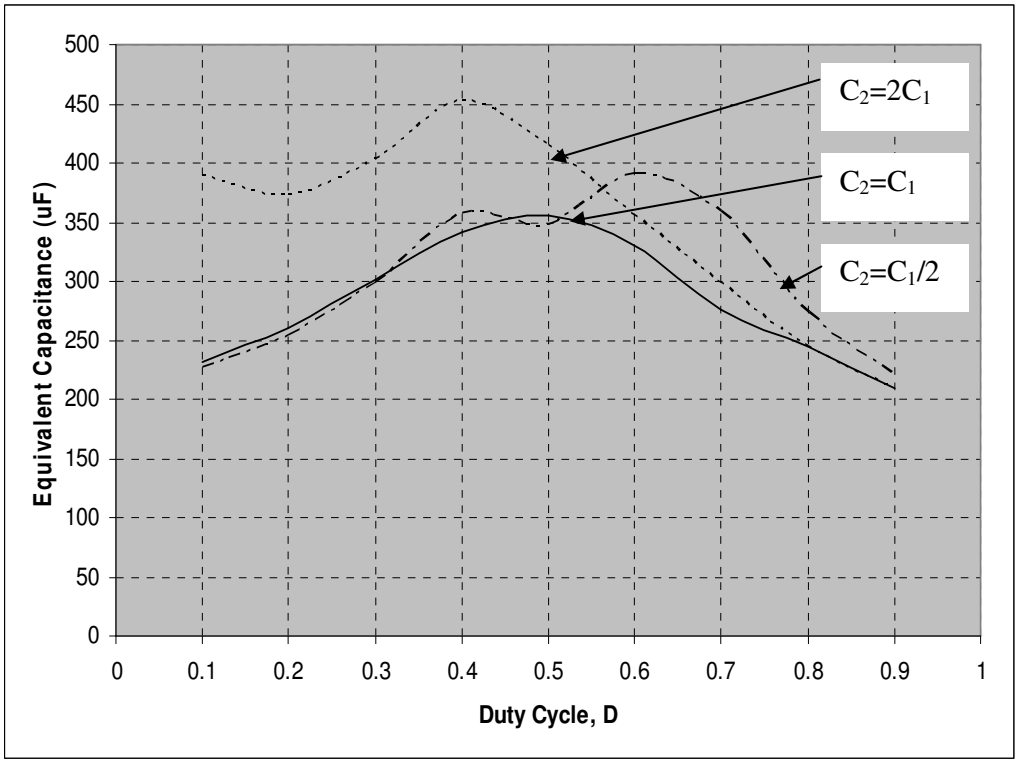

Figure 4.13 Experimental plot of D against C_{eff} for DCDS circuit.

The plot of the experimental results which is obtained for the double-capacitance double switch circuit are shown in Figure 4.13 for three different cases which are comparable to the cases considered in Figure 4.7.

The deviation of the experimental characteristics of both circuits from the theoretical characteristics is due to the fact that the capacitance is calculated from the voltage and current readings which was not accurate due to the gradual accumulation of the voltage across the capacitor which doesn't allow an exact reading of the this voltage, besides the approximation assumed by neglecting the ohmic resistance of the circuit, but the experiment however verifies the effect of the switching capacitance circuit that acts as a variable capacitor between the terminals where the effective capacitance is measured.

4.4 Other topologies of switched capacitance circuit

In the following sections, different topologies of the switched capacitance circuit which were presented in [62] are shown in brief. It is to be considered into account that the switched capacitance circuit could be used in two different modes, the first mode is utilising the resonance energy transfer concept, where the electrical stored energy in the capacitor is interchanged with the magnetic stored energy in the motor inductor or regenerated to the DC supply alternately, the second mode is utilising the switched capacitance circuit as a variable capacitor.

4.4.1 Single-capacitance triple-switch circuit

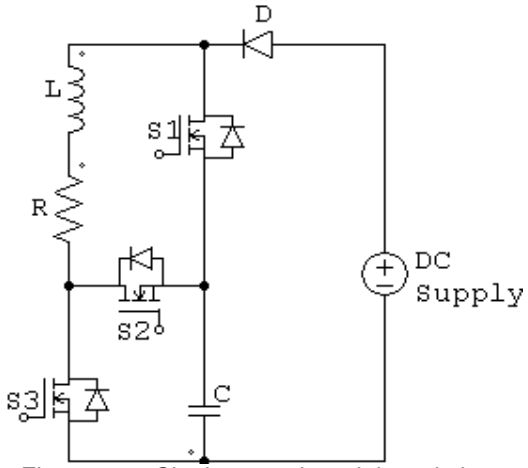

Figure 4.14 Single-capacitor triple-switches.

The system shown in Figure 4.14 illustrates a single-capacitor, triple-switch circuit which utilises the resonance energy transfer concept to interchange energy between the capacitor, C and the motor inductor, L. The capacitor C is charged via switch S_2 by the energy stored in the motor inductor, L. This capacitor, C, discharges its energy back to the motor inductor via switches S_1 and S_3 at the beginning of the energizing period of the motor phase, θ_1 and θ_5 in Figure 3.3.

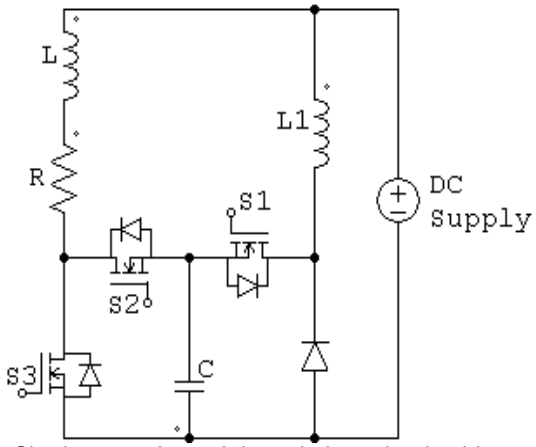

Figure 4.15 Single-capacitor, triple-switches circuit with a coil.

In Figure 4.15, a single-capacitor, triple-switch system with an external coil is illustrated. In this scheme, the resonance energy transfer concept is

applied as before. The energy stored in the inductance of the motor is transferred to the capacitor C when the switch S_3 is open (OFF) and the switch S_2 is closed (ON), this lasts for a time interval equals to $1/2\pi\sqrt{(LC)}$ seconds at the beginning instant of the maximum inductance dead zone, θ_2 in Figure 3.3. During the minimum inductance dead zone, θ_4 in Figure 3.3, switch S_1 is closed for an interval equals to $1/2\pi\sqrt{(L_1C)}$ seconds to transfer the capacitor energy to the DC supply and the inductor L_1. The inductor L_1 acts as a current limiter against high current surge in switch S_1 as well.

4.4.2 Single-capacitor 5-switches circuit

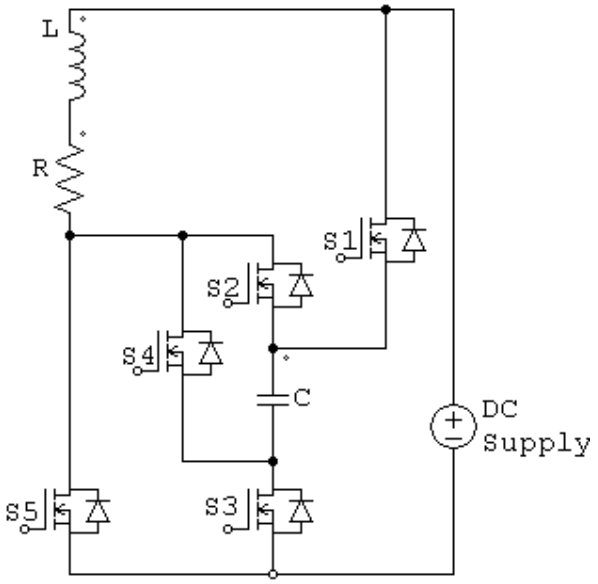

Figure 4.16 Single-capacitor 5-switches circuit.

Another system of a single-capacitor and 5-switches is shown in Figure 4.16 where the capacitor C is charged via switches S_2 and S_3 while discharges its stored energy to the motor inductor via switches S_1 and S_4.

4.4.3 Hybrid switched capacitance systems

In the following, some switched capacitance circuit topologies are shown, such systems are utilising both modes of operation, the resonance energy transfer mode and the variable capacitance mode, hence the name hybrid systems is given to such systems of switched capacitance circuits.

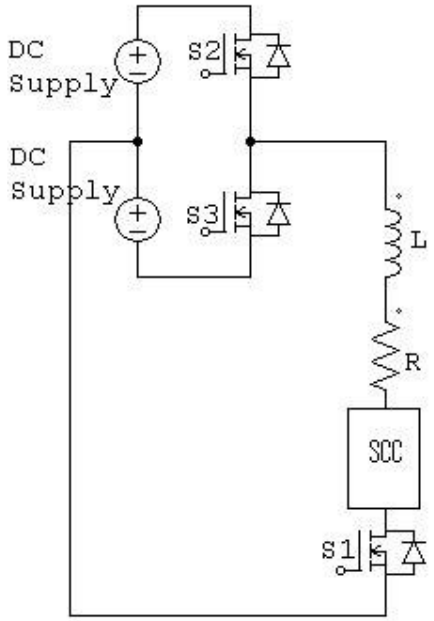

Figure 4.17 Single-capacitor triple-switches system with SCC.

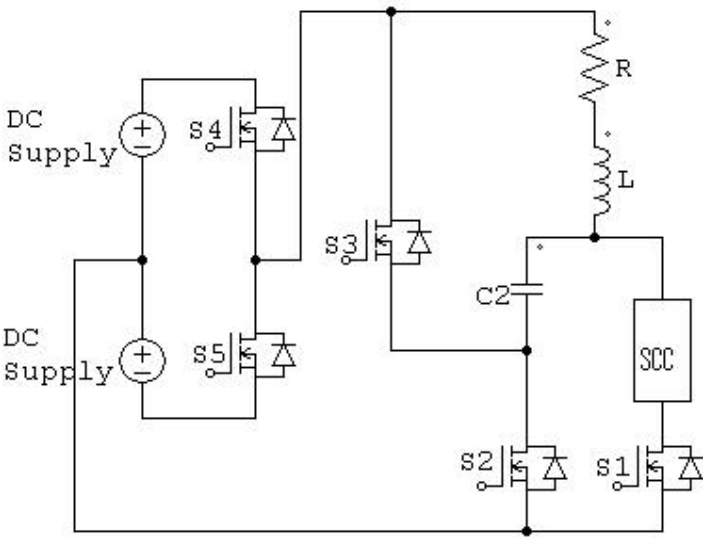

Figure 4.18 Single-capacitor 5-switches system with SCC.

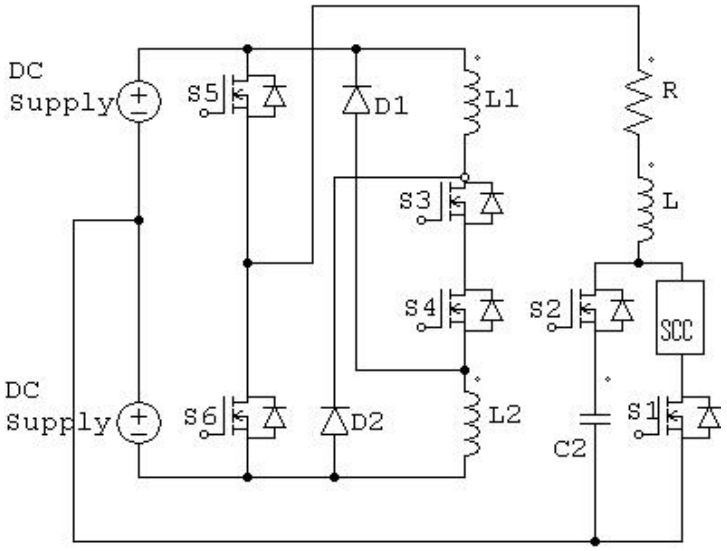

Figure 4.19 Single-capacitor 6-switches system with SCC.

In such systems, the variable capacitance effect of the SCC is used to control the amplitude of the current while the resonance energy transfer is used to improve the time response of the current waveform, in particular, the rising and falling edges. Operation of various circuits is given in [62].

4.5 Applying the switching capacitance circuit to SRM drive topology

In the following chapter, the simulation results will be discussed for each of the two above topologies, the SCDS and DCDS, and the validation of these circuits will be proved and compared with the conventional asymmetric converter from several points of view, including the effect of the switched capacitance circuit on the rise and fall times of the current waveform, the average torque, the harmonic content and the overall efficiency of the drive system.

Chapter 5

Modelling and Simulation of the Proposed Drive Circuit

5.1 Introduction

Most studies concerning dynamic simulation of the switched reluctance machine have been achieved by programming, also software designed to simulate electric network systems as the EMTDC and EMTP have been used. These techniques although very useful, have lack of flexibility [19]. However several simulation studies have been done using the so called circuit-based languages such as SPICE, MATLAB Simulink or M-file, MATRIX, VISSIM and MATHCAD to establish a model of the switched reluctance machine. [11, 16-30, 63]

The SPICE models of the switched reluctance motor systems have the advantage of accurate modelling of the electrical and the electronic components of the drive circuit, but it is not capable of providing an accurate model of the machine due to the fact that the magnetic circuits of the stator, the air gap and the stators can't be separated [64]. The MATLAB model of the switched reluctance motor has the advantages of higher flexibility and open environment which is capable of interacting with many other languages such as C language as well as interface with digital electronic hardware such as PIC Microcontrollers and DSPs which makes it more flexible in the control modelling and processing, yet, the MATLAB environment with both the Simulink and the M-file formats give an approximate model of both the machine and the electronic and electrical components of the drive circuit.

However, few software packages have been developed recently to simulate the switched reluctance machine accurately, such as the PC-SRD developed by the speed laboratory in the university of Glasgow and the Magnet software which is used in this research.

5.2 Magnet Software

The modelling and simulation work of this research has been carried out using the Magnet software, which provides a friendly environment to model the machine with its real mechanical and electrical parameters and computes the electrical, magnetic, mechanical and thermal variables of the machine taking into account the transient with motion effects, Figure 5.1 shows the designed model of a 3-phase, 6/4 switched reluctance machine. For simplicity and time saving, only half of the model is constructed as shown in Figure 5.1 and Figure 5.3 as the other half of the machine will be a mirror image of it.

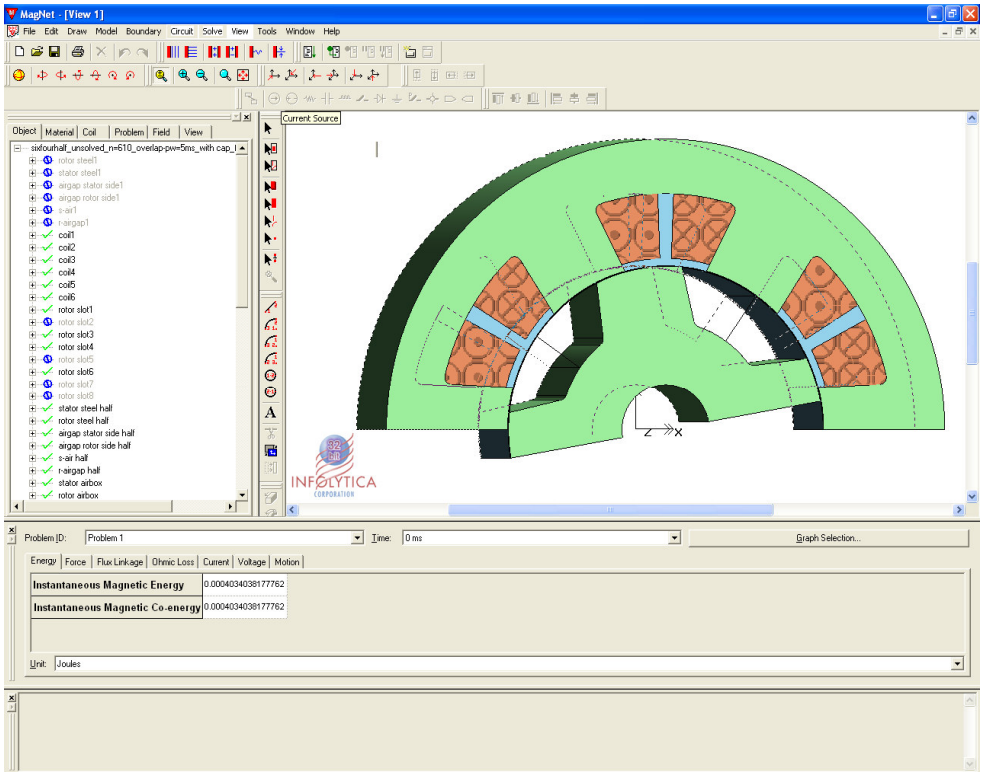

Figure 5.1 Geometric Modeller of Magnet software.

The software supports 2D and 3D solid modelling construction of components besides allowing the users to build their own library of user-defined materials producing a wide and flexible variety of designs.

Magnet includes a circuit modeller, Figure 5.2 which permits the user to connect the designed coils and power electronic devices to circuit drives and loads in order to properly simulate the voltage and current present at the

terminals. It allows the selection of the coil material, the type whether solid or stranded, the number of turns, the internal resistance besides any initial conditions. The circuit components comply with SPICE standards.

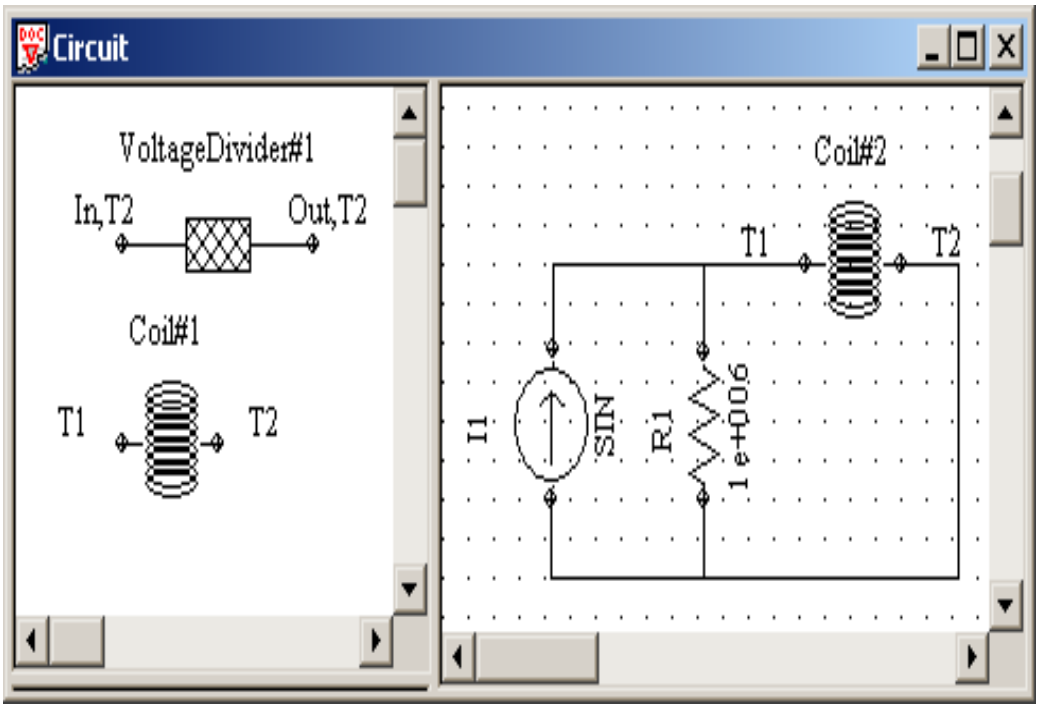

Figure 5.2 Circuit modeller of Magnet software.

Once the geometrical model is produced and the drive circuit is designed, the software utilises the finite element mesh analysis, as shown in Figure 5.3 to calculate the magnetic characteristics of the machine as well as the electrical and thermal characteristics. The limitation of this software with respect to the research purpose, is that it takes very long time to run one simulation for a full cycle, also it plots only one graph at a time with the real time on the x-axis. For comparison reasons or to show the response with respect to the position angle, the curve data has to be exported to excel and re-plotted in terms of the desired parameter.

The Magnet has a plug-in that allows interaction with MATLAB which makes it capable of achieving the advantages of both the SPICE model with respect to the electronic components and the MATLAB model with respect to flexibility and control schemes.

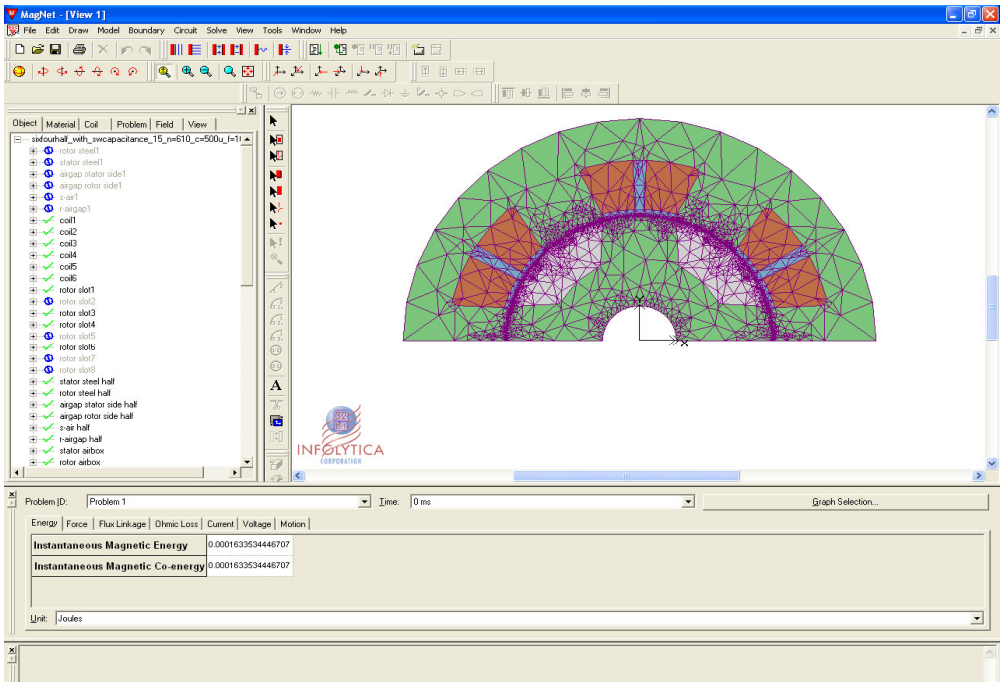

Figure 5.3 Finite element mesh of the solved model.

5.3 Parameters of the Simulated Machine

The parameters of the simulation model is taken from the 3-ph, 6/4 switched reluctance motor as in [48], this machine is a 0.5 kW with the parameters shown in Table 5-1 below.

Table 5-1The machine parameters.

Stator outer diameter.	D_s	134.3 mm.
Stator internal diameter.	D_{si}	114.3 mm.
Stator core axial length.	L_{cs}	100 mm.
Stator core width.	C_s	10 mm.
Rotor pole height.	h_r	13.35 mm.
Air gap.	g	0.25 mm.
Shaft diameter.	D_{ri}	10 mm.
Stator pole arc.	β_s	40^o
Rotor pole arc.	β_r	45^o
Number of turns per phase.	N_{ph}	600
Winding wire diameter.	D_w	0.5 mm.

The machine model is developed using the geometrical modeller as described before with the true mechanical and electrical parameters shown in the above table.

5.4 Drive Circuit

The drive circuit is based on the asymmetric converter circuit with the switched capacitance circuit inserted in series with the phase windings as shown in Figure 5.4.

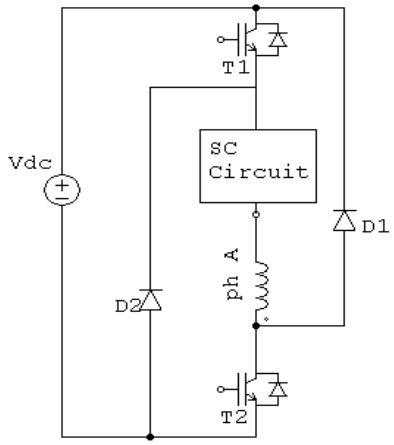

Figure 5.4 Proposed drive circuit.

The two topologies of the switched capacitance circuits which are discussed and analysed in chapter 4, are simulated here, the simulation results of both circuits are compared with each other and with the results obtained from the conventional asymmetric converter alone without inserting the switched capacitance circuit.

For economical and size considerations of the converter circuit, the other topologies of the switched capacitance circuits which include more than two capacitances and/or two switches are not considered, as for each phase there will be two capacitances and two power switches added to the original asymmetric drive circuit besides the control circuit which may lead to a significant increase in the size and volume of the converter, hence a decrease in the power to volume ratio.

5.4.1 Asymmetric Converter Drive

The main aim of this chapter is to study the effect of the proposed drive circuit on profiling the current wave shape and how it affects the output torque as it is the control variable. It was stated before, in chapter 3, that the principal of torque control of the switched reluctance motor depends on two methods, either controlling the amplitude of the phase current or changing the dwell angle. As a matter of fact, changing the dwell angle means in other words allowing the phase current to flow for more time in order to develop positive torque to reduce torque ripples. The proposed drive circuit has shown an achievement of the advantages of both previous methods together, as it allows the control of the amplitude of the phase current and makes the current pulse more flat within the same dwell angle.

For this purpose, which is the study of the effect of the proposed circuit on the current wave shape and the torque ripples, comparison is being held between the output waveforms obtained from the conventional asymmetric drive circuit, Figure 5.5, without inserting the switched capacitance circuit and the waveforms obtained from operating the motor under the same conditions after inserting the switched capacitance circuit.

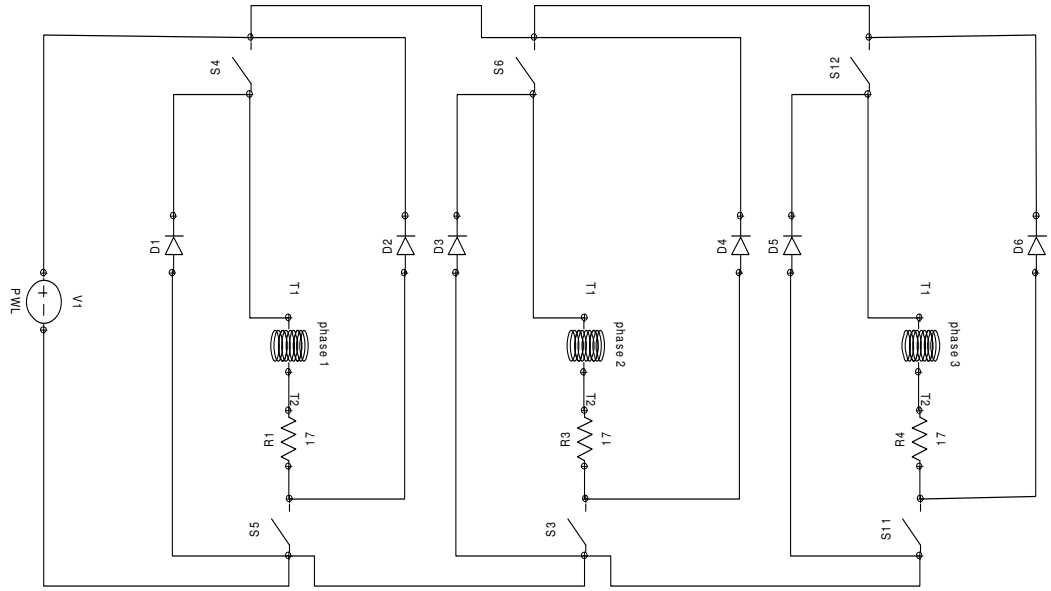

Figure 5.5 Conventional Asymmetric Converter.

The conventional asymmetric drive circuit is setup as shown in Figure 5.5, with the motor parameters shown in Table 5-1.

5.4.1.1 Simulation results for the Asymmetric converter drive

For the study purpose, the motor is derived in two different modes of operations, the single phase operation mode, which means only one phase is energized at any instant while other phases are idle, and the two phase operation mode, where phase two is energized at an instant when current is still flowing in phase one. The single phase operation mode is used only to examine the effect of the switched capacitance circuit on shaping the current waveform. Simulation results of the single phase mode operation with dwell angle of 24° is shown in Figure 5.6 to Figure 5.8 below.

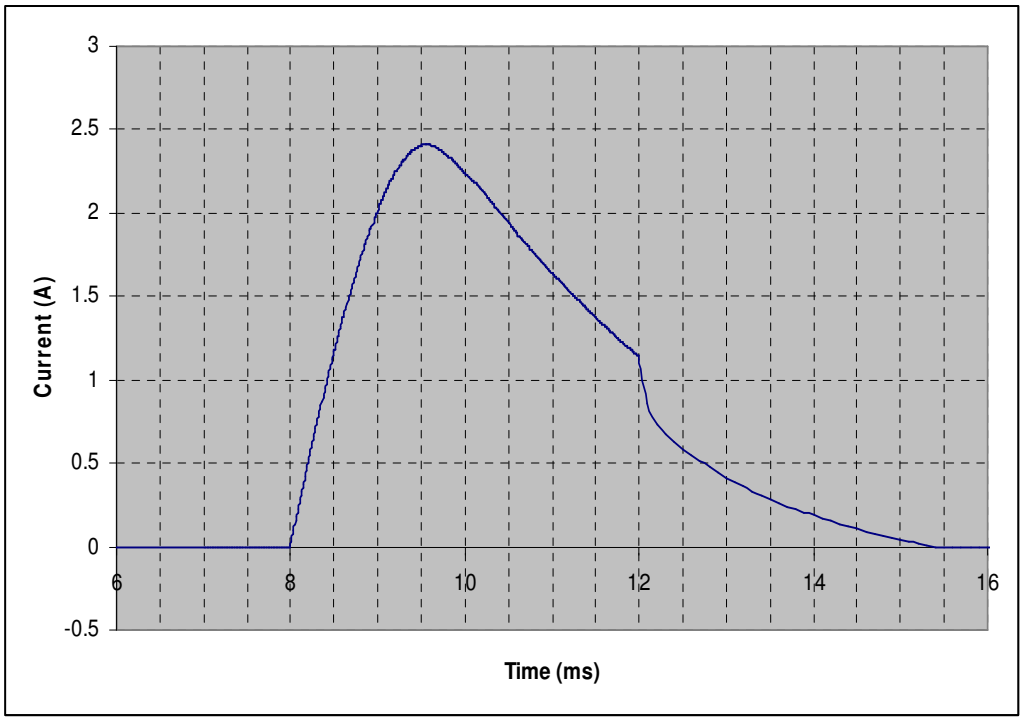

Figure 5.6 Phase current profile for single phase operation mode.

Figure 5.6 shows the current pulse of the machine phase which is energised at the instant t= 8 ms for a period of 4 ms, which corresponds to a dwell angle of 24°. The current reaches its rated value of 2.3 A in 1.5 ms. By definition, the rise time of this current pulse is 0.96 ms, which is the time required for the current to increase from 0.23 A to 2.07 A. Similarly we can find the fall time of this current pulse to be 3.5 ms. The phase voltage and torque pulse of the same phase are shown in Figure 5.7 and Figure 5.8 respectively. These waveforms are to be compared with the corresponding waveforms resulting from the operation of the SRM under the sae conditions after inserting the switched capacitance circuit within the converter.

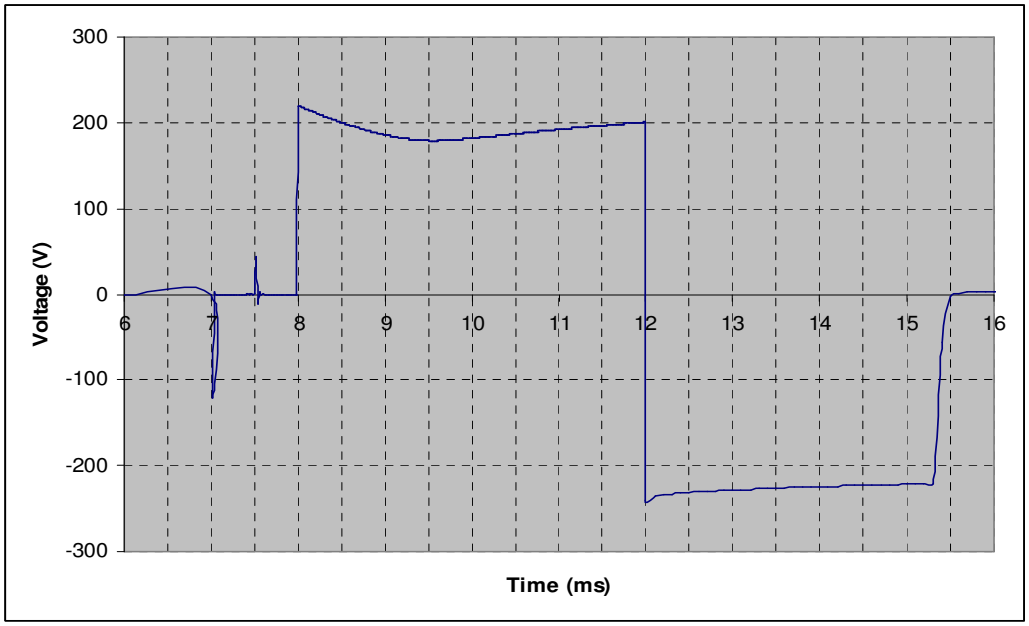

Figure 5.7 Voltage across the motor phase.

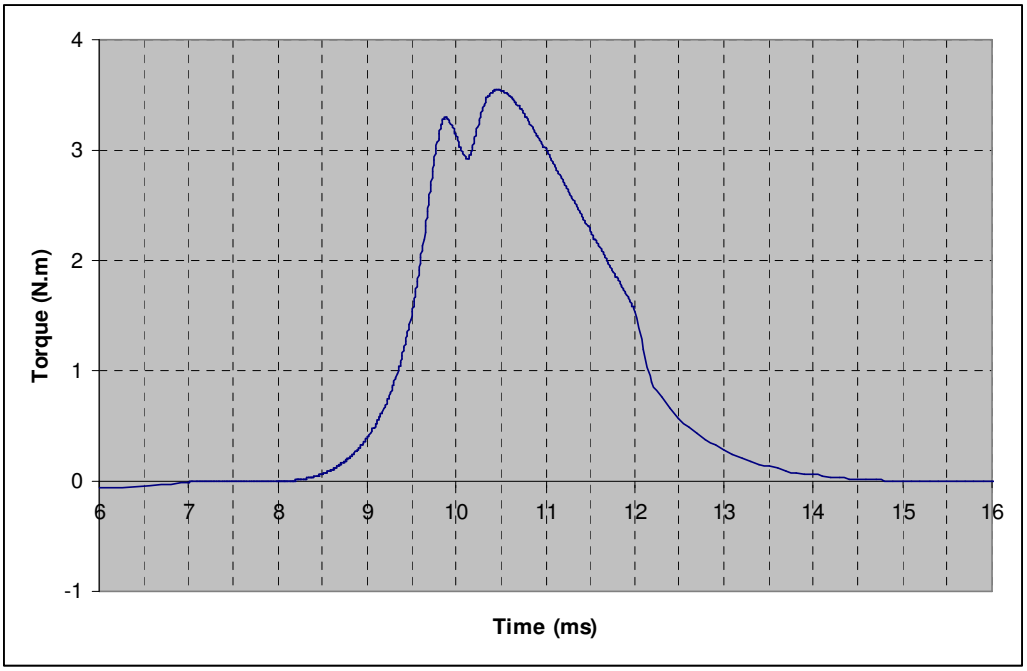

Figure 5.8 Torque pulse developed by a single phase.

The torque pulse of Figure 5.8 has a peak of 3.54 Nm.

In the following section, the new drive circuit topology is presented using the single-capacitance double-switches, switched capacitance circuit.

5.4.2 Single Capacitance Double Switch (SCDS) drive Circuit

The switched capacitance circuit is inserted in series with the motor phase, the circuit consists of a single capacitance connected in series with a semiconductor switch to form one branch which is connected in parallel with another semiconductor switch as shown in Figure 5.9 below. The 17 Ω resistor represents the phase ohmic resistance measured in section 3.5.1.1.

The value of the fixed capacitors, C_1, C_2 and C_3 is selected to be 60μF as will be explained below.

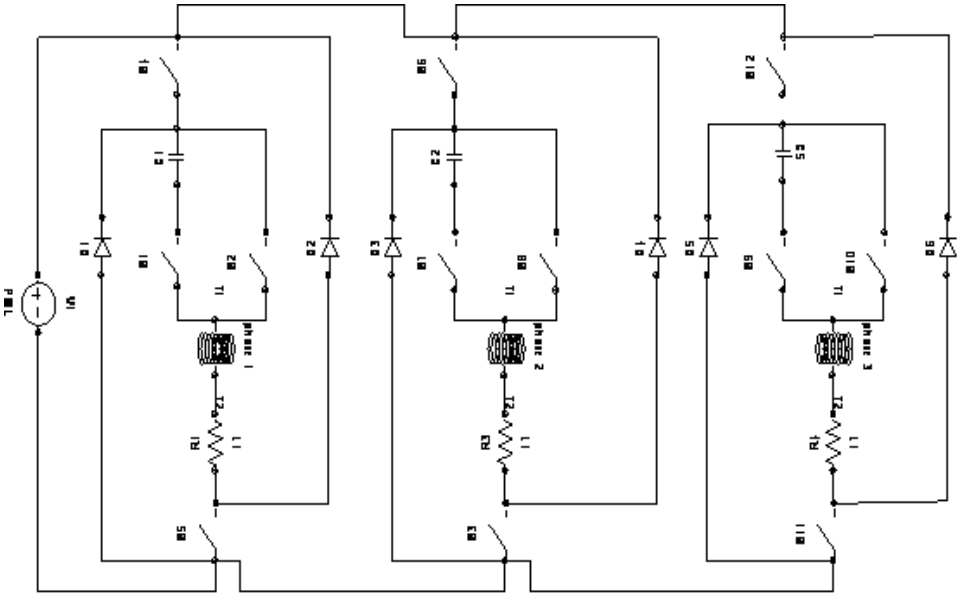

Figure 5.9 Drive circuit utilising single-capacitance double-switch circuit.

5.4.2.1 Switching Strategy

In order to hold a valid comparison between the current case where the single-capacitance double-switch switched capacitance circuit (SCC) is inserted in series with the motor phase, and the previous case where the conventional asymmetric converter is used, the switching pattern of the main switches of each phase (S_3, S_4, S_5, S_6, S_{11} and S_{12}) is kept the same, while the switching pattern of the switched capacitance circuit switches (S_1, S_2, S_7, S_8, S_9 and S_{10}) is designed so that the resulting effective capacitance of the

circuit tracks the variation of the phase inductance profile to resonate with it at the supply frequency.

5.4.2.2 Calculation of the effective capacitance, C_{eff}

From the above discussion and for a given value of the phase inductance, L at any instant, the relation between L and C_{eff} can be written as stated in equation 5.1 below which represents the resonance frequency of an RLC series circuit:

$$f_0 = \frac{1}{2\pi\sqrt{L\,C_{eff}}} \qquad 5.1$$

Where; f_0 is the supply frequency in our case, from which, C_{eff} could be found from equation 5.2 as:

$$C_{eff} = \frac{1}{2\pi L f_0^2} \qquad 5.2$$

5.4.2.3 Calculation of Duty Cycle, D

For the single capacitance double switch SCC, the duty cycle is calculated straight forward from equation 4.33 to be as stated in equation 5.3 below.

$$D = \sqrt{\frac{C}{C_{eff}}} \qquad 5.3$$

In the above equation, in order to calculate for D, the value of C, which is the fixed capacitor, is the only unknown as C_{eff} is calculated as above. So, the switching strategy is based on the estimation of the value of L at each instant of the operation, from which the corresponding value of C_{eff} is calculated, hence the duty cycle D which is continuously varying with the variation of the phase inductance.

5.4.2.4 Determining the value of the fixed capacitor, C

The value of the fixed capacitor, C is a factor of determining the duty cycle at which the semiconductor switch is operated, although it is arbitrary, there has to be a minimum value of C so that the duty cycle is not less than 10% of the period of the switching function, so from equation 5.3 the value of the fixed capacitor, C can be found as follows:

$$D_{min} = \sqrt{\frac{C}{(C_{eff})_{max}}} \quad 5.4$$

$$C = (C_{eff})_{max} \cdot D_{min}^{2} \quad 5.5$$

According to the maximum value of the effective capacitance which is 366 μF (this is the value of C_{eff} which resonates with the minimum inductance) and setting D_{min} to 0.1 the exact value of C could be found, this value will be the maximum effective capacitance which could be obtained between the terminals XX of Figure 4.1 at D=0.1. The max value of C_{eff} according to Figure 4.4 is the value of the fixed capacitor, C divided by D^2 which is 0.01 in this case. As the value of C is arbitrary, so it is selected to be 60 μF as this value will require a duty cycle greater than 0.15 to get the 366 μF and the maximum value of D will be around 0.9 which will be more convenient for practical implementation.

5.4.2.5 Simulation results for SCDS drive circuit

The corresponding waveforms for those shown above are presented below for the phase current, voltage and torque pulse at the transient (starting) period.

In this case, the switching frequency of the switched capacitance circuit is varied over a wide range in order to study its effect on the current profile and on the overall performance of the drive circuit, the shown waveforms are for a switching frequency of 1kHz as it is recommended in [61] to keep the ratio of the switching frequency to the supply frequency greater than 10 in order to reduce the switching harmonics. Study has been carried out for a wide range of switching frequencies between 300 Hz up to 100 kHz with 0.5

kHz increment in order to examine the effect of the switching frequency on various characteristics of the motor and drive circuit.

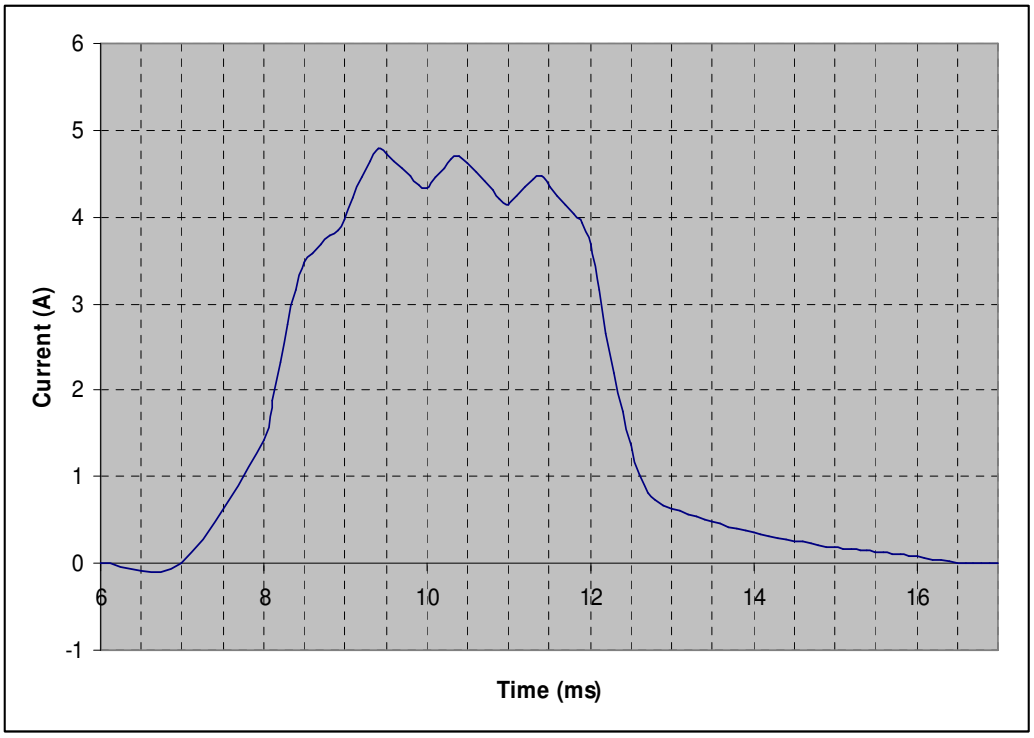

Figure 5.10 Phase current profile for SCDS circuit, f=1kHz.

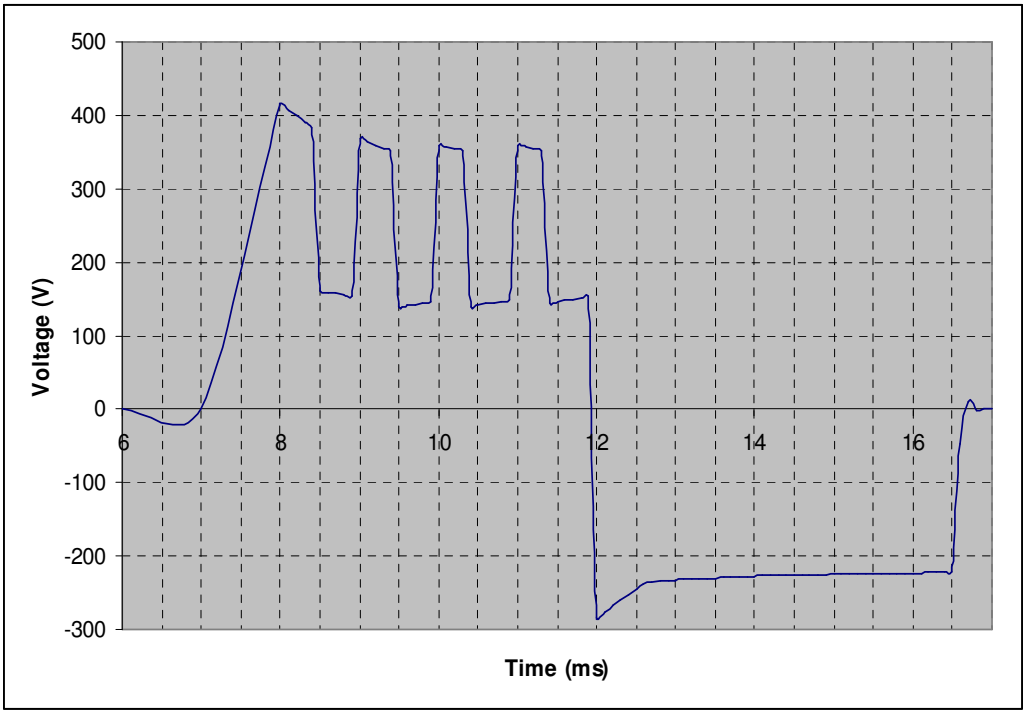

Figure 5.11 Voltage across the motor phase for SCDS circuit, f=1kHz.

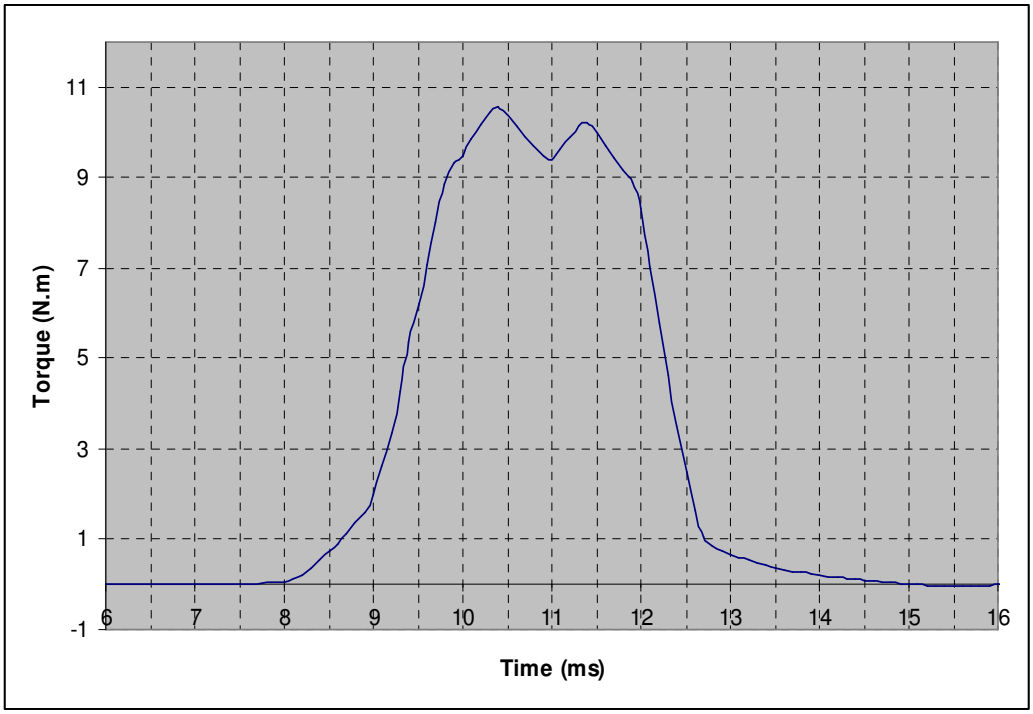

Figure 5.12 Torque pulse developed by a single phase for SCDS circuit, f=1kHz.

As it can be seen from the above figures of the phase current profile, Figure 5.10, the phase voltage, Figure 5.11, and the torque pulse developed per phase, Figure 5.12, some significant effects of the switching capacitance circuit can be found compared to the case of the asymmetric converter drive circuit on both the current shaping and the torque pulse consequently, the effect of the switched capacitance circuit on the phase current and the developed torque is discussed below.

(a) Effect of SCC on the phase current profile

Figure 5.13 shows the combination of the two current waveforms resulting from the simulation of the two cases, these are: the asymmetric converter without the SCC, and the same converter with the SCC inserted in series with the motor phase, setting the switching frequency of the SCC to 1kHz. From Figure 5.13 the following points can be obviously found out:

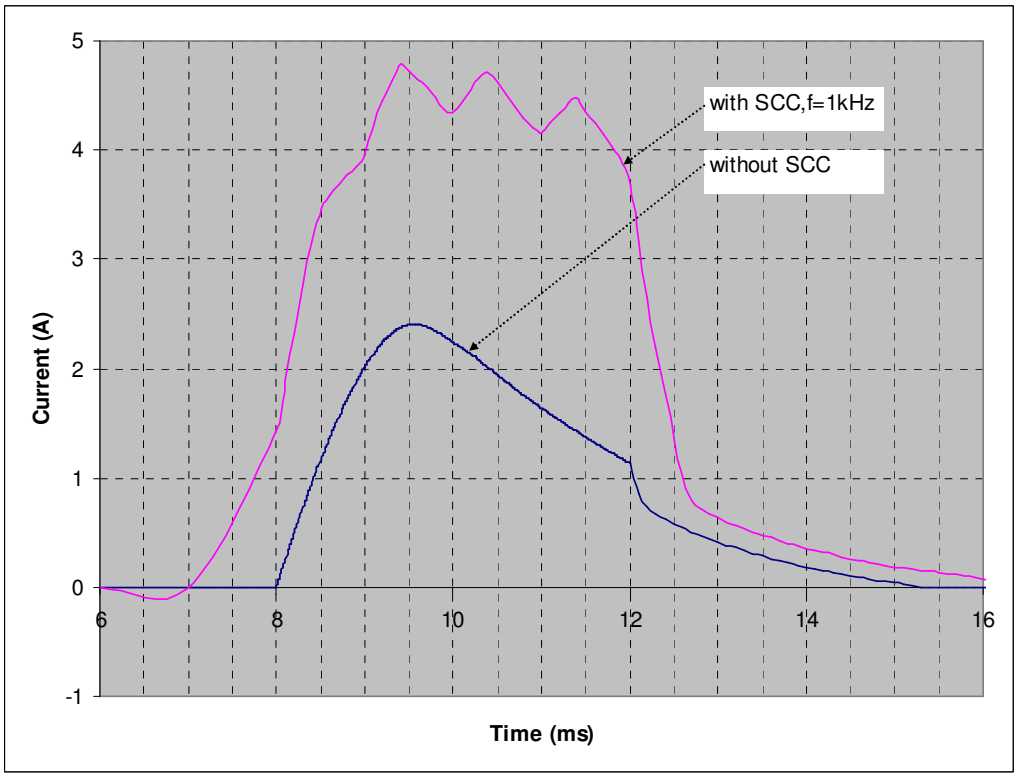

Figure 5.13 Current profiles for the asymmetric converter with and without SCC.

1. The amplitude of the current pulse is increased in the second case to 4.79 A instead of 2.3 A in the first case, which represents 108% increase of the amplitude of the starting current.
2. The current pulse starts rising up at the instant t=7ms instead of 8 ms (the exact switching instant of phase 1), which in other words is equivalent to an advance angle of 6°.
3. Comparing the two current profiles show that the new technique allows the control of the phase current profile to give the effect of controlling of both the dwell angle and the amplitude of the phase current. The dwell angle is a factor of optimizing the efficiency, while the current amplitude is a factor of maximizing the developed torque. Actually the dwell angle in the second case is the same as the first case, but the flat top pulse with the fast rise and fall times gives the same effect as if the dwell angle has been increased.

(b) Effect of SCC on the developed torque

Considering Figure 5.14 below, which represents the two torque pulses resulting from the two above cases, the significant effect on the torque pulse is clearly shown under the same operating conditions which is due to the fact that the torque developed by the switched reluctance machine is actually proportional to the square of the phase current (i^2). This fact leads to make the effect of any slight change of the current profile more significant on the developed torque as could be seen in Figure 5.14. The torque pulse in the case of using the SCC starts to build up exactly at instant t=8 ms or slightly before it, instead of starting at t=8.5 ms in the first case. Also, the flat top of the torque pulse means an increase of the average value of the developed torque and hence the overall efficiency of the drive system. Finally it could be noted that the peak value of the torque pulse is increased from 3.54 Nm to 10.58 Nm which is equivalent to 198.9 % increase.

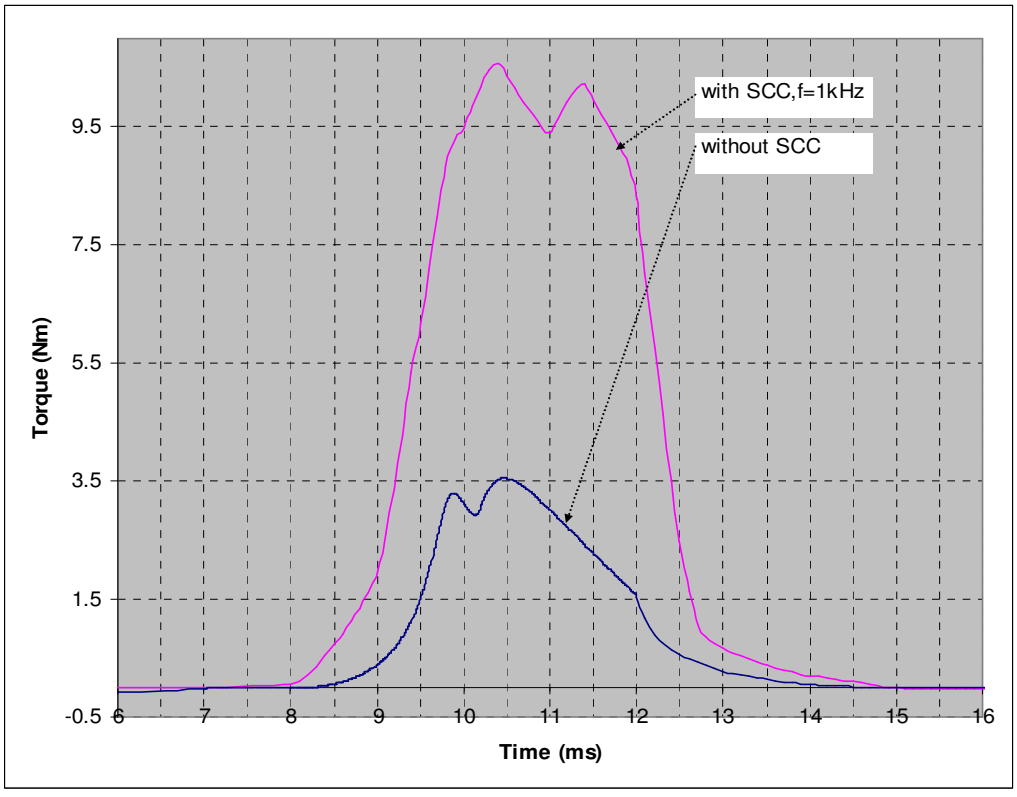

Figure 5.14 Developed torque for the asymmetric converter with and without SCC.

(c) Effect of SCC on the voltage stresses

The effect of using the switched capacitance circuit on the phase voltage could be seen in Figure 5.15 below, which shows the voltage being chopped during the ON period at the switching frequency (1kHz) in this case. The voltage chopping increases the voltage stress over the motor phase to 271 V (RMS) which represents 23% more than the asymmetric converter case before inserting the switched capacitance circuit. However, this increase of voltage across the machine phase doesn't reflect on the voltage stress across the upper semiconductor switch as it occurs only between the instants 8 ms and 12 ms, while the switch is ON, this can be clearly seen in Figure 5.16.

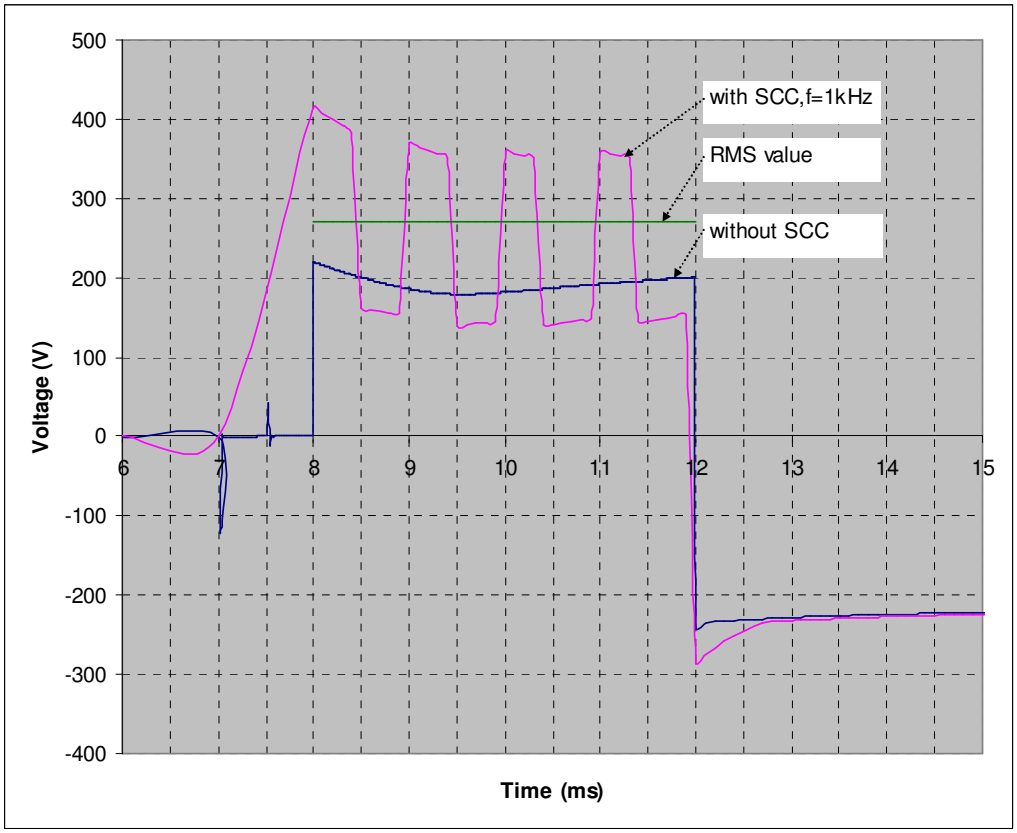

Figure 5.15 Voltage stress over the machine phase.

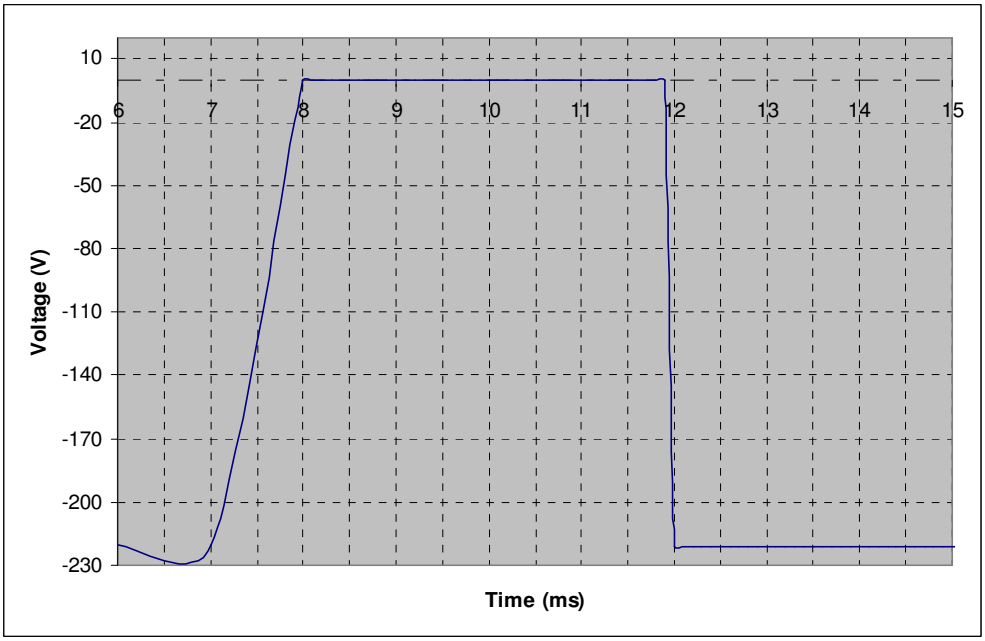

Figure 5.16 Voltage stress across the upper switch, S_4.

(d) Effect of SCC on the current harmonics

The effect of using the switched capacitance circuit is studied for the previous case which is the single-capacitor double-switch circuit with a switching frequency of 1kHz compared with the case of the conventional asymmetric converter without using the switched capacitance circuit.

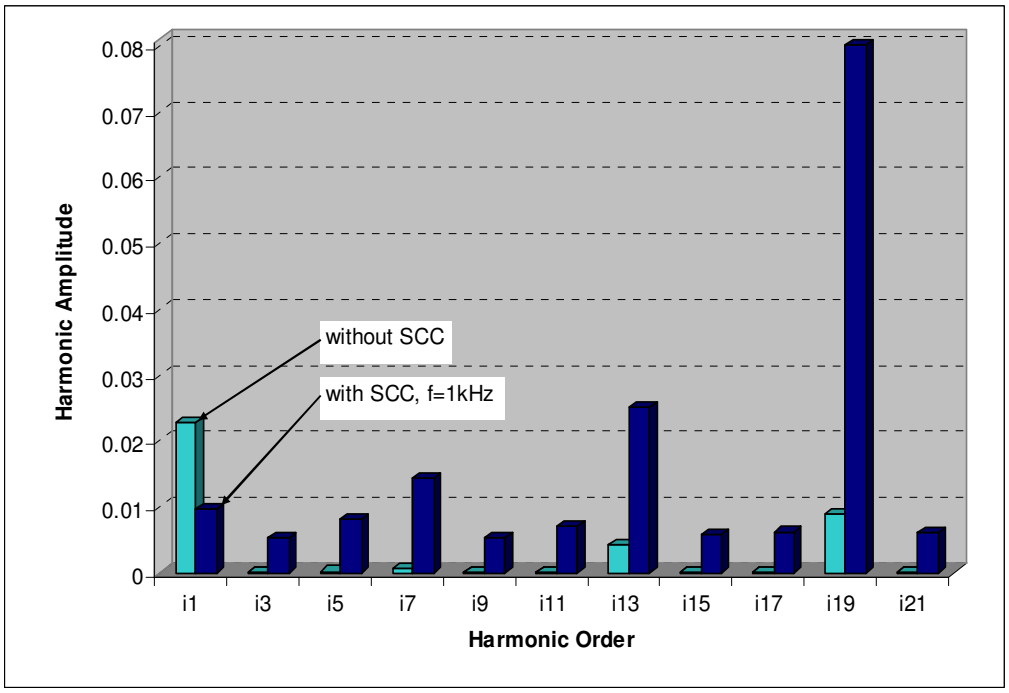

Figure 5.17 Respective Harmonic Amplitudes.

The respective amplitudes of odd harmonics in both cases are shown in Figure 5.17 while the total harmonic distortion factor (THD) is shown in Figure 5.18 for both cases. However, the THD decreases with increasing the switching frequency according to the profile shown in Figure 5.19.

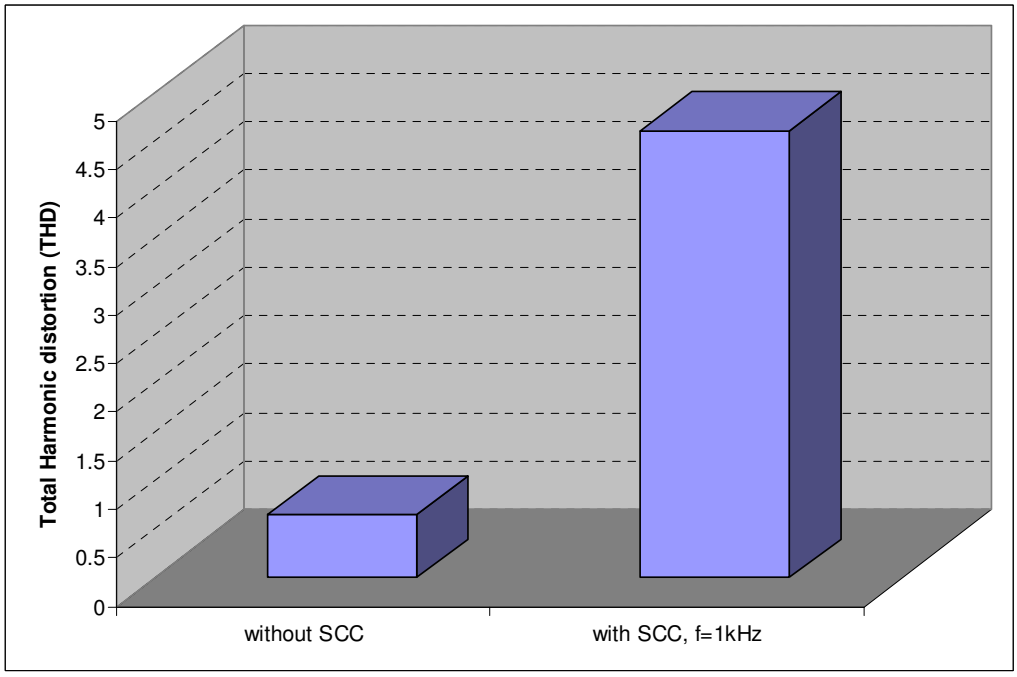

Figure 5.18 Total Harmonic Distortion (THD).

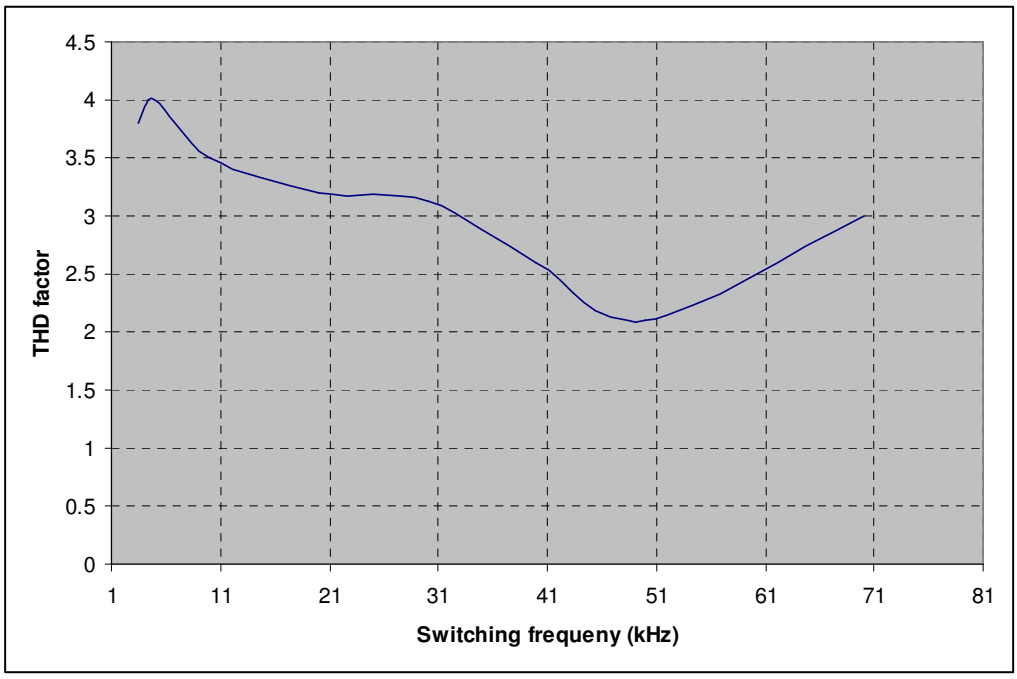

Figure 5.19 Variation of THD with switching frequency.

However, the calculation of the THD is not very accurate as it has been calculated using a semi-analytical semi-numerical method [63] which needs at least 200 samples to be read which was not available in some cases due to technical issues with the software, also some of the undesired harmonic orders could be eliminated, but it is not in the scope of this research.

(e) Effect of the SCC on the overall efficiency

Referring to equations 3.8 and 3.9, the mechanical output of the motor could be written as:

$$\frac{d\ w_m}{dt} = vi\ - i^2 R_m - \frac{d\ w_f}{dt} \qquad 5.6$$

That is, taking the ohmic losses and the magnetic stored power away of the electrical input power. Hence, by determining the ohmic losses and the magnetic energy in both cases (the one of the asymmetrical converter and the one with the switched capacitance circuit), comparison of the effect of using the switched capacitance circuit on the overall efficiency of the system can be achieved.

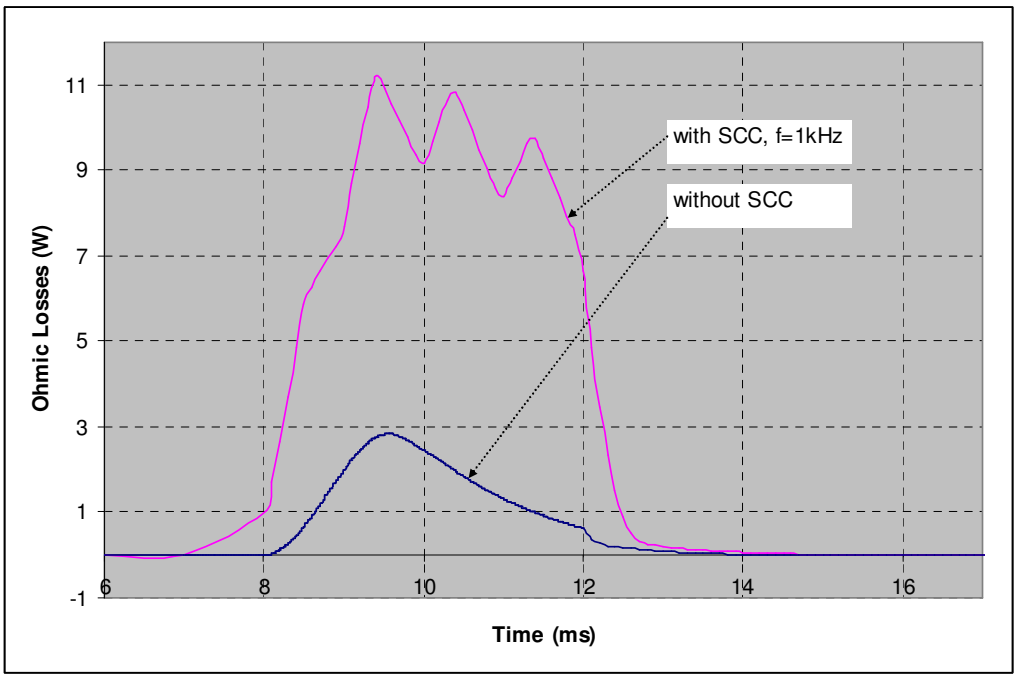

Figure 5.20 Ohmic Losses per coil.

The ohmic losses profiles in both cases as obtained from the simulation results are shown in Figure 5.20, where the shown ohmic loss is per coil of the stator winding (this value has to be multiplied by 2 to find the ohmic losses per phase) while the instantaneous magnetic energy profiles are shown in Figure 5.21.

Substituting the average values of the ohmic losses (i^2R_m), and the magnetic power (dw_f/dt) into equation 5.6, the overall efficiency, η is found to be η=93.06% for the asymmetric converter circuit and η=91.43% for the switched capacitance converter circuit.

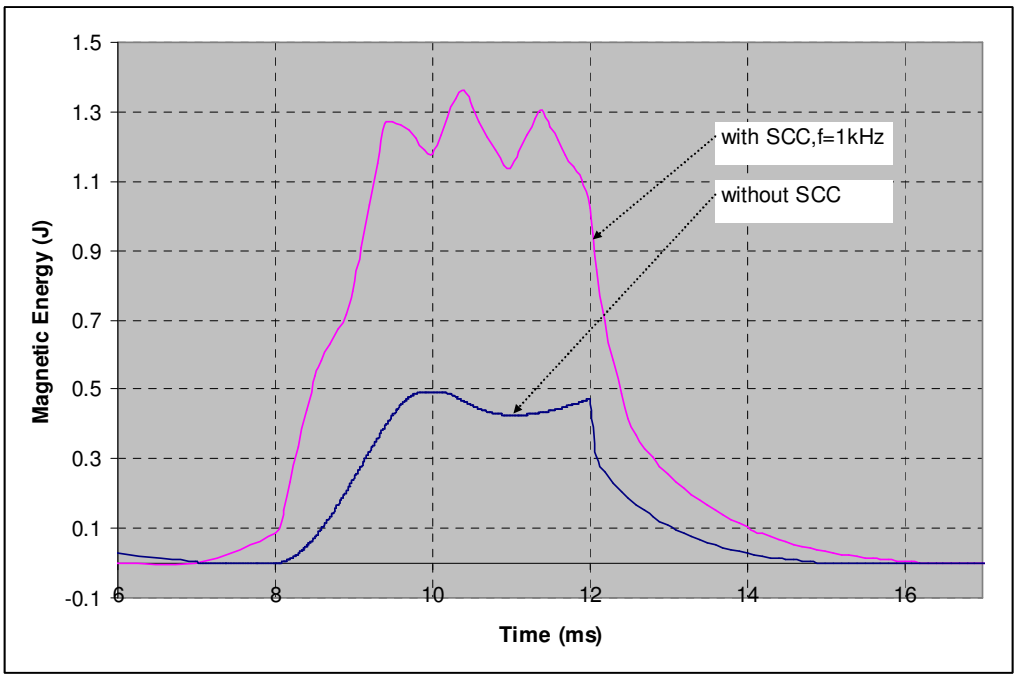

Figure 5.21 Instantaneous Magnetic Energy.

(f) Effect of the SCC on the switching losses

The reduction in the overall efficiency can be referred to the increased harmonic content of the phase current and the switching losses in the switched capacitance circuit. The contribution of the switched capacitance circuit to the switching losses is carried out by comparing the switching losses in the two cases, the asymmetric converter without the SCC and the case with the use of the SCC at 1kHz, bearing in mind that in the first case, nearly all of the power dissipated in the MOSFETs occurs when the device is in the ON state [65] and this is included in the ohmic losses.

The switching losses, P_s can be calculated to a good approximation using equation 5.7 below. [66]

$$P_s = \frac{V_m I_m}{2} f_s \tau \qquad 5.7$$

Where; V_m is the maximum voltage stress on the switch; I_m is the maximum current through the switch; f_s is the switching frequency; and τ is

the period of the switching interval, which is the sum of the delay time plus the rise time specified in the device datasheet.[64]

Equation 5.7 is applied to the current case study with referring to Figure 5.22 below, which shows the voltage stresses over the two power switches associated with the switched capacitance circuit at a switching frequency of 1kHz, from which τ can be estimated, hence the switching losses can be calculated. A compromise has to be done between the harmonic content which decreases with increasing the switching frequency and the switching losses which increases with increasing the switching frequency.

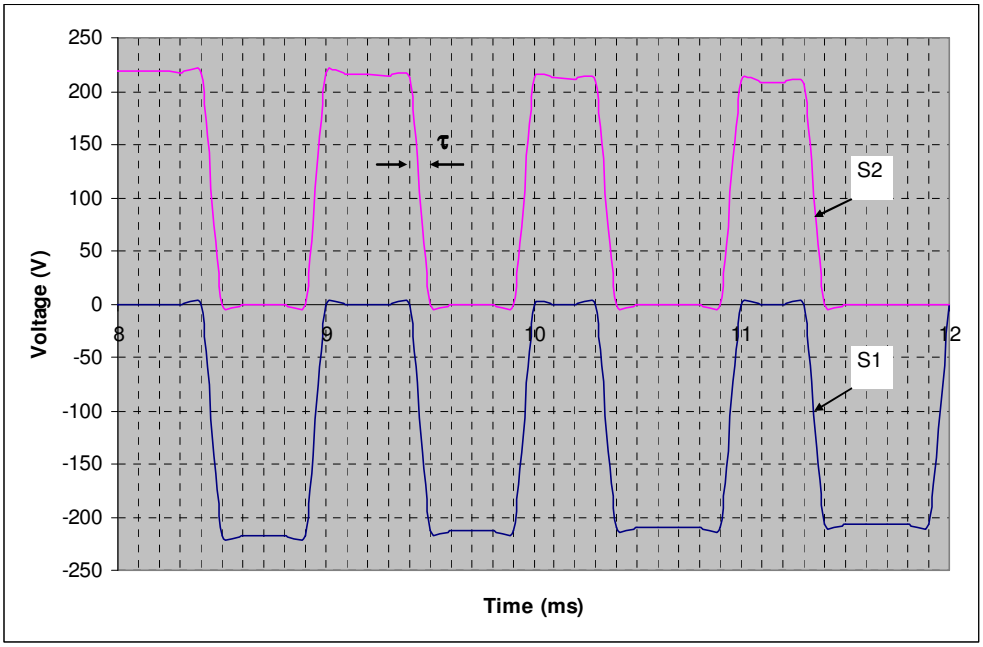

Figure 5.22 Voltage stresses over S_1 and S_2 at 1kHz.

5.4.2.6 Effect of the Switching Frequency

The effect of the switching frequency of the switched capacitance circuit has been studied over a wide range of switching frequencies between 300 Hz and 100 kHz in order to examine the effect of the switching frequency on profiling the phase current and its influence on the developed torque, the harmonic distortion, the switching losses hence the overall efficiency of the drive system.

The following figures from Figure 5.23 to Figure 5.34 show the different profiles of phase current for switching frequencies between 300 Hz and 100 kHz at the same dwell angle of 24° as stated earlier. The current profiles are compared with the asymmetric converter current profile, which is shown in dotted line in all graphs.

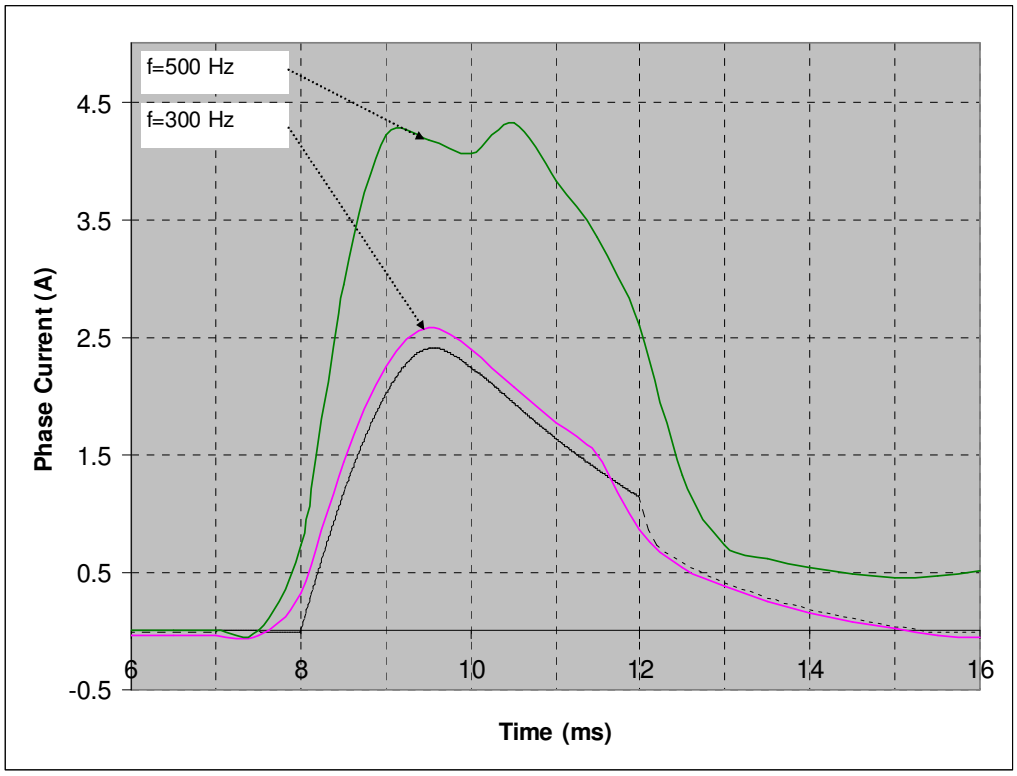

Figure 5.23 Current profiles for 300 Hz and 500 Hz.

At 300 kHz the current waveform is as shown in Figure 5.23, the simulation results showed high current and voltage spikes over the motor phase after the second switching interval at this frequency, the voltage spike reached few kilovolts which led to a significant deformation of the magnetic characteristics (the flux linkage, the magnetic energy, and the magnetic co-energy) of the machine, however, it was recommended in [61] not to use a switching frequency less than 10 times the supply frequency which means a switching frequency of 500 Hz minimum.

The full details of the case of 1 kHz have been shown above as it was the case of lowest switching losses, with a relatively high peak and good time response.

At 1.5 kHz, the simulation results showed lower peak of the current waveform than that at 1 kHz, with higher switching losses and a negative flux linkage-peak of about 0.35 Wb as shown in Figure 5.24. Also, the simulation results showed high voltage spikes (10 kV) over the switches S_1 and S_2 under the same operating conditions as the 1 kHz case.

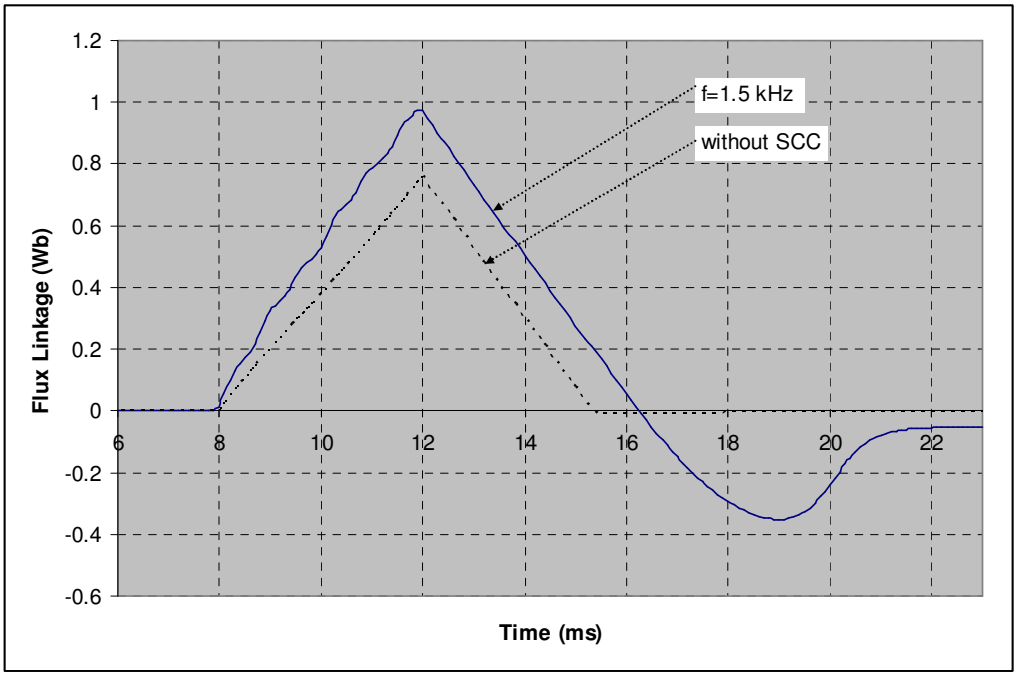

Figure 5.24 Flux linkage at 1.5 kHz.

The results of switching frequencies between 2 kHz and 7 kHz have shown good current and voltage profiles of the motor phase with normal operating conditions of the power electronic switches, the limitation of this range of frequencies is the high switching losses shown in Figure 5.35.

There has been an unexpected failure of the system at a frequency of 7.5 kHz.

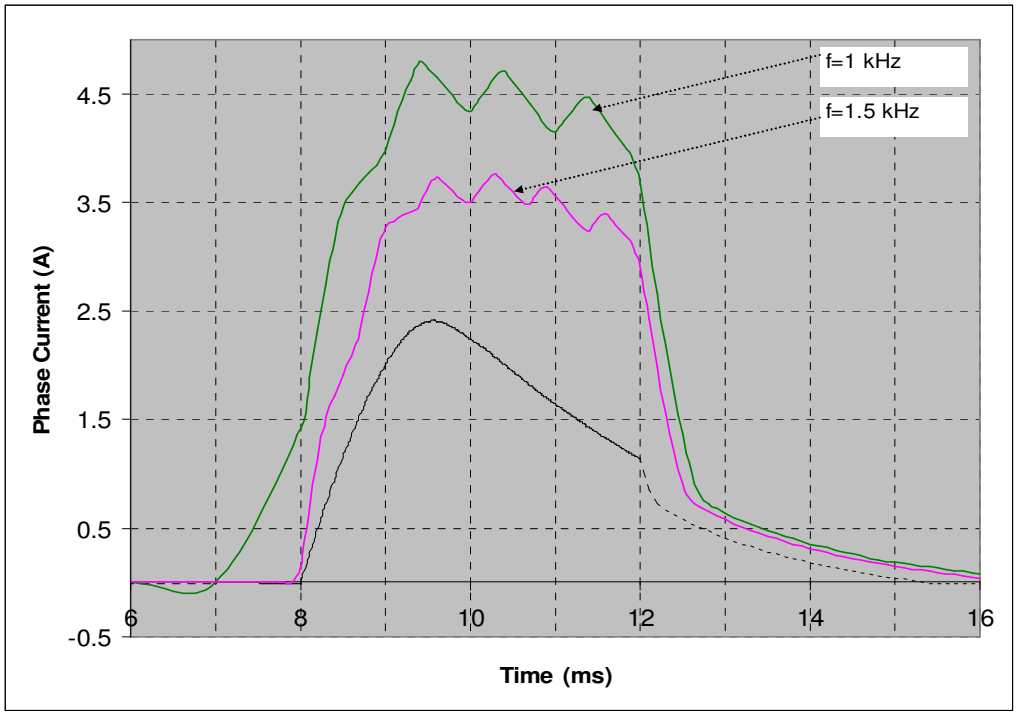

Figure 5.25 Current profiles for 1kHz and 1.5 kHz.

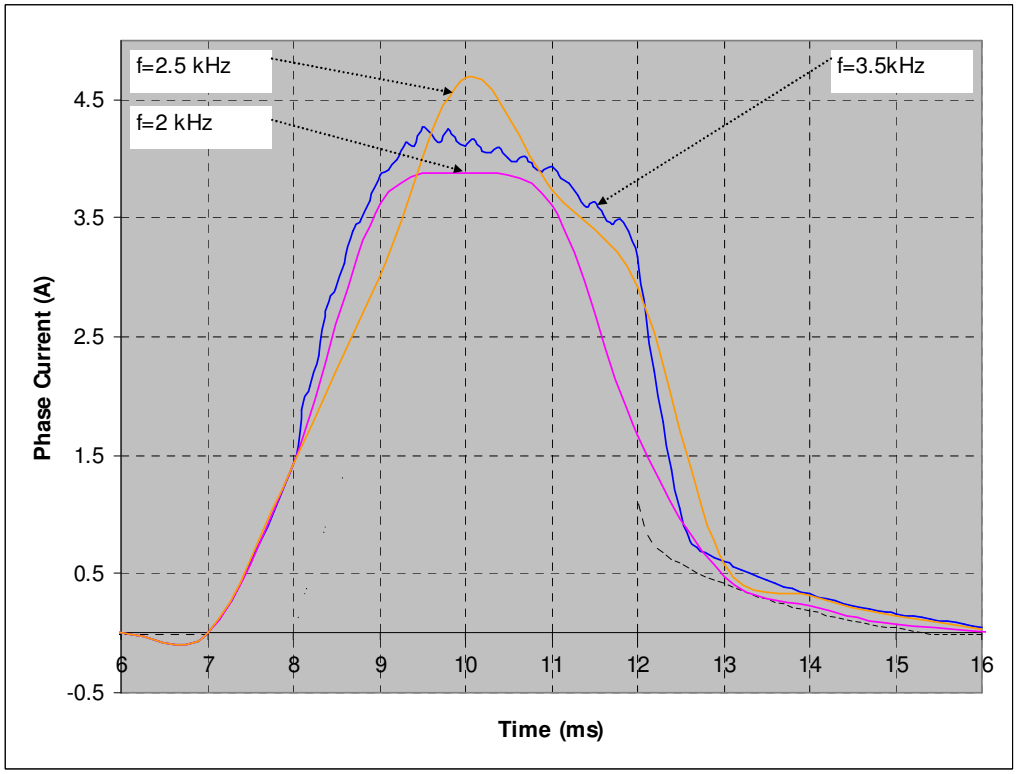

Figure 5.26 Current profiles for 2 kHz, 2.5 kHz and 3 kHz.

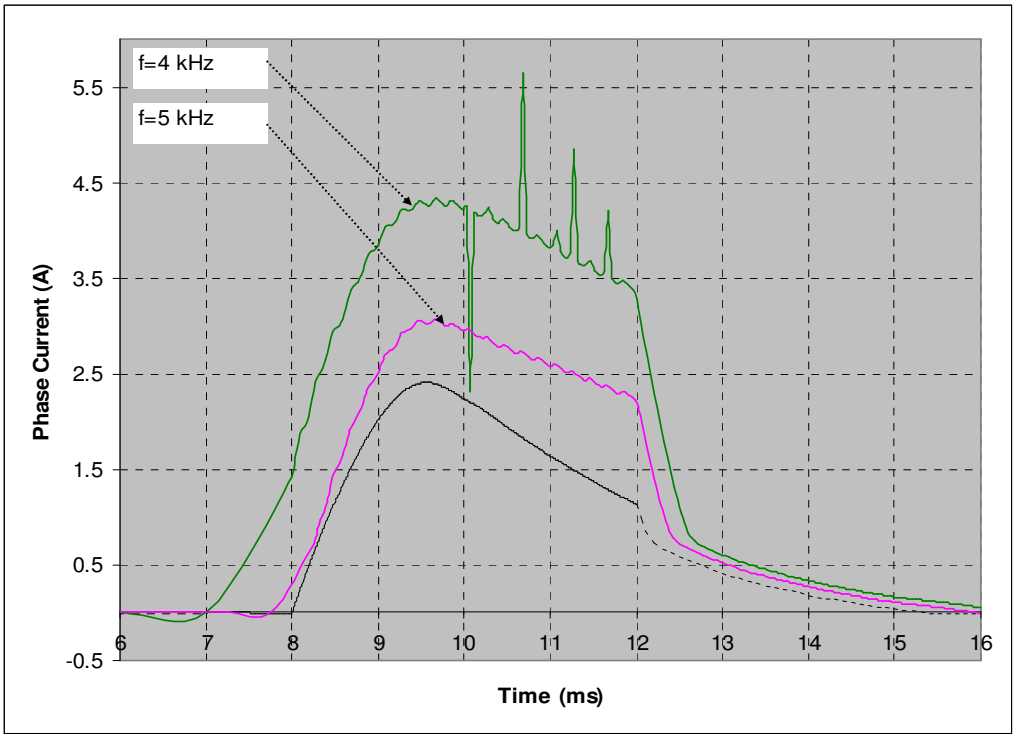

Figure 5.27 Current profiles for 4 kHz and 5 kHz.

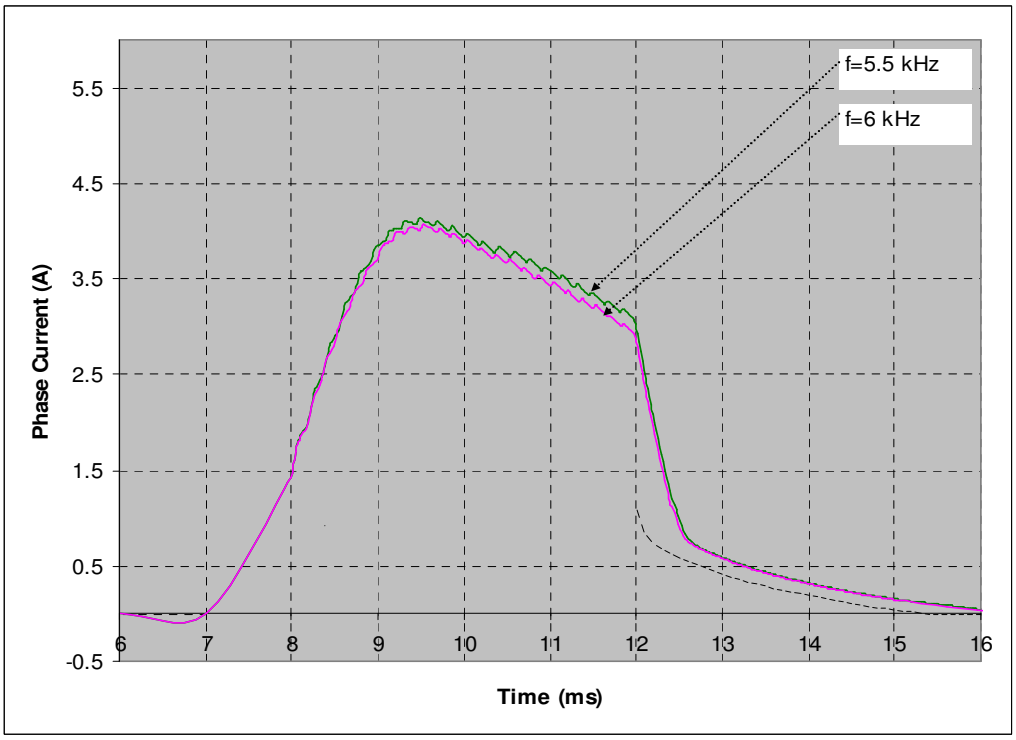

Figure 5.28 Current profiles for 5.5 kHz and 6 kHz.

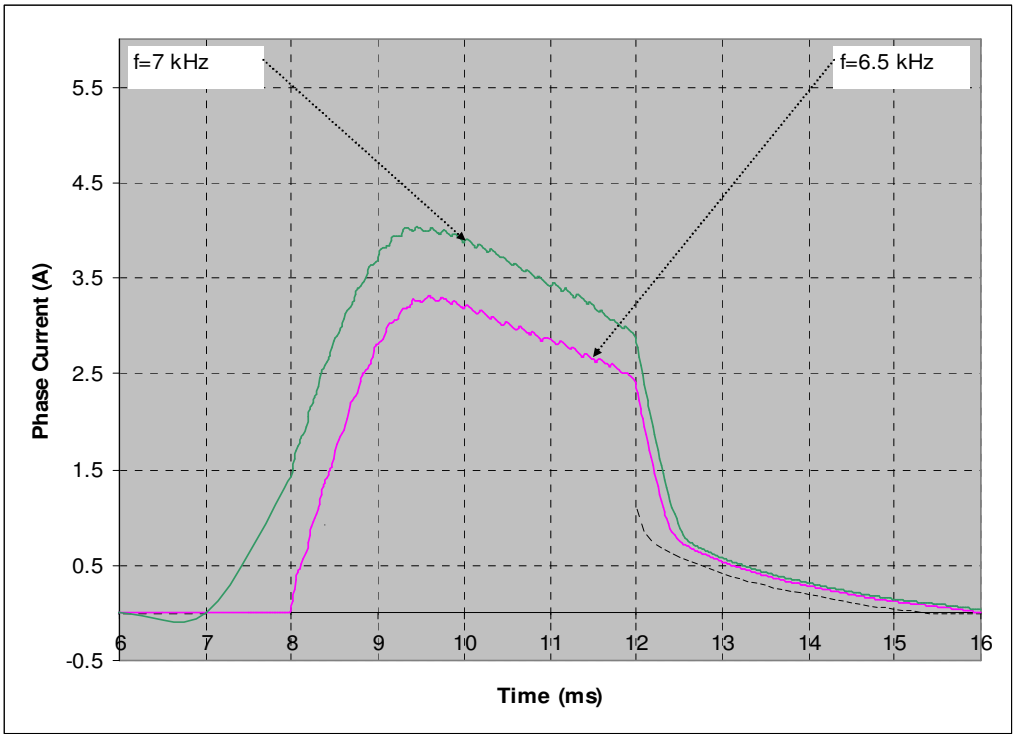

Figure 5.29 Current profiles for 6.5 kHz and 7 kHz.

The examination of the behaviour of the converter-motor system in the switching frequency range between 8 kHz and 30 kHz has shown the current profiles as in Figure 5.30 and Figure 5.31 below, with normal voltage stresses and peak currents, while it has shown maximum increase in the output mechanical energy at a switching frequency of 20 kHz as shown in Figure 5.47.

The switching frequency range above 40 kHz has proved to have very slow time response of the current waveform in most cases as could be seen from figures below, besides the extremely higher switching losses in the power electronic switches and a significant deformation of the magnetic characteristics of the machine which led to a very low value of the average developed torque due to negative torque pulses and a very poor overall efficiency due to the extremely high switching losses.

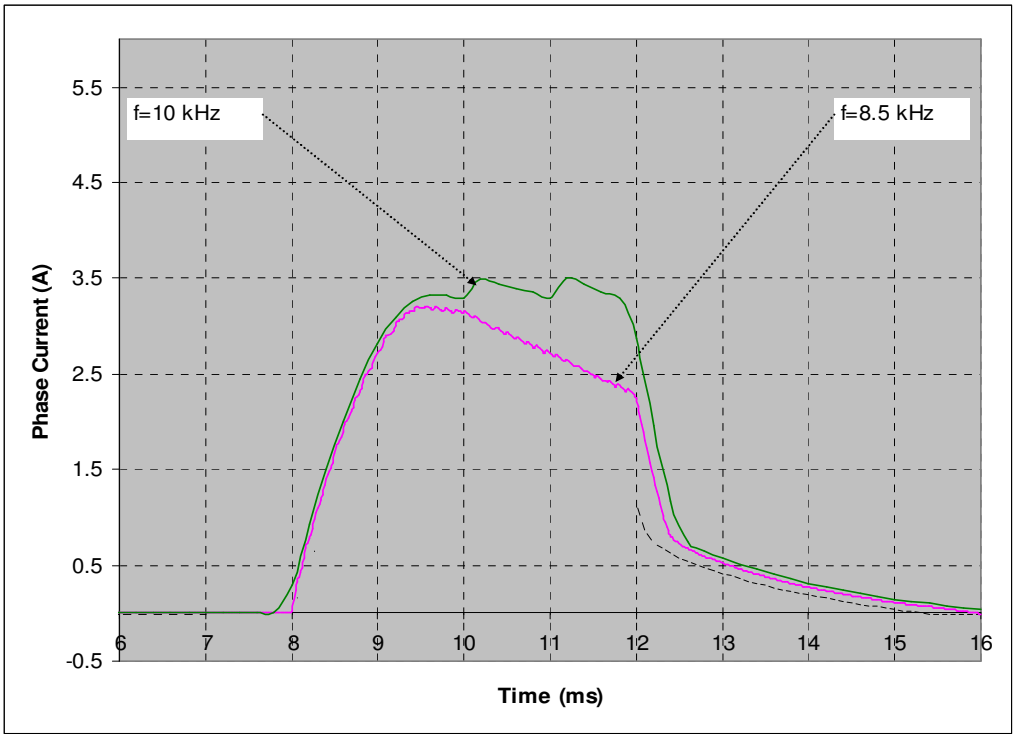

Figure 5.30 Current profiles for 8.5 kHz and 10 kHz.

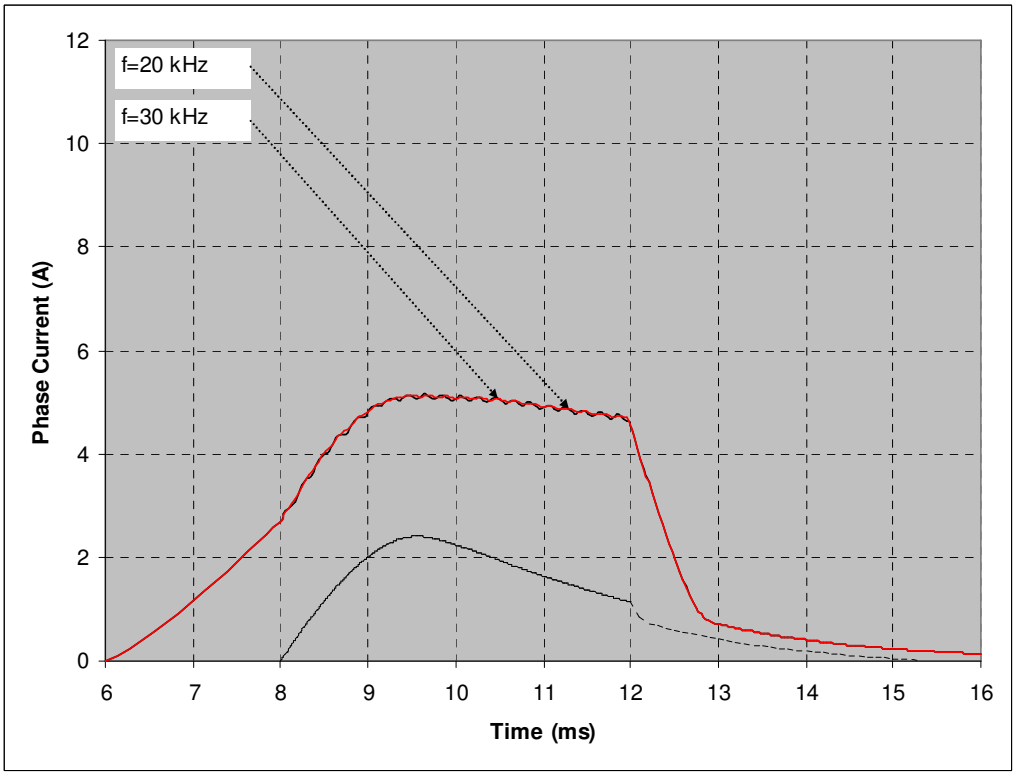

Figure 5.31 Current profiles for 20 kHz and 30 kHz.

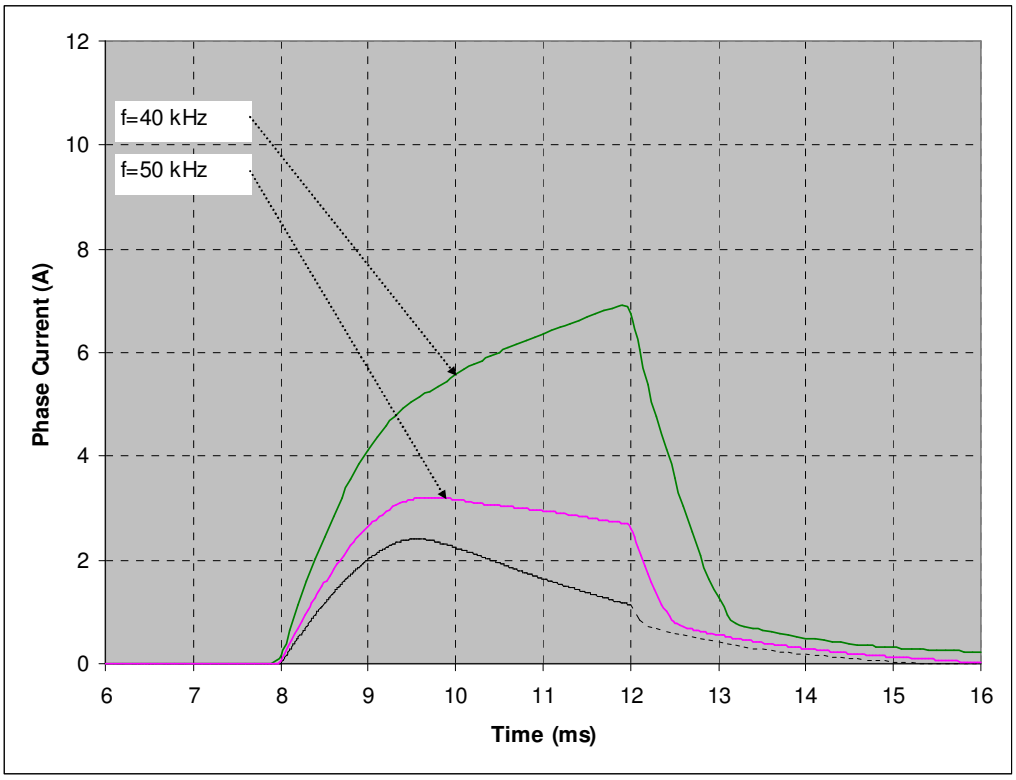

Figure 5.32 Current profiles for 40 kHz and 50 kHz.

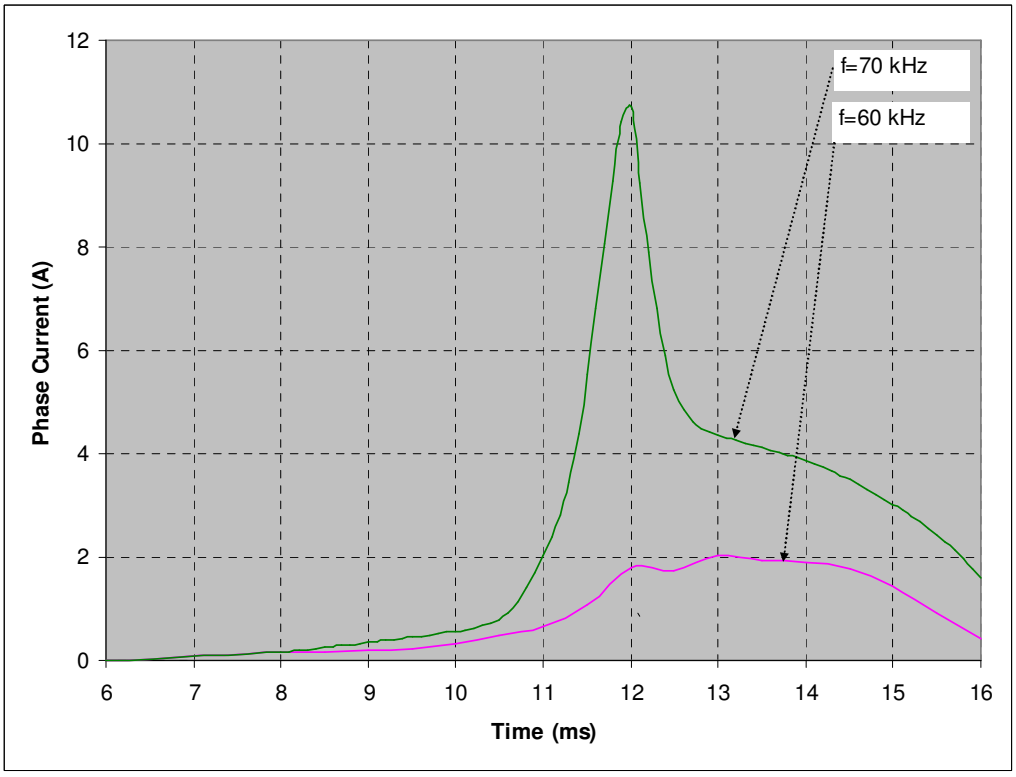

Figure 5.33 Current profiles for 60 kHz and 70 kHz.

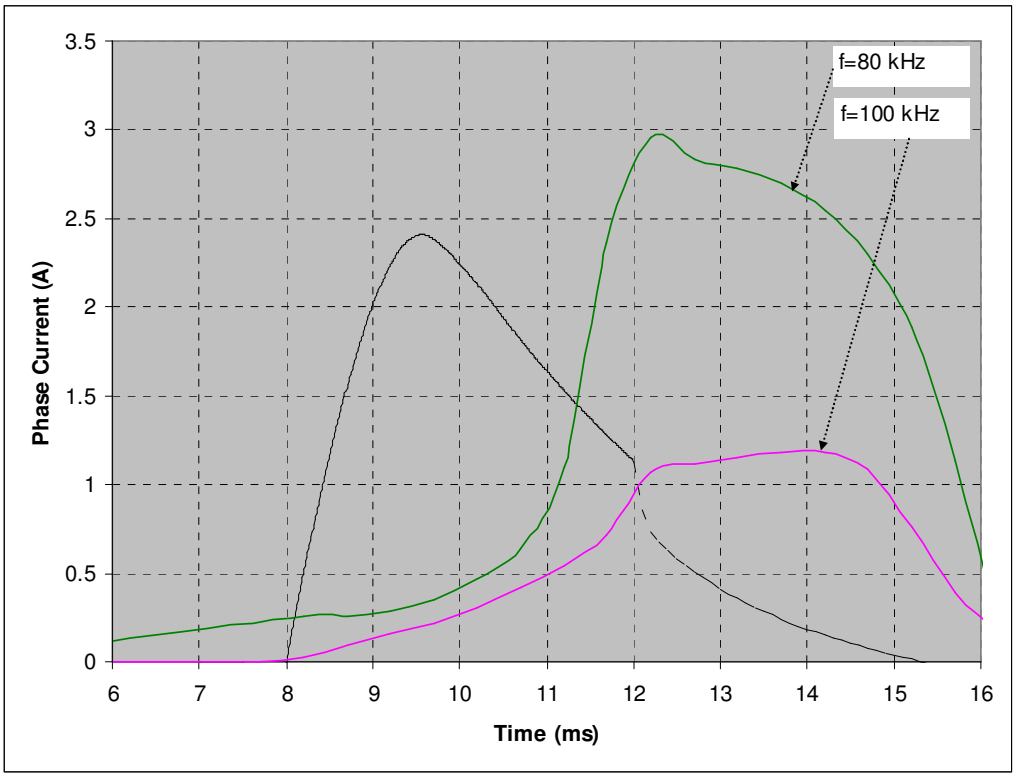

Figure 5.34 Current profiles for 80 kHz and 100 kHz.

The effect of changing the switching frequency of the switched capacitance circuit is obviously readable from the above figures, which show the change of the current profile with changing the frequency including the amplitude, the rise and fall times, the flatness of the top, and the advance angle, however the comments and detailed calculations are shown for a case study of the 1 kHz frequency as stated in section 5.4.2.5 (a).

The relation between the different parameters of the current profile and the switching frequency of the switched capacitance circuit could not be represented by neither a mathematical nor an empirical relation up to the end of this research, but it will be an interesting field of research for the future work.

The significant parameter according to which the switching frequency could be decided is the switching losses as if it goes to high levels with increasing the switching frequency it will severely affect the overall efficiency of the system besides the increased size and cost of the heat sinks associated to overcome the problems of overheating of the power semiconductor switches.

Figure 5.35 below shows the calculated switching losses for each switching frequency within the studied range.

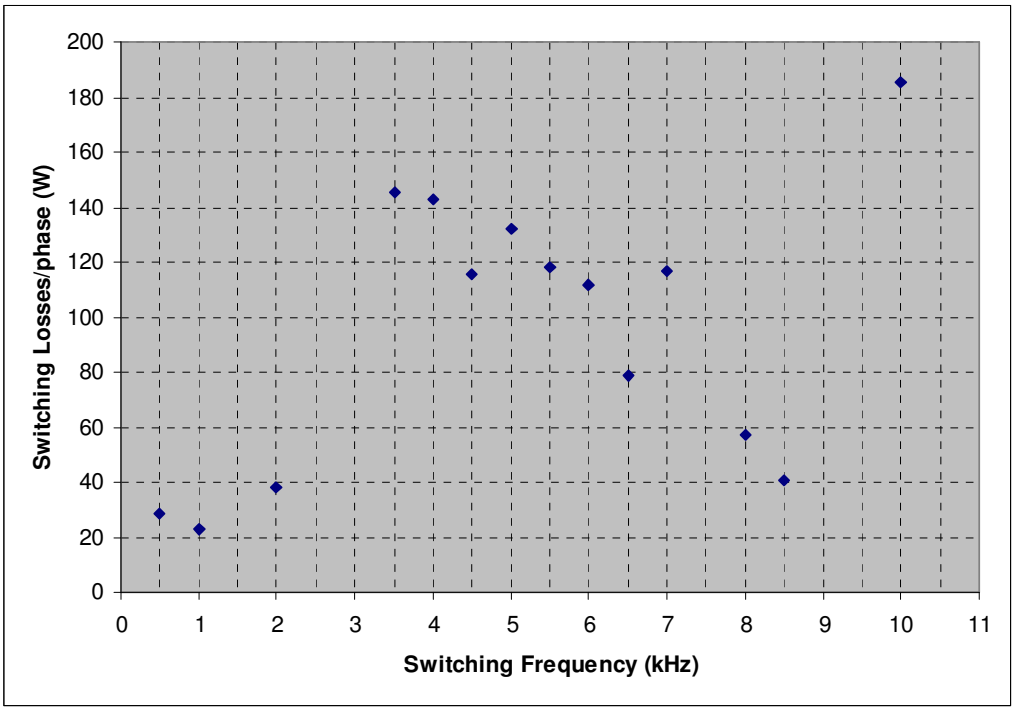

Figure 5.35 Switching losses in terms of the switching frequency.

According to the calculations of the switching losses and as it could be seen in Figure 5.35, the minimum switching losses occurs at the frequency f_s=1 kHz, hence it is selected as a case study for the comparisons and discussions above. The frequencies above 10 kHz are neglected as they have shown unacceptable levels of the switching losses compared with the power level of the drive system under consideration.

5.4.3 Two Phase Operation

The above discussion has been considering the single phase operation of the SRM in order to compare the influence of inserting the switched capacitance circuit on different parameters of the drive system, the single phase operation means that one phase of the machine is energised at a time, while the other phases are idle. But from the practical point of view, the single phase operation mode leads to high torque ripples which contribute to the acoustic noise, mechanical vibration, and velocity errors due to the

torque pulsation during the operation of the machine, therefore the two or multi-phase operation is recommended as one factor to reduce the torque ripples, the other factors are minimizing the hysteresis band of the current control loop and keeping the dwell angle constant over the operation range.

Therefore, simulation is repeated under the same conditions as before while allowing the phase currents to overlap.

The maximum limit of the overlap angle, θ_{omax}, could be calculated from equation 5.8 below. [1]

$$\theta_{o\max} = -\frac{2\pi}{P_r}\left(\frac{1}{2} - \frac{1}{q}\right) \qquad 5.8$$

Where; P_r is the number of rotor poles and q is the number of phases. The maximum overlap angle according to equation 5.8 is found to be 15°.

However, the overlap angle is adjusted to 9° and the simulation results for this case are shown in the following figures, where Figure 5.36 and Figure 5.37 are showing the phase currents and the developed torque respectively for the asymmetric converter without the SCC circuit while Figure 5.38 and Figure 5.39 are showing the phase currents and the developed torque respectively for the converter with the SCC at a switching frequency of 1 kHz. The significant factor to be monitored in this case is the influence of using the switched capacitance circuit on the torque ripples.

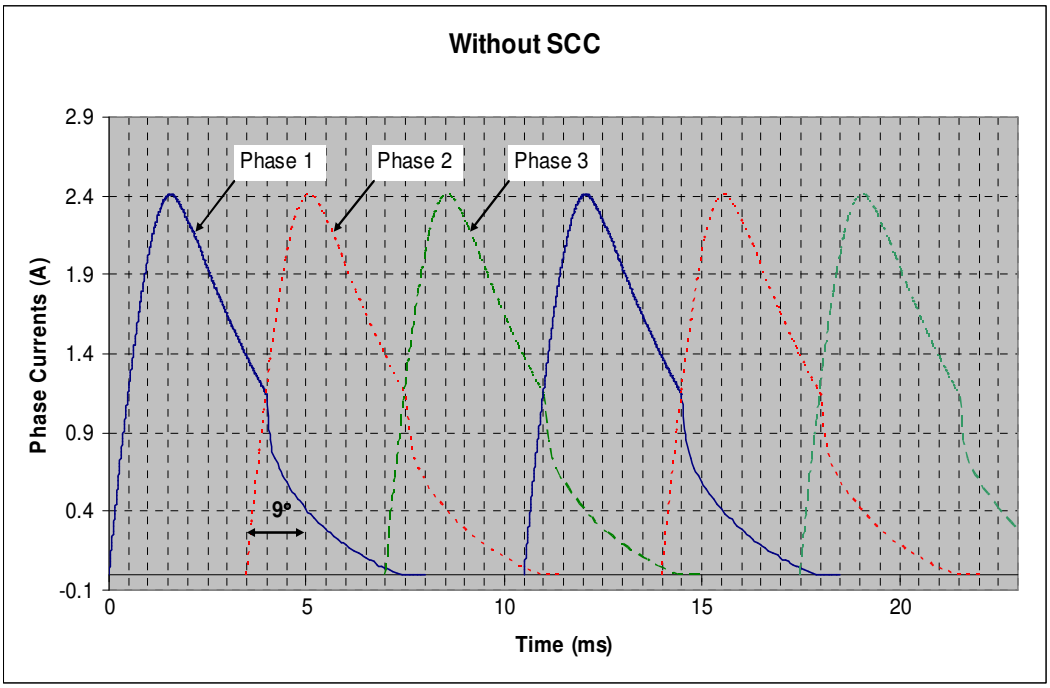

Figure 5.36 Phase Currents in case of overlap, without SCC.

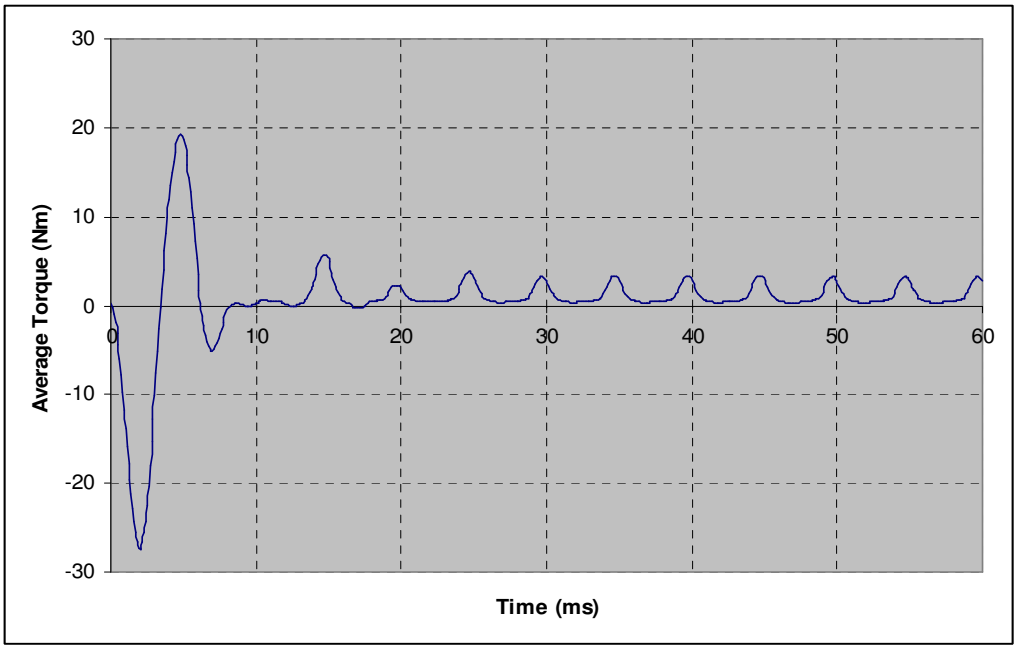

Figure 5.37 Developed torque in case of overlap, without SCC.

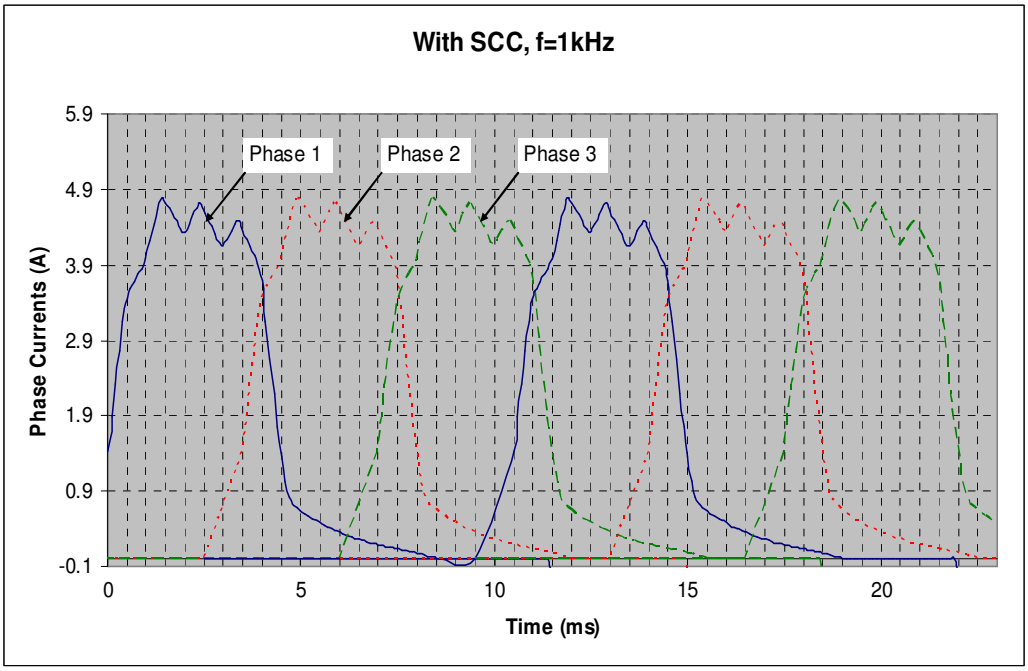

Figure 5.38 Phase Currents in case of overlap, using SCC.

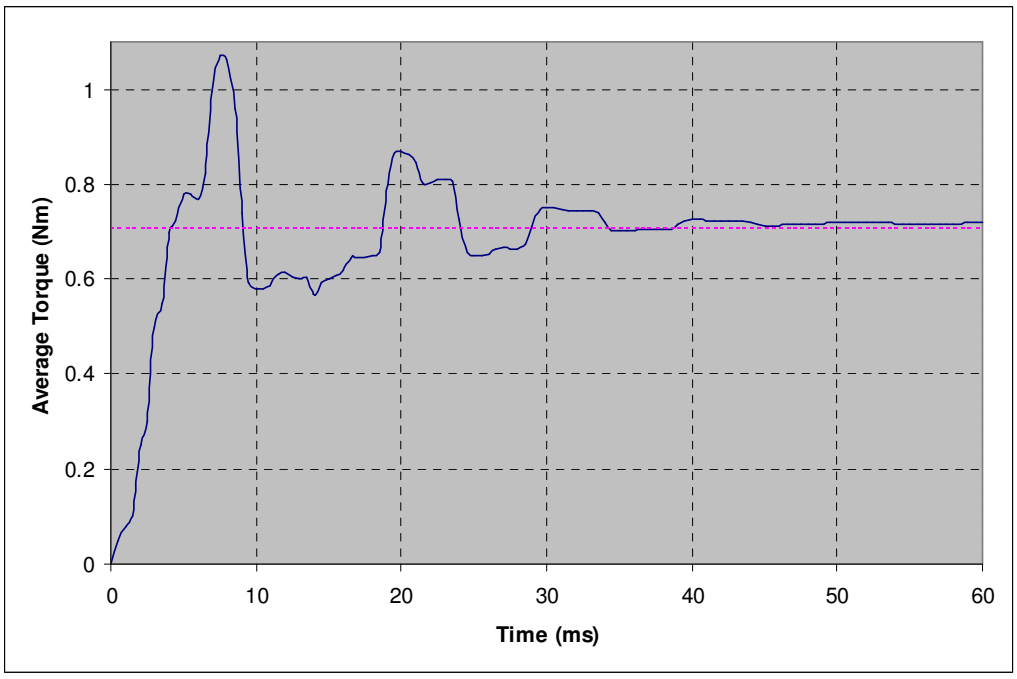

Figure 5.39 Developed torque in case of overlap, using SCC.

Referring to Figure 5.37 and Figure 5.39, where the average developed torques by the three-phase motor are shown in the continuous torque development mode, it could be seen obviously by comparing the two figures the effect of using the switched capacitance circuit in reducing the torque ripples at steady state. To calculate the torque ripples in the first case of Figure 5.37, the steady state period is zoomed in Figure 5.40, which shows a torque ripple (TR) of 2.15 Nm measured from the average value of the developed torque of 0.65 Nm.

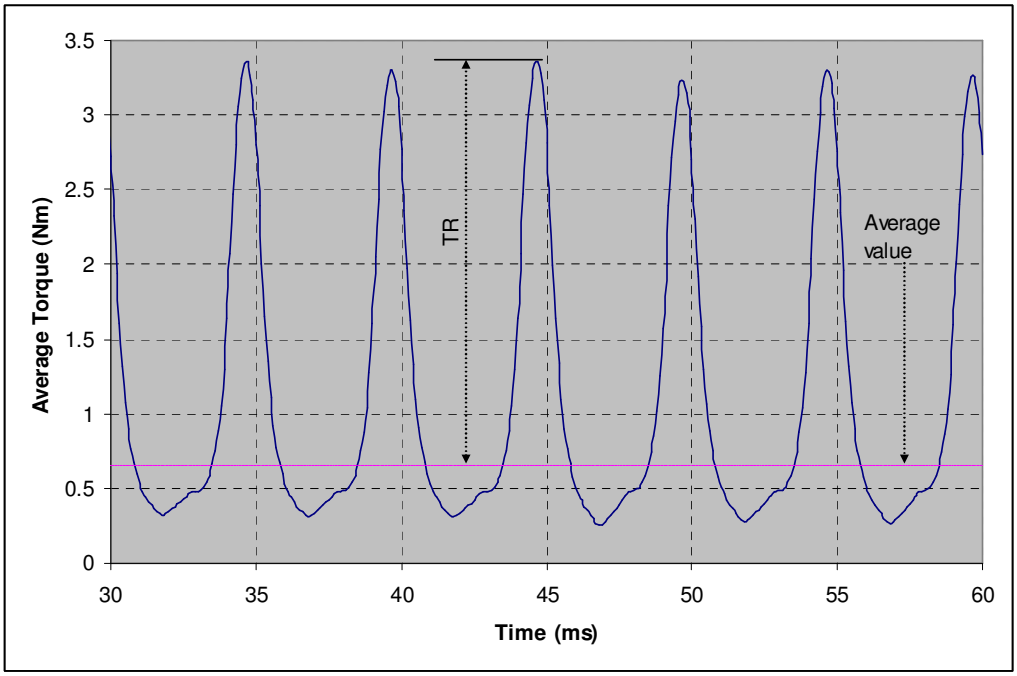

Figure 5.40 Torque ripples in asymmetric converter.

The following figures from Figure 5.41 to Figure 5.45 show the average torque developed by the switched reluctance motor for different switching frequencies of the switched capacitance circuit, the average torque is shown in dotted line in all figures.

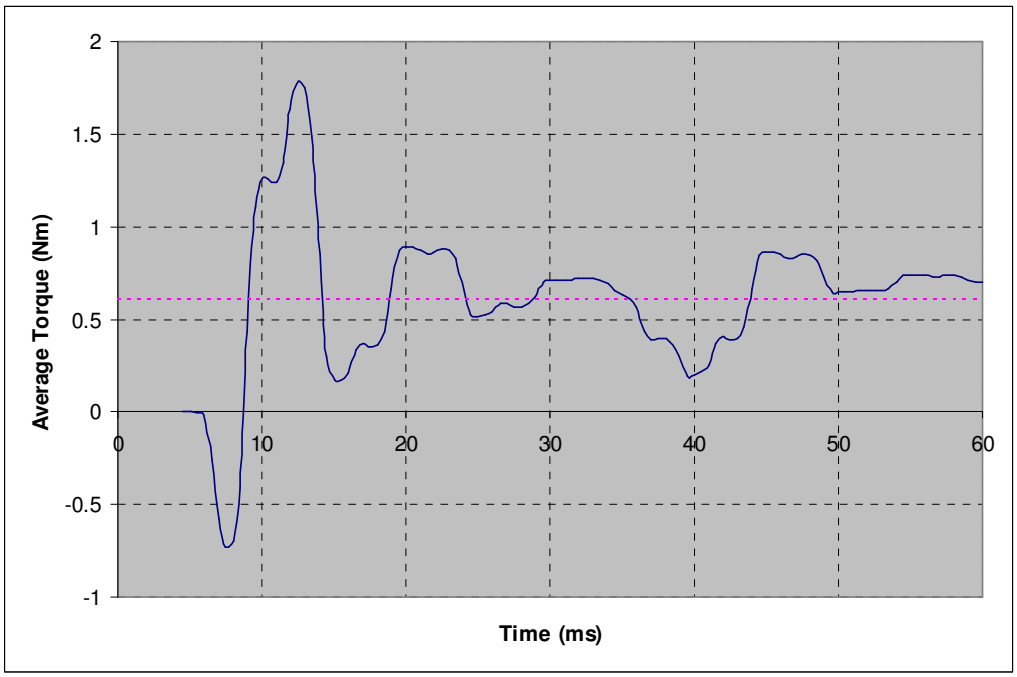

Figure 5.41 Developed torque at f=30 kHz.

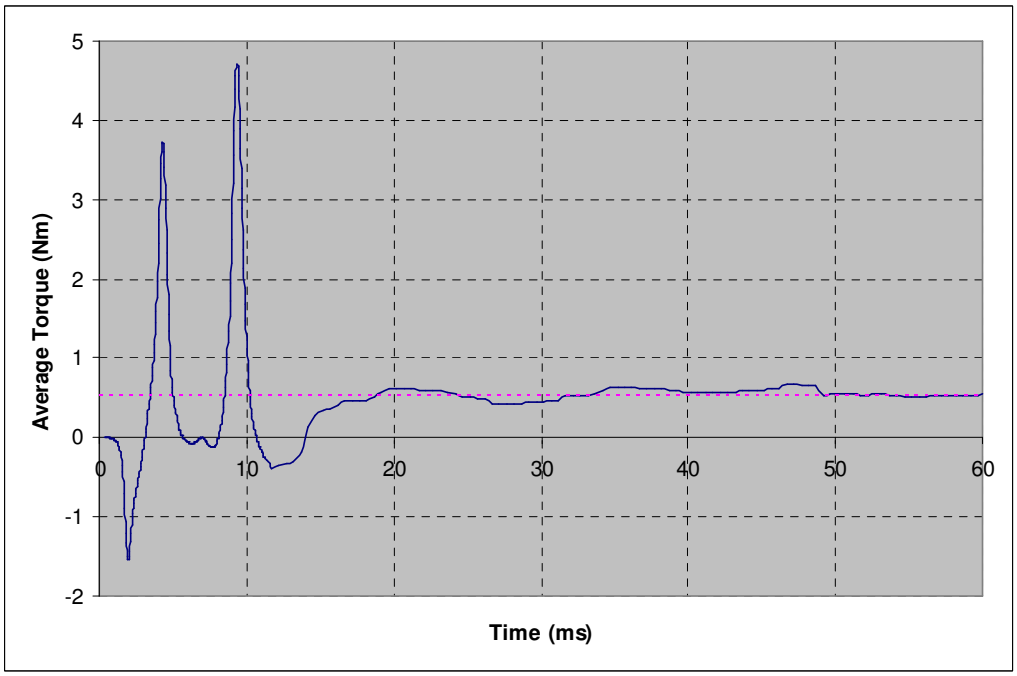

Figure 5.42 Developed torque at f=40 kHz.

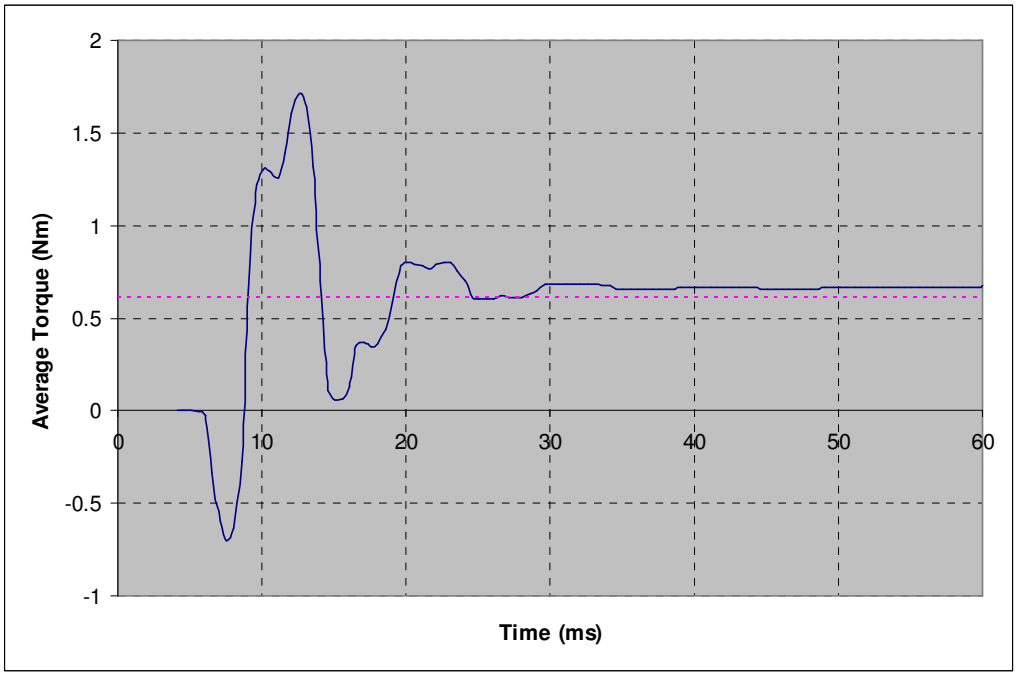

Figure 5.43 Developed torque at f=70 kHz.

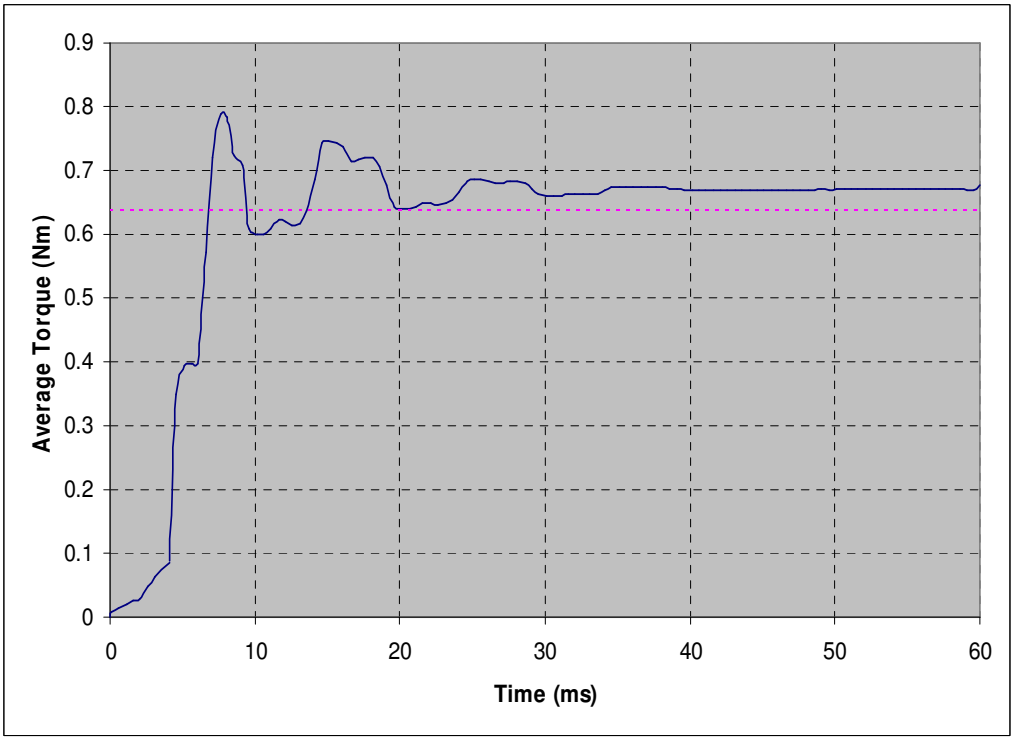

Figure 5.44 Developed torque at f=80 kHz.

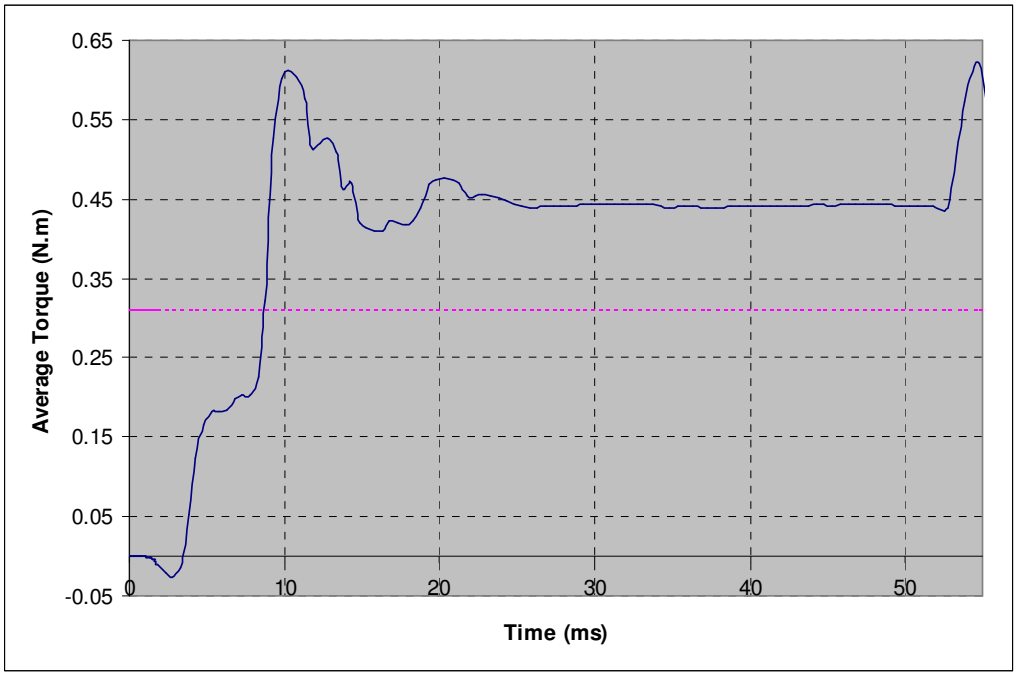

Figure 5.45 Developed torque at f=100 kHz.

The simulation results have shown a maximum torque ripple of 0.13 Nm which occurs at a switching frequency of 100 kHz compared with a peak torque ripple of 2.15 Nm in the case of the asymmetric converter before inserting the switched capacitance circuit.

The change in the magnetic characteristics of the switched reluctance motor due to the use of the switched capacitance driver circuit is shown in Figure 5.46 which indicates the increase in the output mechanical energy represented by the area enclosed by OABCO in the asymmetric converter case and the area enclosed by $OA_1B_1C_1O$ in the switched capacitance converter case.

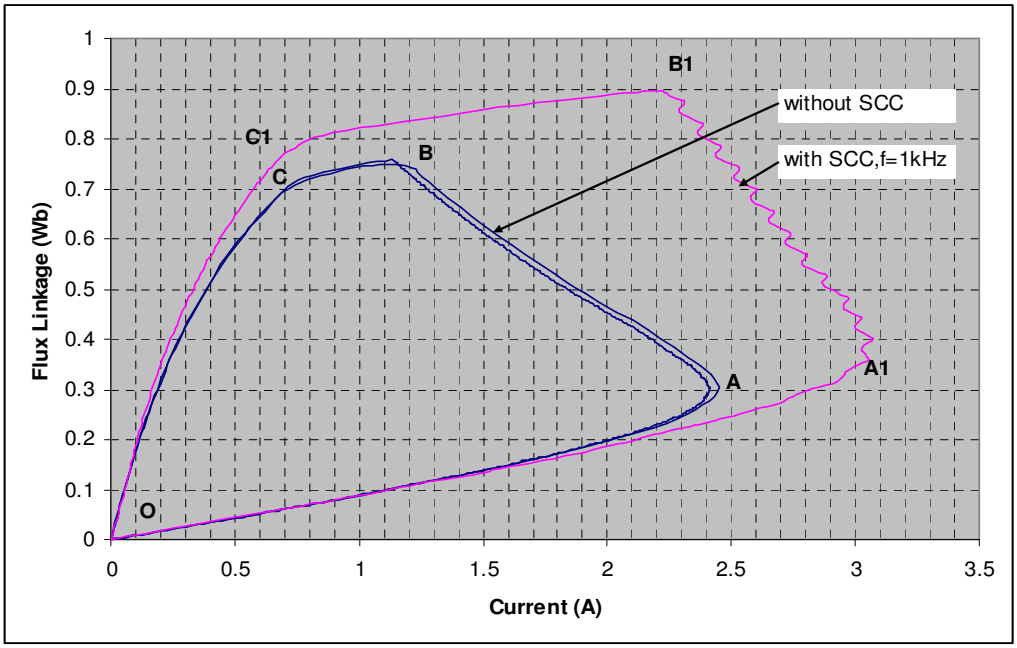

Figure 5.46 Flux Linkage versus Stator Current (Simulated).

The maximum increase in the output mechanical energy occurred at a frequency of 20 kHz under same operating conditions as shown in Figure 5.47 below.

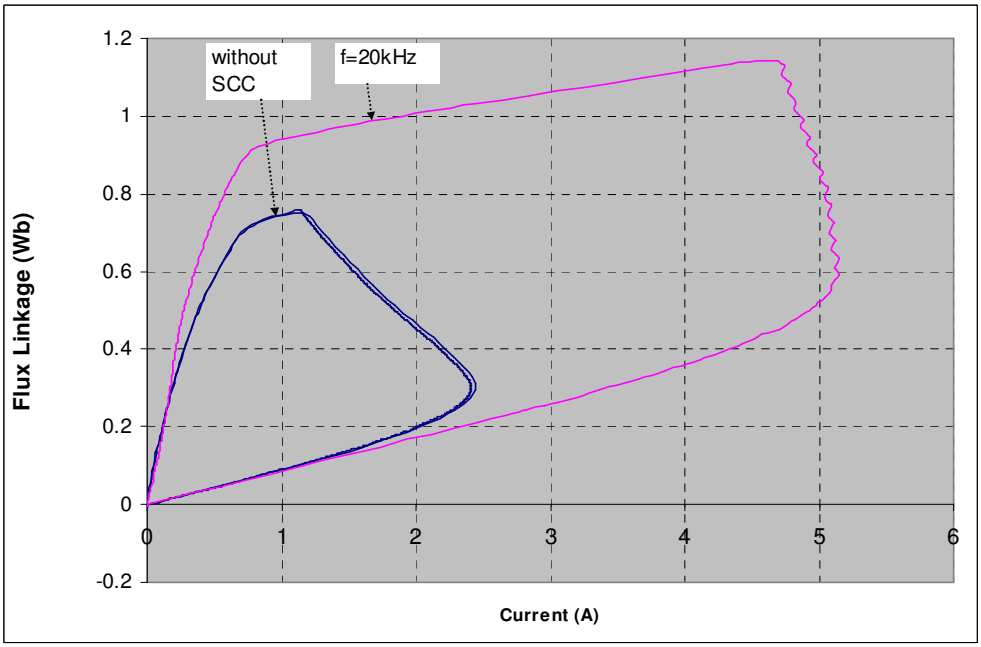

Figure 5.47 maximum increase in output energy at 20 kHz.

5.4.4 Double-Capacitance Double-Switch Circuit

The second topology of the switched capacitance circuit considered in this research is the double-capacitance double-switch circuit shown in Figure 5.48 below.

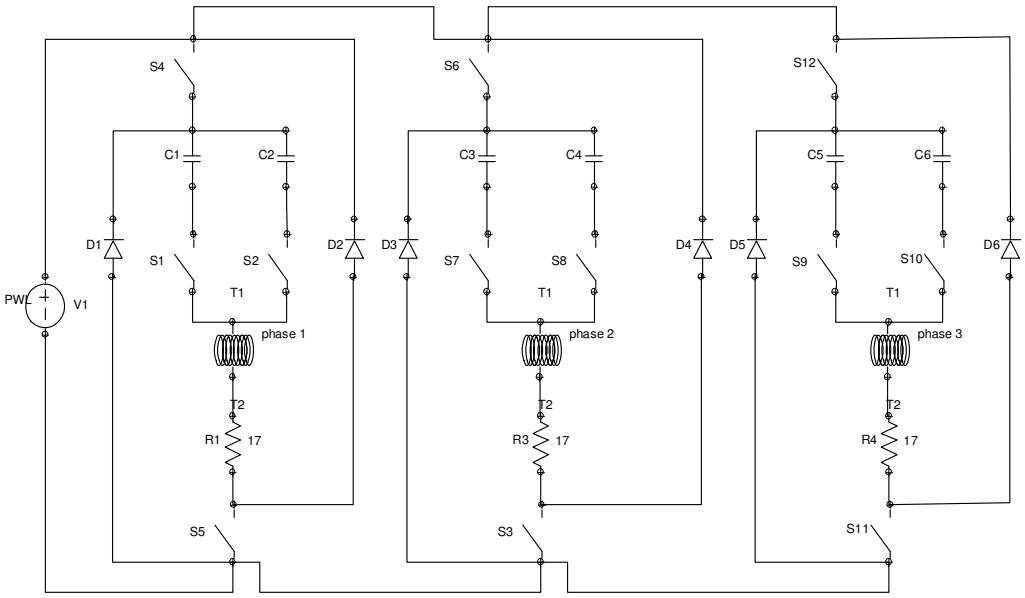

Figure 5.48 Double-Capacitance Double-Switch Circuit.

The double-capacitance double-switch circuit utilises two fixed capacitors instead of one in the case of single-capacitance double-switch circuit. The same procedure as the previous case is followed to calculate the effective capacitance and the values of the two fixed capacitors.

5.4.4.1 Determining the values of C_1 and C_2

Referring to Figure 4.7, it is shown that the relation between the effective capacitance, C_{eff} and the duty cycle, D in the case of double-capacitance double-switch circuit is a second order relation, which means there will be two possible values of D, for each value of C_{eff}.

As has been done in the case of single-capacitance double-switch circuit, the value of the fixed capacitor was calculated based on the value which resonates with the minimum motor inductance at the supply frequency. For the double-capacitance double switch case, the value of the capacitor C_1

is calculated to be less than or equal to the value which resonates with the maximum value of the inductance of the motor phase (this is the minimum value of the effective capacitance), while the value of the fixed capacitor C_2 is calculated so that the sum of C_1+C_2 is greater than or equal to the value of the capacitance which resonates with the minimum value of the phase inductance (this value is the maximum value of the effective capacitance).

The calculated values of the capacitances which resonate with the minimum and maximum values of the phase inductance at the supply frequency are 100 μF and 6 μF respectively.

5.4.4.2 Calculation of the duty cycle

Referring to equation 4.47 which states the relation between the effective capacitance, C_{eff} and the duty cycle, D, this equation can be re-written as follows:

$$C_{eff}\,\gamma\,D^2 + C_{eff}(1-D)^2 - C_2 = 0 \qquad 5.9$$

$$C_{eff}\,\gamma\,D^2 + C_{eff}(1-2D+D^2) - C_2 = 0 \qquad 5.10$$

$$C_{eff}\,\gamma\,D^2 + C_{eff} - 2C_{eff}D + C_{eff}D^2 - C_2 = 0 \qquad 5.11$$

$$C_{eff}(\gamma+1)D^2 + C_{eff} - 2C_{eff}D + (C_{eff} - C_2) = 0 \qquad 5.12$$

Equation 5.12 is a second order equation which can be solved for D, provided that the effective capacitance, C_{eff} and the values of the fixed capacitors C_1 and C_2 are known.

A simple program is written to solve equation 5.12 for each instantaneous value of C_{eff} to get the corresponding value of the duty cycle, D and provide it to the simulation software.

5.4.4.3 Simulation results of the DCDS drive circuit

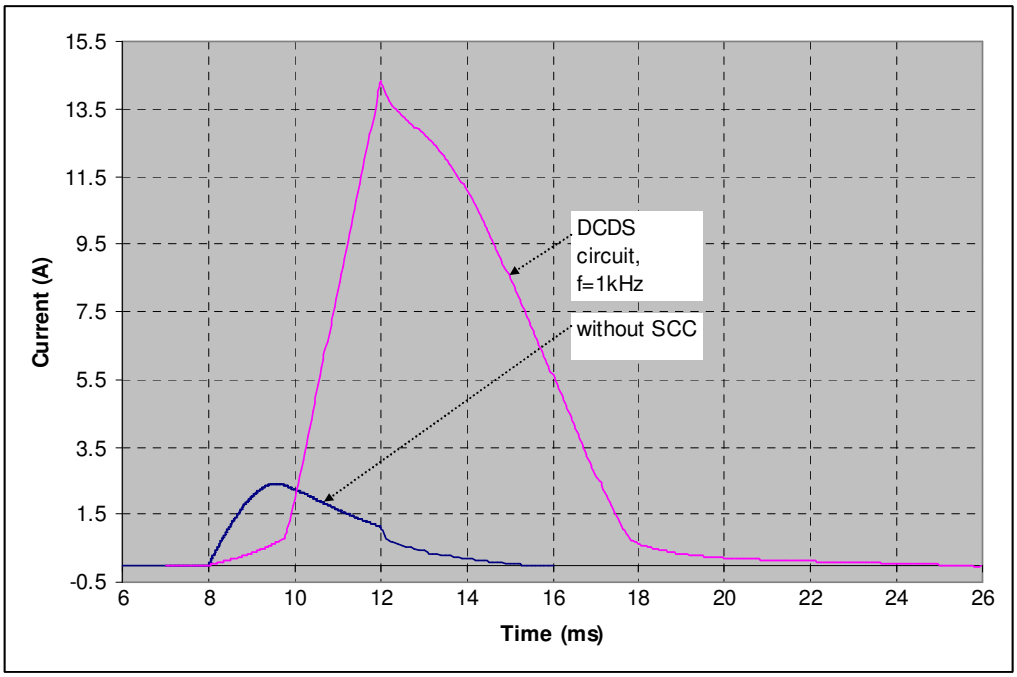

Figure 5.49 DCDS circuit for f=1 kHz.

Figure 5.49 shows the current profile resulting from the double-capacitance double-switch (DCDS) circuit compared with the current profile of the asymmetric converter without using the SCC.

The current in the case of the DCDS circuit at a switching frequency of 1 kHz reaches a peak of 14.5 A with a very bad characteristics with respect to the rise time and fall time.

The DCDS circuit didn't show encouraging results along the range of frequency between 1 kHz and 10 kHz, which is shown in Figure 5.50. As a matter of fact, the low controllability of the DCDS circuit is referred to the fact that there is always one capacitor at least has to be connected in series with the motor phase, unlike the SCDS case, where the capacitor can be expelled out of the loop by switching off the electronic switch in series with it, reverting the drive circuit back to the case of the asymmetric converter circuit, this gives more controllability to the SCDS circuit which is not available in the DCDS case.

The results have shown high current peaks with poor time-characteristics, high negative torque peaks, and deformation of the voltage and flux linkage of the motor phases besides an ohmic loss which is 5 times more than the SCDS drive circuit.

Not enough study of the double-capacitance double-switch circuit has been conducted in this research due to the expiration of the licence of the software used in carrying out the simulation, but it might be of interest in the future work.

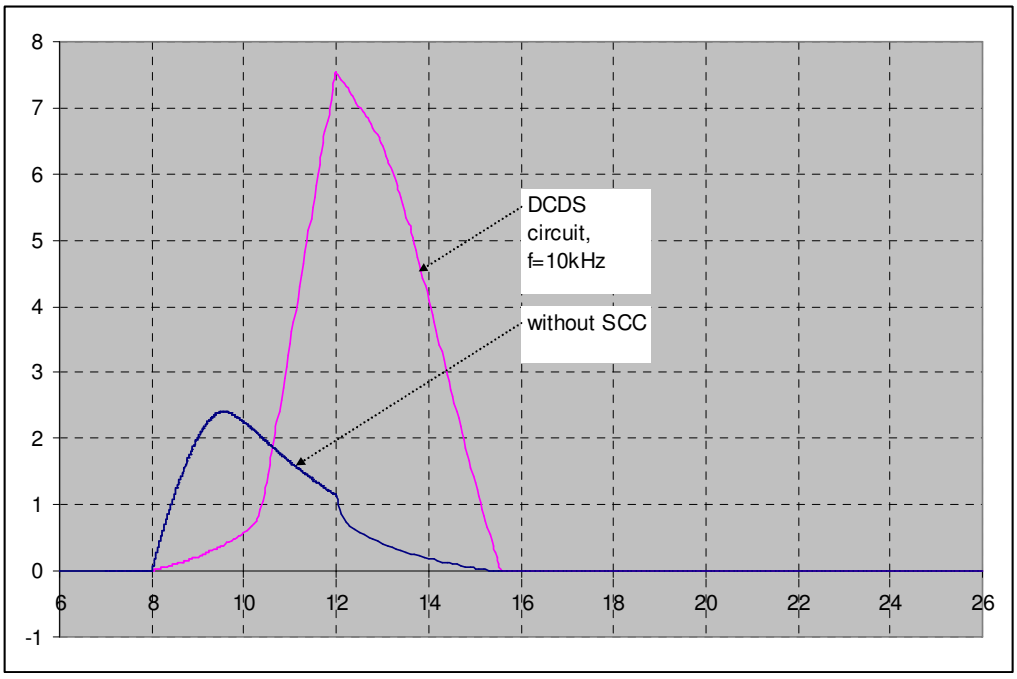

Figure 5.50 DCDS circuit for f=10 kHz.

Chapter 6
Conclusions and Future Work

6.1 Conclusions

This study has introduced the switched capacitance circuit as a new topology of a drive circuit of a three phase, 6/4 switched reluctance machine which hasn't been covered by any published research until the time when this thesis was completed.

The literature work considering the switched reluctance machine drive circuits has been critically reviewed in both the design of the switched reluctance machine and the design of its drive circuit topologies. Comparison of the most common drive circuit topologies has been held showing the major advantages and disadvantages of each topology together with its major field of application. The literature review showed that no research has been conducted on the application of the switched capacitance circuit in the field of switched reluctance machine drive circuits.

The analysis and mathematical evaluation of the switched capacitance circuit as a variable capacitor has been developed for two cases, which are the single-capacitance double-switch case and the double-capacitance double-switch case which have been introduced as drive circuits of the switched reluctance motor in this research and the relation between the effective capacitance and the duty cycle has been derived for both cases.

Other topologies of the switched capacitance circuits which utilise more than two switches have been introduced in brief, besides those topologies of the switched capacitance circuits based on resonance energy transfer concept.

The latter two topologies were not discussed in details for economical and design considerations of the drive circuits, as for example, if the single-capacitor, triple-switches switched capacitance circuit is considered as a drive circuit of a three-phase switched reluctance motor, this will add extra nine switches and three capacitors to the conventional drive circuit with their drive circuits and heat sinks which will contribute significantly to the increase in size and weight of the drive system, besides the increase in the switching losses associated. For these reasons, only the single-capacitance double-switch and the double-capacitance double-switch were considered in details.

The mathematical derivation of the characteristics of both topologies proved the behaviour of the switched capacitance circuit as a variable capacitor in direct relation with the duty cycle of the power electronic switch which gives an advantage of the new drive circuit topology which uses the switched capacitance circuit as a variable capacitor to track the variation of the phase inductance enabling a significant change of the phase current profile with respect to the fall and rise times, the pulse duration, and the amplitude.

In the literature, each one of the previous parameters of the phase current pulse is controlled separately through certain techniques to meet the requirement of a certain application, for example, to maximise the developed torque, it is required to increase the dwell angle, which in contradiction, decreases the overall efficiency of the drive system, also for optimum operation, the dwell angle may be changed which leads to higher torque ripples.

On the other hand, hysteresis current controller is usually used to keep the current pulse flat topped.

The new technique of the switched capacitance circuit enables the control f the phase current pulse to change its amplitude, its flat top, and its rise and fall times all in one technique which gives an important advantage to this research.

The characteristics of the switched capacitance circuit as a variable capacitor has been verified experimentally and the characteristic curves have been compared with the theoretical ones for both cases of the switched capacitance circuits discussed in the theoretical part of the study. The comparison showed an excellent agreement between the theoretical and the practical behaviour of the switched capacitance circuit as a variable capacitor if the reading errors and the measuring instruments tolerance are taken into consideration.

The switched capacitance circuit has been imposed to the conventional asymmetric converter as it is the most common converter topology which is used in many SRM applications. It has been found to be an effective way of shaping the phase current profile which gives a significant advantage of this research. The literature showed that the principal of torque control of the switched reluctance motor depends on one of two methods, either controlling the amplitude of the phase current or changing the dwell angle. The simulation results has proven that the switched capacitance circuit allows control over both the current amplitude and the dwell angle both in one technique.

By reviewing the different software programmes used to model and simulate the SRM drive systems, there were few alternatives to be used in this research, these were Pspice, MATLAB or one of the special purpose software packages which have been recently developed. At the early stage of the research, a full model of the motor with its conventional asymmetric converter has been constructed using MATLAB –Simulink, few figures of this model is shown in the appendix.

The limitation of the MATLAB model is represented in the following major points:

- The switched reluctance machine model on MATLAB is idealised specially with respect to the phase inductance where it is represented by five linear segments summed together to give the ideal profile of the phase inductance, this might be a good approximation for a controller design, but in our case, the inductance value was very important to be accurate as it is the

main parameter used to decide the value of the effective capacitance to resonate with it at the supply frequency.

- The power electronics part of the drive system couldn't be modelled on MATLAB, such as the power supply, and the converter circuit. Also, there was a necessary need to access the component levels of the drive circuit to examine the effect of different operating conditions on each passive and power electronic component in the circuit.

The second alternative was the Pspice, but due to the fact that it is only few researches in the literature which used Pspice to model a switched reluctance machine no serious attempts were undertaken to use it in this research.

The third alternative was the special purpose software packages specially developed to model and simulate the switched reluctance motor with its full drive and control system.

As a first option the PC-SRD software developed by professor T. J. Miller and his team in Glasgow University was selected, but due to budget limitations, it was not possible to use it in this research.

The SRM with its complete drive circuit has been modelled utilising the Magnet software which allowed accurate modelling of the machine geometry and magnetic characteristics besides the PSPICE-complying models of the passive components and power electronic switches of the drive circuit provided by its circuit modeller.

The simulation results of the single-capacitance double-switch drive circuit has shown a very encouraging results which allows control over the phase current wave shape and peak, which contributes significantly to the mechanical output energy of the motor and hence the overall efficiency as well as a significant enhancement in the torque ripples.

Simulation of the single-capacitance double-switch circuit has been carried out to for a wide range of switching frequencies in an attempt to achieve an empirical relation between the switching frequency and the different significant parameters of the phase current profile.

However, to decide the optimum switching frequency of the switched capacitance circuit, a compromise has to be done between the switching losses which increase with increasing the switching frequency and the total current harmonic distortion which decreases with increasing the switching frequency. The use of a current limiter might be a good solution of this problem.

The single-capacitance double-switch converter circuit would be a perfect solution for SRM applications which require a high starting torque, where the capacitor might be inserted in the circuit at the starting transient period, then it could be expelled out of the circuit during normal operation.

Also, it is suitable for high speed applications due to its positive effect on building up the phase current and improving its transient response at both the turn-on and turn-off periods.

The double-capacitance double-switch drive circuit didn't show encouraging results compared with the single-capacitance one, as it has shown high current peaks with negative torque peaks which significantly reduces the average developed torque besides the low controllability due to the permanent existence of at least one capacitor connected in series with the machine phase. However, more research is required to be conducted on such a topology for more validation.

6.2 Future work

The following points might be of great interest for future work related to the utilisation of switched capacitance circuit as a drive system of the switched reluctance machines:

- More analysis and research has to be conducted to find an empirical or a mathematical relation between the switching frequency of the switched capacitance circuit and the various parameters of the resulting current profile, such as the rise and fall times, the peak value, and the average or RMS value.
- Also, It is desired to undertake more research on the reduction of the current harmonic content associated with the insertion of the switched

capacitance circuit within the converter in order to keep the THD as low as possible.

- More research on the DCDS topology has to be conducted to validate its performance. One suggestion is to use the DCDS to resonate in parallel with the phase inductance so that it could be expelled out of the circuit at any instant when that is desired.
- The switched capacitance circuit can be introduced to other converter topologies of the SRM drivers such as the resonant converter topology which has been confirmed to show discouraging results in [1] in order to enhance its performance.

References

[1] R. Krishnan, *Switched Reluctance Motor Drives : Modeling, Simulation, Analysis, Design, and Applications.* Boca Raton, FL: CRC Press, 2001, pp. 398.

[2] T. J. E. Miller, *Electronic Control of Switched Reluctance Machines.* Oxford: Newnes, 2001, pp. 272.

[3] T. J. E. Miller, "Optimal design of switched reluctance motors," *IEEE Trans. Ind. Electron.,* vol. 49, pp. 15-27, 02/. 2002.

[4] K. Nakamura, T. Ono, H. Goto, T. Watanabe and O. Ichinokura, "A novel switched reluctance motor with wound-cores put on stator and rotor poles," *IEEE Trans. Magn.,* vol.
41, pp. 3919-3921, 2005.

[5] S. Song, W. Liu and Y. Wang, "Modeling, dynamic simulation and control of a four-phase switched reluctance motor," in *2007 IEEE International Conference on Control and Automation, ICCA,* 2008, pp. 1290-1295.

[6] S. Song, W. Liu and Y. Wang, "Modeling, dynamic simulation and control of a four-phase switched reluctance motor," in *2007 IEEE International Conference on Control and Automation, ICCA,* 2008, pp. 1290-1295.

[7] J. H. Leong, "Design consideration and implementation of switched reluctance motor drive," in *2002 Student Conference on Research and Development. SCOReD2002. Proceedings. Global Research and Development in Electrical and Electronics Engineering, 16-17 July 2002,* 2002, pp. 196-9.

[8] G. Rim and R. Krishnan, "Variable speed constant frequency power conversion with a switched reluctance machine," in *Proceedings of 1994 IEEE Applied Power Electronics Conference and Exposition - ASPEC'94, 13-17 Feb. 1994,* 1994, pp. 63-71.

[9] J. Choi, T. H. Kim, Y. Kim, S. Lim, S. Lee, Y. Kim and J. Lee, "The finite element analysis of switched reluctance motor considering asymmetric bridge converter and DC link voltage ripple," *IEEE Trans. Magn.,* vol. 41, pp. 1640-1643, 2005.

[10] S. Paramasivam, R. Arumugan, B. Umamaheswari, S. Vijayan, S. Balamurugan and G. Venkatesan, "Accurate rotor position estimation for switched reluctance motor using ANFIS," in *IEEE TENCON 2003. Conference on Convergent Technologies for the Asia-Pacific Region, 15-17 Oct. 2003,* 2003, pp. 1493-7.

[11] N. H. Fuengwarodsakul, R. W. De Doncker and R. B. Inderka, "Simulation model of a switched reluctance drive in 42 V application," in *IECON'03. 29th Annual Conference of the IEEE Industrial Electronics Society, 2-6 Nov. 2003,* 2003, pp. 2871-6.

[12] D. N. Essah and S. D. Sudhoff, "An improved analytical model for the switched reluctance motor," *IEEE Trans. Energy Convers.,* vol. 18, pp. 349-356, 2003.

[13] B. P. Loop and S. D. Sudhoff, "Switched reluctance machine model using inverse inductance characterization," in *Proceedings of 2002 IEEE Industry Applications Society Annual Meeting, 13-18 Oct. 2002,* 2002, pp. 13-21.

[14] J. H. Chen, K. T. Chau, Q. Jiang, C. C. Chan and S. Z. Jiang, "Modeling and analysis of chaotic behavior in switched reluctance motor drives," in *Proceedings of the 2000 Power Electronics Specialist Conference, 18-23 June 2000,* 2000, pp. 1551-6.

[15] K. T. Chau and J. H. Chen, "Analysis of chaotic behavior in switched reluctance motors using current hysteresis regulation," *Electric Power Components and Systems,* vol. 30, pp. 607-24, 06/. 2002.

[16] H. Le-Huy and G. Sybille, "MATLAB/Simulink and PSpice as modelling tools for power systems and power electronics," in *Proceedings of the 2000 Power Engineering Society Summer Meeting, Jul 16-20 2000,* 2000, pp. 766-767.

[17] H. Chen, J. Jiang, S. Sun and D. Zhang, "Dynamic simulation models of switched reluctance motor drivers," in *Proceedings of the 3th World Congress on Intelligent Control and Automation, Jun 28-Jul 2 2000,* 2000, pp. 2111-2115.

[18] H. Chen, X. Meng and L. Zheng, "Design and simulation software package of switched reluctance machine systems for windows 9x in english,"

in *2000 IEEE Asia-Pacific Conference on Circuits and Systems: Electronic Communication Systems, Dec 4-6 2000,* 2000, pp. 489-492.

[19] Chong-Chul Kim, Jin Hur and Dong-Seok Hyun, "Simulation of a switched reluctance motors using Matlab/M-file," in *28th Annual Conference of the IEEE Industrial Electronics Society, 5-8 Nov. 2002,* 2002, pp. 1066-71.

[20] G. Gallegos-Lopez, P. C. Kjaer, T. J. E. Miller and G. W. White, "Simulation study of resonant DC link inverter for current-controlled switched reluctance motors," in *Proceedings of the 1997 2nd International Conference on Power Electronics and Drive Systems, PEDS. Part 2 (of 2), may 26-29 1997,* 1997, pp. 757-761.

[21] K. N. Srinivas and R. Arumugam, "Circuit simulation of dynamic performances of the switched reluctance motor," in *Proceedings of IEEE Region 10 International Conference on Electrical and Electronic Technology, 19-22 Aug. 2001,* 2001, pp. 592-6.

[22] H. Chen, J. Jiang, D. Zhang and S. Sun, "Models and simulation of the switched reluctance motor drive with the microcomputer control based on MATLAB software package," in *IEEE APCCAS 2000. 2000 IEEE Asia-Pacific Conference on Circuits and Systems. Electronic Communication Systems. Proceedings, 4-6 Dec. 2000,* 2000, pp. 493-6.

[23] F. Soares and P. J. Costa Branco, "Simulation of a 6/4 switched reluctance motor based on Matlab/Simulink environment," *IEEE Trans. Aerospace Electron. Syst.,* vol. 37, pp. 989-1009, 07/. 2001.

[24] O. Ichinokura, S. Suyama, T. Watanabe and H. J. Guo, "A new calculation model of switched reluctance motor for use on spice," in *8th Joint Magnetism and Magnetic Materials -International Magnetic Conference-(MMM-Intermag), Jan 7-11 2001,* 2001, pp. 2834-2836.

[25] J. Faiz, J. Raddadi and J. W. Finch, "Spice-based dynamic analysis of a switched reluctance motor with multiple teeth per stator pole," *IEEE Trans. Magn.,* vol. 38, pp. 1780-8, 07/. 2002.

[26] J. Mahdavi, G. Suresh, B. Fahimi and M. Ehsani, "Dynamic modeling of non-linear SRM drive with pspice," in *Proceedings of the 1997 IEEE Industry Applications Conference 32nd IAS Annual Meeting. Part 1 (of 3), Oct 5-9 1997,* 1997, pp. 661-667.

[27] G. Franceschini, S. Pirani, M. Rinaldi and C. Tassoni, "SPICE-assisted simulation of controlled electric drives: an application to switched reluctance drives," *IEEE Trans. Ind. Appl.,* vol. 27, pp. 1103-10, 11/. 1991.

[28] M. G. Giesselmann, "Dynamic modeling of switched reluctance machines with PSpice for windows," in *Proceedings of the 1996 31st Intersociety Energy Conversion Engineering Conference. Part 1 (of 4), Aug 11-16 1996,* 1996, pp. 298-303.

[29] Chang-Chou Hwang and J. N. Lou, "Transient analysis of capacitance switching for industrial power system by PSpice," *Electr. Power Syst. Res.,* vol. 45, pp. 29-38, 04/. 1998.

[30] I. Moson, K. Iwan and J. Nieznanski, "Circuit-oriented model of the switched reluctance motor for drive systems simulation," in *28th Annual Conference of the IEEE Industrial Electronics Society, 5-8 Nov. 2002,* 2002, pp. 497-501.

[31] C. Pollock and A. Michaelides, "Switched reluctance drives: A comparative evaluation," *Power Eng J,* vol. 9, pp. 257-266, 1995.

[32] J. Oyama, T. Higuchi, T. Abe, K. Haraguchi, E. Yamada and F. Profumo, "Hybrid type novel switched reluctance motor," in *Proceedings of Power Electronics Specialist Conference - PESC'98, 17-22 may 1998,* 1998, pp. 857-63.

[33] P. Rafajdus, V. Hrabovcova, M. Liptak and I. Zrak, "New design of switched reluctance motor for improving its efficiency," in *16th International Conference on Electrical Machines. Conference Proceedings, 5-8 Sept. 2004,* 2004, pp. 6.

[34] M. A. El-Khazendar and J. M. Stephenson, "Analysis and optimisation of the 2-phase self-starting switched reluctance motor," in *ICEM '86 Munchen. International Conference on Electrical Machines, 8-10 Sept. 1986,* 1986, pp. 1031-4.

[35] Mi-Ching Tsai, Chien-Chin Huang and Zheng-Yi Huang, "A new two-phase homopolar switched reluctance motor for electric vehicle applications," *J Magn Magn Mater,* vol. 267, pp. 173-81, 12/. 2003.

[36] Shang-Hsun Mao and Mi-Ching Tsai, "A novel switched reluctance motor with C-core stators," *IEEE Trans. Magn.,* vol. 41, pp. 4413-20, 12/. 2005.

[37] Y. Ozoglu, M. Garip and E. Mese, "New pole tip shapes mitigating torque ripple in short pitched and fully pitched switched reluctance motors," *Electr. Power Syst. Res.,* vol. 74, pp. 95-103, 2005.

[38] Jin Woo Lee, Hong Seok Kim, Byung Il Kwon and Byung Taek Kim, "New rotor shape design for minimum torque ripple of SRM using FEM," *IEEE Trans. Magn.,* vol. 40, pp. 754-7, 03/. 2004.

[39] Geun-Hie Rim, Won-Ho Kim, Eun-Soo Kim and Ki-Chul Lee, "A choppingless converter for switched reluctance motor with unity power factor and sinusoidal input current," in *Proceedings of 1994 Power Electronics Specialist Conference - PESC'94, 20-25 June 1994,* 1994, pp. 500-7.

[40] R. C. Becerra, M. Ehsani and T. J. E. Miller, "Commutation of SR motors," *IEEE Transactions on Power Electronics,* vol. 8, pp. 257-263, 1993.

[41] R. Krishnan and P. N. Materu, "Analysis and design of a low-cost converter for switched reluctance motor drives," *IEEE Trans. Ind. Appl.,* vol. 29, pp. 320-7, 03/. 1993.

[42] A. Hava, V. Blasko and T. A. Lipo, "A modified C-dump converter for variable reluctance machines," in *Conference Record of the 1991 IEEE Industry Applications Society Annual Meeting (Cat. no.91CH3077-5), 28 Sept.-4 Oct. 1991,* 1991, pp. 886-9.

[43] S. Mir, I. Husain and M. E. Elbuluk, "Energy-efficient C-dump converters for switched reluctance motors," *IEEE Transactions on Power Electronics,* vol. 12, pp. 912-921, 1997.

[44] King-Jet Tseng, Shuyu Cao and Jijiu Wang, "A new hybrid C-dump and buck-fronted converter for switched reluctance motors," *IEEE Trans. Ind. Electron.,* vol. 47, pp. 1228-36, 12/. 2000.

[45] S. -. Park and T. A. Lipo, "New series resonant converter for variable reluctance motor drive," in *PESC '92 Record. 23rd Annual IEEE Power Electronics Specialists Conference (Cat. no.92CH3163-3), 29 June-3 July 1992,* 1992, pp. 833-8.

[46] A. Hava, J. Wacknov and T. A. Lipo, "New ZCS resonant power converter topologies for variable reluctance machine drives," in *Proceedings of IEEE Power Electronics Specialist Conference - PESC '93, 20-24 June 1993,* 1993, pp. 432-9.

[47] Anonymous (1997, Digital signal processing solutions for the switched reluctance motor. Texas Instruments Europe, Available: http://focus.ti.com/lit/an/bpra058/bpra058.pdf

[48] Mohamed, A. A. Morsy, "Design and Implementation of Fuzzy Sliding Mode Controller for Switched Reluctance Motor," 2007.

[49] J. M. Stephenson and J. Corda, "Computation of torque and current in doubly salient reluctance motors from nonlinear magnetisation data," *Proceedings of the Institution of Electrical Engineers,* vol. 126, pp. 393-6, 05. 1979.

[50] D. Panda and V. Ramanarayanan, "A composite control strategy for sensorless and low-noise operation of switched reluctance motor drive," in *Proceedings of World Congress on Industrial Applications of Electrical Energy and 35th IEEE-IAS Annual Meeting, 8-12 Oct. 2000,* 2000, pp. 1751-8.

[51] B. Fahimi, A. Emadi and R. B. Sepe Jr., "Four-quadrant position sensorless control in SRM drives over the entire speed range," *IEEE Transactions on Power Electronics,* vol. 20, pp. 154-163, 2005.

[52] G. Gallegos-Lopez, P. C. Kjaer and T. J. E. Miller, "High-grade position estimation for SRM drives using flux linkage/current correction model," in *Conference Record of 1998 IEEE Industry Applications Conference. Thirty-Third IAS Annual Meeting, 12-15 Oct. 1998,* 1998, pp. 731-8.

[53] P. C. Kjaer, J. J. Gribble and T. J. E. Miller, "High-grade control of switched reluctance machines," *IEEE Trans. Ind. Appl.,* vol. 33, pp. 1585-93, 11/. 1997.

[54] A. D. Cheok and N. Ertugrul, "Computer-based automated test measurement system for determining magnetization characteristics of switched reluctance motors," *IEEE Transactions on Instrumentation and Measurement,* vol. 50, pp. 690-6, 06/. 2001.

[55] I. H. Al-Bahadly, "Analysis of position estimation method for switched reluctance drives," in *Proceedings First IEEE International Workshop on Electronic Design, Test and Applications '2002, 29-31 Jan. 2002,* 2002, pp. 262-6.

[56] H. Vasquez, J. Parker and T. Haskew, "Control of a 6/4 switched reluctance motor in a variable speed pumping application," *Mechatronics,* vol. 15, pp. 1061-1071, 2005.

[57] M. T. DiRenzo, M. K. Masten and C. P. Cole, "Switched reluctance motor control techniques," in *Proceedings of the 1997 American Control Conference. Part 1 (of 6), Jun 4-6 1997,* 1997, pp. 272-277.

[58] P. Vas, *Artificial-Intelligence-Based Electrical Machines and Drives : Application of Fuzzy, Neural, Fuzzy-Neural and Genetic-Algorithm-Based Techniques.* UK: Oxford University Press, 1999, pp. 625.

[59] W. Ding and D. Liang, "Modeling of a 6/4 switched reluctance motor using adaptive neural fuzzy inference system," *IEEE Trans. Magn.,* vol. 44, pp. 1796-1804, 2008.

[60] B. Mirzaeian, M. Moallem, V. Tahani and C. Lucas, "Multiobjective optimization method based on a genetic algorithm for switched reluctance motor design," *IEEE Trans. Magn.,* vol. 38, pp. 1524-1527, 2002.

[61] W. H. Koch, "A Novel Excitation for the Control of Stand Alone Induction Generators," 1984.

[62] Muhammad Riaz, "Novel Switched Reluctance Motor Drive Systems," *Thesis,* 1985.

[63] BELA, E. F. KARSA, "Analysis of A.C. waveforms harmonic analysis," in *Electrical Measuring Instruments and Measurements* Anonymous BUDAPEST: AKADEMIAI KIADO, 1967, pp. 783-789.

[64] Muhammad H. Rashid, *Power Electronics Circuits, Devices, and Applications.* ,3rd ed.USA: Pearson Education International, Printice Hall, 2004, pp. 880.

[65] N. Mohan, *Power Electronics Converters, Applications and Design.* ,2nd ed.New York: John Wiley & Sons, Inc., 1995, pp. 802.

[66] B. W. Williams, *Power Electronics Devices, Drives, Applications and Passive Components.* ,2nd ed.Hong Kong: Macmillan, 1992, pp. 542.

Appendix
MATLAB model of SRM

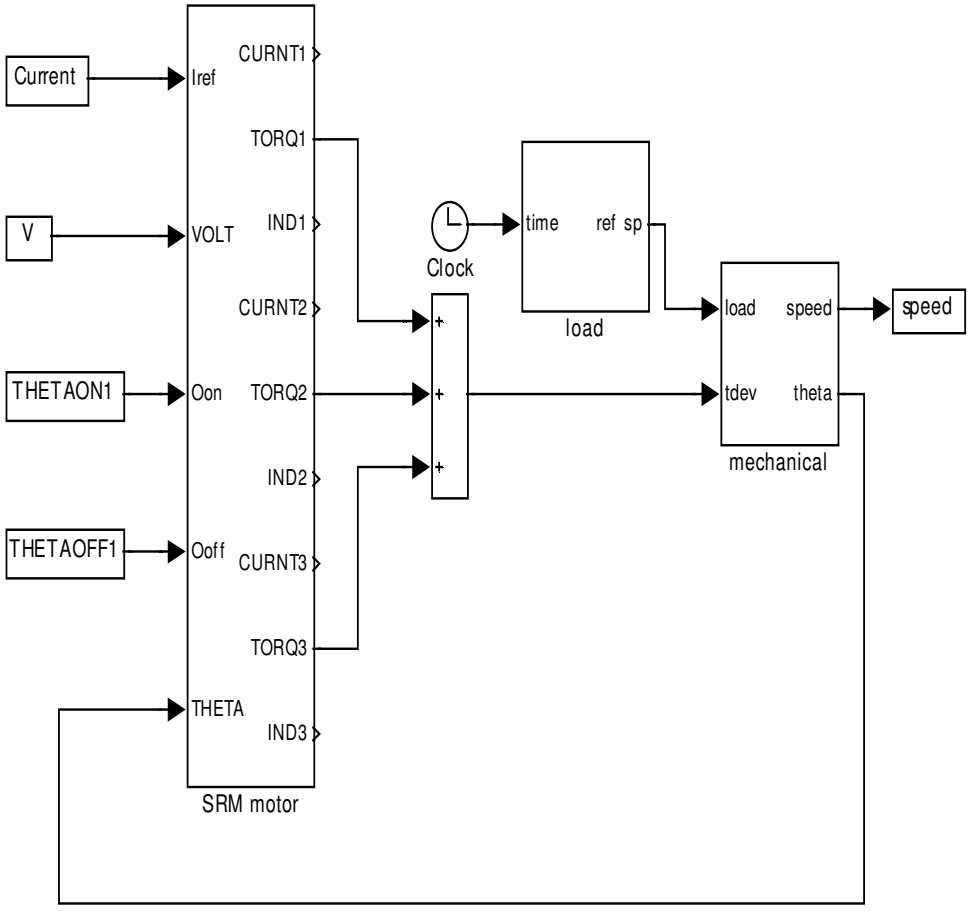

Figure A.1 SRM model.

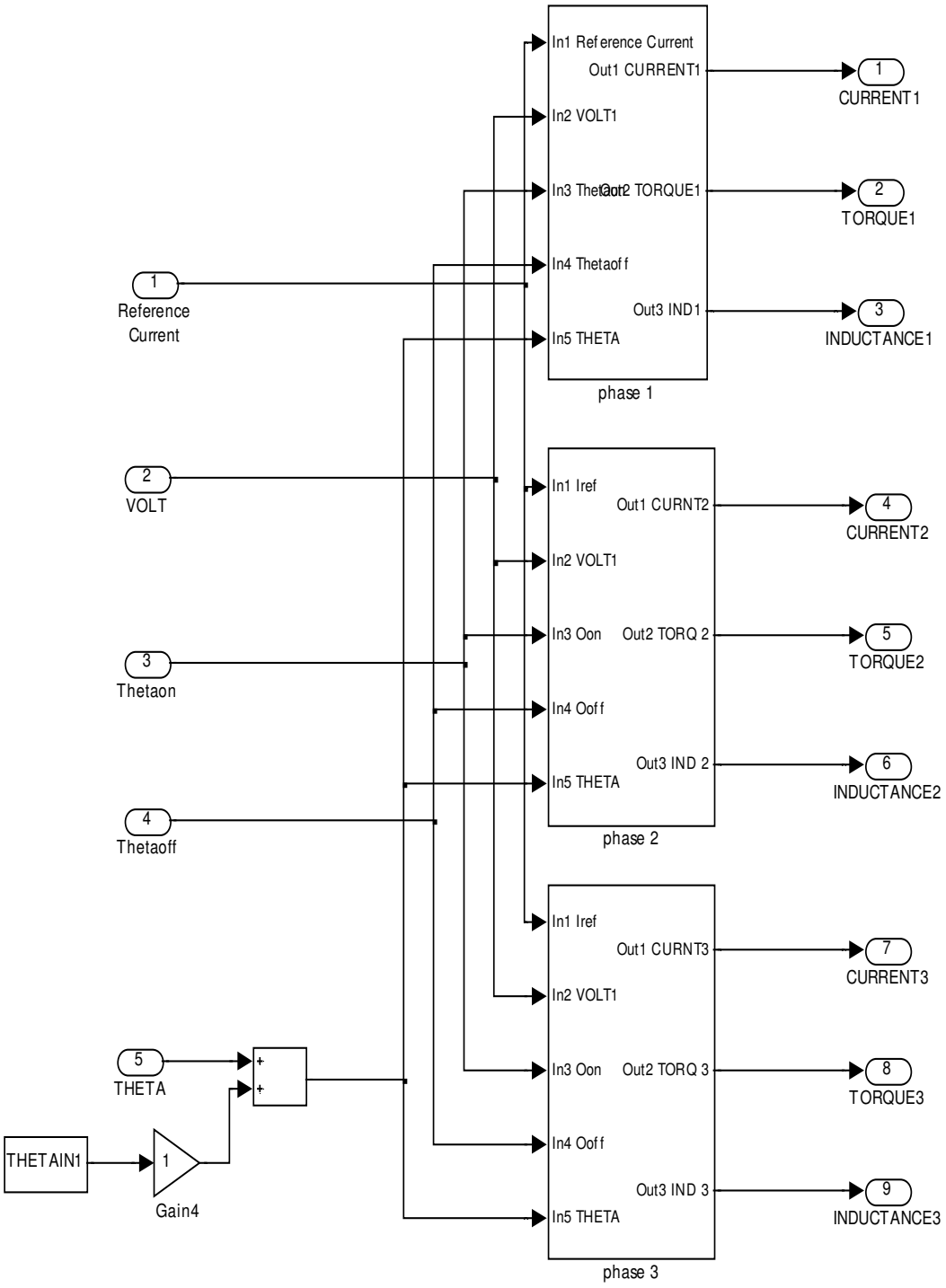

Figure A.2 Three phases modelling.

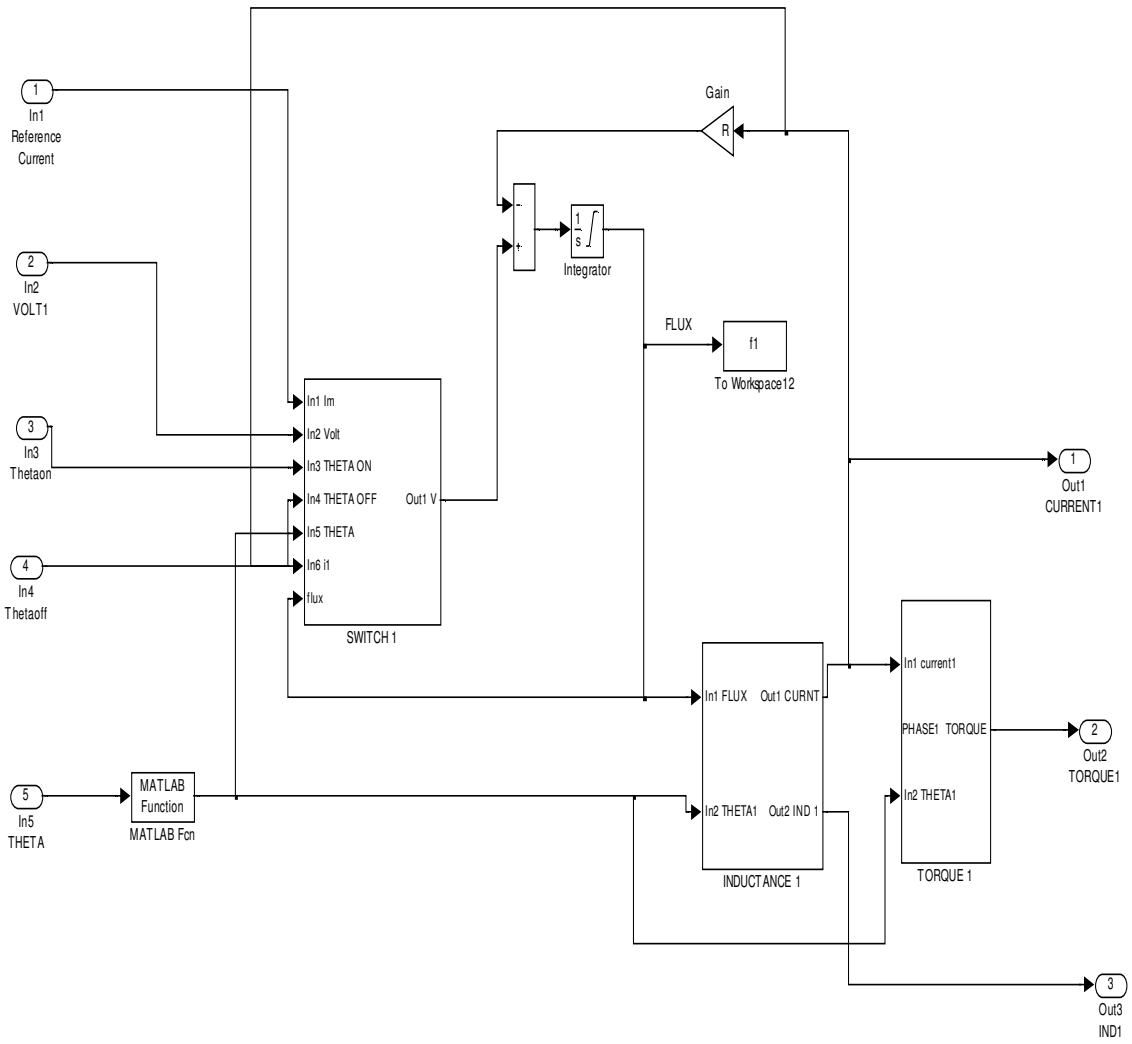

Figure A.3 Single-phase model of the SRM.